MRI-based radiotherapy of brain tumours: Implementing MRI-only radiotherapy and exploring diffusion MRI for response assessment

Lerner, Minna

2025

Document Version:
Publisher's PDF, also known as Version of record

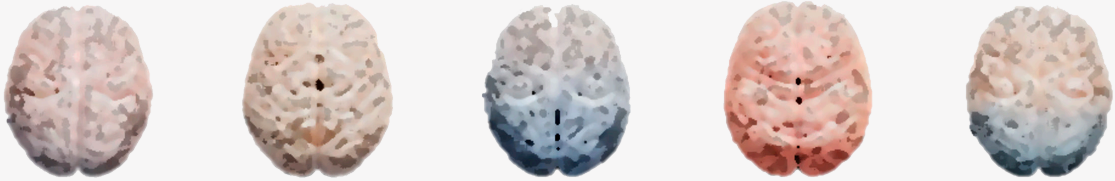

MRI-based radiotherapy of brain tumours

Implementing MRI-only radiotherapy and exploring diffusion MRI for response assessment

MINNA LERNER
MEDICAL RADIATION PHYSICS | FACULTY OF MEDICINE | LUND UNIVERSITY

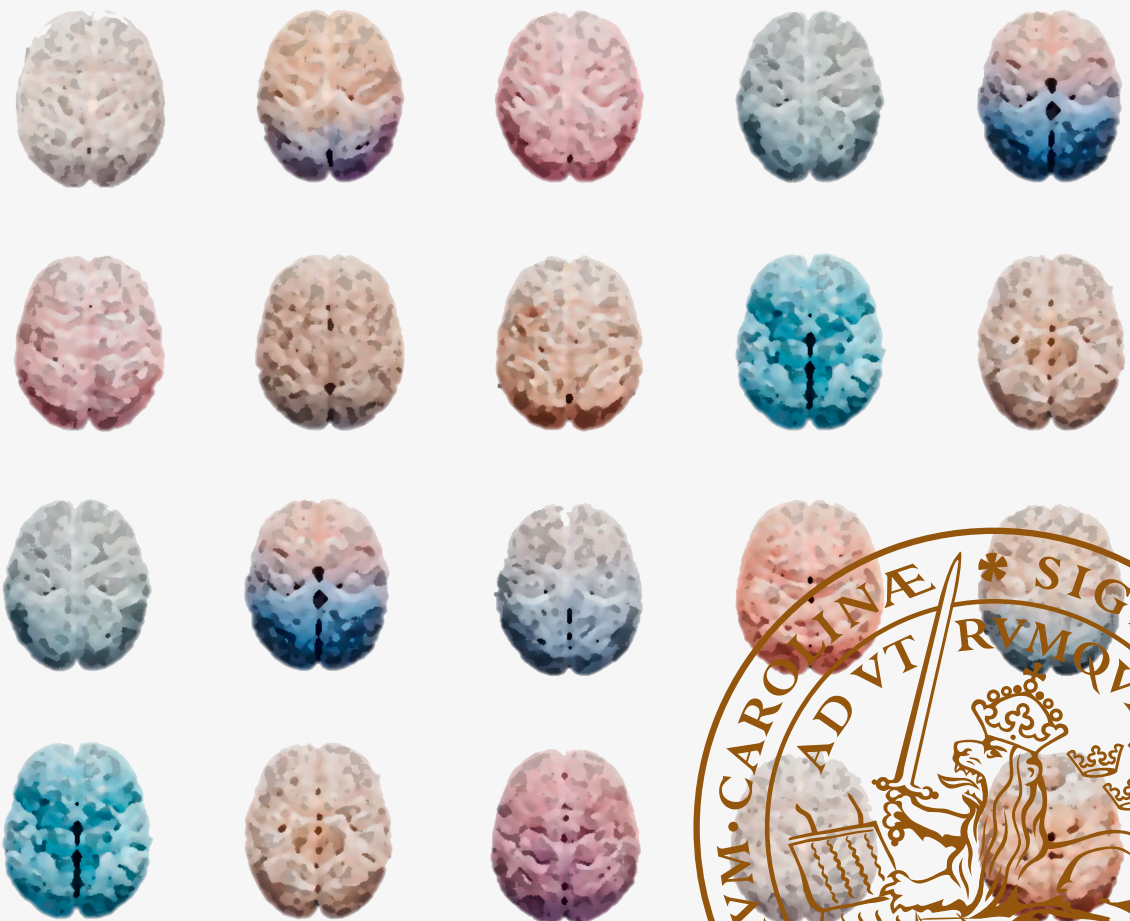

MRI-based radiotherapy of brain tumours

MRI-based radiotherapy of brain tumours

Implementing MRI-only radiotherapy and exploring diffusion MRI for response assessment

Minna Lerner

LUND
UNIVERSITY

DOCTORAL DISSERTATION
Doctoral dissertation for the degree of Doctor of Philosophy (PhD) at the Faculty of Medicine, Lund University, Sweden to be publicly defended on 9th of May at 13.00 in the Torsten Landberg Lecture Hall, 3rd floor of the Radiotherapy Building, Skåne University Hospital, Klinikgatan 5 in Lund, Sweden.

Faculty opponent
Dr. Richard Speight, Leeds Cancer Centre, Leeds, United Kingdom

Organization LUND UNIVERSITY Medical Radiation Physics Department of Translational Medicine Faculty of Medicine	**Document name** Doctoral dissertation **Date of issue** 2025-05-09
Author Minna Lerner	**Sponsoring organisation**

Title and subtitle

MRI-based radiotherapy of brain tumours: *Implementing MRI-only radiotherapy and exploring diffusion MRI for response assessment*

Abstract

During the last decades, magnetic resonance imaging (MRI) has become increasingly important in radiotherapy workflows. Its superior soft tissue contrast, compared to computed tomography (CT), enables accurate target delineations. MRI is also standard during radiotherapy follow-up to assess treatment response.

A workflow based solely on MRI, i.e. MRI-only radiotherapy, has the potential to reduce systematic uncertainties by excluding the otherwise required image registration between CT and MRI. Electron density maps for dose calculations can be provided by synthetic CT (sCT) data, generated from MRI. The first aim of our research was to validate and clinically implement an MRI-only workflow for patients with brain tumours. Dose calculations on sCT were compared to original treatment plans on CT, which demonstrated that sCT was a possible substitute for conventional CT during treatment planning of brain malignancies (Paper I). A prospective evaluation including high-grade glioma patients focused on the feasibility of the MRI-only workflow in clinical practice (Paper II). Criteria for dosimetry and patient positioning were fulfilled, and MRI-only radiotherapy was delivered to 20 patients. This work led to one of the first implementations of MRI-only radiotherapy for glioblastoma, which is now clinical routine at Skåne University Hospital.

The second aim was also to explore new imaging biomarkers for early response assessment, derived from tensor-valued diffusion MRI. By implementing and optimising the imaging sequence, feasibility was demonstrated in a radiotherapy setting (Paper III). The method was further explored in patients with brain metastases. It was shown that parameters derived from tensor-valued diffusion MRI differed significantly between responding and non-responding tumours, both before and during radiotherapy (Paper IV). These findings suggest that meaningful radiotherapy-related changes may be detected based on these parameters. Finally, denoising methods applied to tensor-valued diffusion MRI were studied to improve the inherently low signal-to-noise ratios of the diffusion images (Paper V). The results indicate that appropriate denoising of diffusion data enables higher spatial resolution and increased precision in diffusion parameters. This is an important step towards clinical applicability of imaging biomarkers for radiotherapy applications.

In conclusion, the work presented in this thesis demonstrate feasibility of both MRI-only radiotherapy and tensor-valued diffusion MRI in a radiotherapy setting. The findings have changed the local clinical practice of glioblastoma radiotherapy and enabled novel research possibilities of potential imaging biomarkers for early response assessment.

Key words

MRI-only, radiotherapy, synthetic CT, diffusion MRI, imaging biomarkers, brain tumours

Classification system and/or index terms (if any)	Supplementary bibliographic information	
ISSN and key title 1652-8220, Lund University, Faculty of Medicine Doctoral Dissertation Series 2025:46	**Language** English **Number of pages** 110	
ISBN 978-91-8021-699-9	Price	Security classification
	Recipient's notes	

Signature Date 2025-03-24

MRI-based radiotherapy of brain tumours

Implementing MRI-only radiotherapy and exploring diffusion MRI for response assessment

Minna Lerner

LUND
UNIVERSITY

Coverphoto: “Pastel brains” – the image was initially generated using OpenAI’s DALL·E and subsequently modified by the author. The modifications, enhancements, and creative alterations are the intellectual propery of the author.

Medical Radiation Physics,
Department of Translational Medicine,
Faculty of Medicine, Lund University, Sweden

ISBN 978-91-8021-699-9

ISSN 1652-8220

Lund University, Faculty of Medicine Doctoral Dissertation Series 2025:46

Printed in Sweden by Media-Tryck, Lund University, Lund 2025

"Not everything that can be counted counts, and not everything that counts can be counted."

- William Bruce Cameron

Abstract

During the last decades, magnetic resonance imaging (MRI) has become increasingly important in radiotherapy workflows. Its superior soft tissue contrast, compared to computed tomography (CT), enables accurate target delineations. MRI is also standard during radiotherapy follow-up to assess treatment response.

A workflow based solely on MRI, i.e. MRI-only radiotherapy, has the potential to reduce systematic uncertainties by excluding the otherwise required image registration between CT and MRI. Electron density maps for dose calculations can be provided by synthetic CT (sCT) data, generated from MRI. The first aim of our research was to validate and clinically implement an MRI-only workflow for patients with brain tumours. Dose calculations on sCT were compared to original treatment plans on CT, which demonstrated that sCT was a possible substitute for conventional CT during treatment planning of brain malignancies (**Paper I**). A prospective evaluation including high-grade glioma patients focused on the feasibility of the MRI-only workflow in clinical practice (**Paper II**). Criteria for dosimetry and patient positioning were fulfilled, and MRI-only radiotherapy was delivered to 20 patients. This work led to one of the first implementations of MRI-only radiotherapy for glioblastoma, which is now clinical routine at Skåne University Hospital.

The second aim was also to explore new imaging biomarkers for early response assessment, derived from tensor-valued diffusion MRI. By implementing and optimising the imaging sequence, feasibility was demonstrated in a radiotherapy setting (**Paper III**). The method was further explored in patients with brain metastases. It was shown that parameters derived from tensor-valued diffusion MRI differed significantly between responding and non-responding tumours, both before and during radiotherapy (**Paper IV**). These findings suggest that meaningful radiotherapy-related changes may be detected based on these parameters. Finally, denoising methods applied to tensor-valued diffusion MRI were studied to improve the inherently low signal-to-noise ratios of the diffusion images (**Paper V**). The results indicate that appropriate denoising of diffusion data enables higher spatial resolution and increased precision in diffusion parameters. This is an important step towards clinical applicability of imaging biomarkers for radiotherapy applications.

In conclusion, the work presented in this thesis demonstrate feasibility of both MRI-only radiotherapy and tensor-valued diffusion MRI in a radiotherapy setting. The findings have changed the local clinical practice of glioblastoma radiotherapy and enabled novel research possibilities of potential imaging biomarkers for early response assessment.

Summary in Swedish

Cancer är en av de vanligaste sjukdomarna i världen, och i Sverige får ungefär var tredje person ett cancerbesked någon gång under sin livstid. Ungefär hälften av dessa personer får strålbehandling, som är en av de mest vanliga och effektiva behandlingsmetoderna mot cancer. Målet med strålbehandlingen är att döda tumörcellerna genom att ge en hög stråldos till tumören men samtidigt skona omkringliggande frisk vävnad för att hålla nere biverkningarna.

När det gäller hjärntumörer är strålbehandling särskilt viktigt. I Sverige diagnosticeras ungefär 1400 personer med primär hjärntumör varje år, och ännu fler drabbas av spridd cancer till hjärnan, så kallade hjärnmetastaser. Hjärntumörer kan vara svåra att operera bort helt, och strålbehandlingen kan användas för att döda eventuella kvarvarande tumörceller eller användas som huvudbehandling när operation inte är möjlig. För att kunna leverera strålningen på ett så precist och noggrant sätt som möjligt är bildtagning av tumören och området runtomkring mycket viktig. För detta används ofta både datortomografi (CT) och magnetkamerabildtagning (MR). MR är speciellt användbart för patienter med hjärntumörer eftersom det tydligt visar små skillnader i mjukvävnad och är därför grunden för tumörutritning. CT-bilderna, som i stället återspeglar densitetsskillnader, används för att beräkna hur strålningen ska levereras. CT-bilderna används också för att kontrollera att patientens kropp ligger likadant vid varje behandlingstillfälle genom att jämföra dem med dagliga röntgenbilder.

De senaste åren har ett nytt arbetssätt introducerats där enbart MR-bilder används för att planera strålbehandlingen. Att utesluta CT-undersökningen kommer med flera fördelar: ökad noggrannhet genom att inte behöva överföra information mellan MR- och CT-bilder (s.k. registrering), minskad stråldos till patienten och ett mer strömlinjeformat arbetssätt i kliniken. Däremot behövs fortfarande ett underlag för att kunna beräkna stråldosen och hur behandlingen ska levereras. För detta har olika metoder utvecklats för att kunna omvandla MR-bilder till så kallade syntetiska CT-bilder, med samma egenskaper som en riktig CT-bild men utan den extra undersökningen. De syntetiska CT-bilderna ersätter den riktiga CTn i alla steg. När ett nytt arbetssätt ska införas i kliniken är det dock viktigt med omfattande tester och utvärderingar av både mjukvara och arbetsflöde för att säkerställa att resultatet blir minst lika bra som med de tidigare metoderna.

Två av studierna inom detta avhandlingsarbete fokuserade på att ta fram metoder och att utvärdera användandet av syntetiska CT-bilder för strålbehandling baserat på endast MR-bilder. Metoden för syntetisk CT är baserad på artificiell intelligens (AI) och utvecklades tillsammans med ett svenskt företag. Resultaten visade att de syntetiska CT-

bilderna på ett säkert och noggrant sätt kunde användas för att beräkna strålningen i patienten. Med den nya framtagna tekniken behandlades 20 patienter, enbart baserat på MR-bilder. En patient fick planeras om på riktigt CT-underlag då den hade en blödningsstillande gel kvar kring skallbenet efter en tidigare operation, vilket påverkade de syntetiska CT-bildernas utseende. Efter ytterligare kontroller visade det sig dock att bilderna var tillförlitliga, både vad gällde dos och för att positionera patienten rätt vid behandling. Totalt sett kunde det konstateras att den MR-baserade strålbehandlingen av hjärntumörer var säker att implementera i kliniken.

Den andra delen av detta avhandlingsarbete fokuserade på uppföljning av behandling snarare än planering inför behandling. Trots att strålbehandling är en av grundpelarna vid behandling av hjärnmetastaser är det inte alla patienter som svarar på behandlingen. Idag saknas det metoder för att avgöra hur strålkänslig en tumör är i förväg och därför behandlas till exempel alla patienter med hjärnmetastaser med samma mängd strålning. Om tumören är väldigt stor eller ligger nära strålkänsliga organ kan dock stråldosen i vissa fall sänkas. Vidare finns det inte heller någon metod för att under, eller tidigt efter, behandling kunna bestämma hur tumören svarat på strålningen. Dagens bildmetoder kan bara mäta storleksförändringar i tumören, vilket innebär att det slutliga resultatet blir synligt först efter flera veckor eller månader efter avslutad behandling.

Som tidigare nämnts är en av fördelarna med MR-bildtagning att den ger bra kontrast mellan olika mjukvävnader. En annan fördel med MR är att olika fysiologiska processer i kroppen kan fångas i bilderna. Detta kallas för funktionell MR och kan till exempel ge information som kan kopplas till vävnadens underliggande struktur. I det här arbetet har vi använt en avancerad typ av funktionell MR-bildtagning som kallas för diffusions-MR för att undersöka möjligheterna till förbättrad uppföljning av hjärnmetastaser och eventuellt kunna förutspå behandlingsrespons redan innan, eller tidigt under strålbehandlingen. MR-signalen i bilderna härstammar till stor del från vattenmolekylerna som finns i kroppen. Vattenmolekylerna rör sig slumpmässigt, både inom och mellan celler. Genom att mäta vattnets rörlighet, som kallas diffusion, kan vi få information om vävnadens struktur och egenskaper. Om cellerna ligger väldigt tätt packade, t.ex. som de gör i en tumör, rör sig vattnet långsamt och begränsat. Om cellstrukturen i stället är avlång, som t.ex. i nervbanor, rör sig vattnet lättare i riktningen längs med strukturen.

I det här arbetet har vi för första gången infört en metod för en avancerad typ av diffusionsmätning på en strålbehandlingsanpassad MR-kamera. Vi testade bildtagningen noga genom att undersöka friska försökspersoner och göra olika utvärderingar av bilderna. När vi försäkrat oss om att bildkvaliteten var tillräckligt bra och stabil gick vi vidare med en patientstudie. Patienter med hjärnmetastataser som skulle få strålbehandling på kliniken i Lund tillfrågades. Totalt inkluderades 26

patienter, som var och en genomgick upp till fyra MR-undersökningar: innan strålbehandling, mellan andra och tredje behandlingstillfället och 3 och 6 månader efter avslutad behandling.

Analysen i patientstudien försvårades av att hälften av patienterna behövde uteslutas, vissa på grund av sin långt gångna sjukdom och andra på grund av begränsad bildkvalitet i diffusions-bilderna. Bland de patienter som kvarstod identifierades 10 som svarade på behandling och 3 som inte gjorde det. Analys av diffusionsegenskaper antydde att medeldiffusionen var lite högre i de tumörer som svarade på behandling och att de eventuellt hade lite högre mikroskopiskt riktningsberoende diffusion än de som inte svarade på behandling. Det krävs dock större studier för att bekräfta resultaten och möjliggöra generella slutsatser. Den sista studien i detta avhandlingsarbete fokuserade på hur vi kan förbättra bildkvaliteten i diffusionsbilderna med hjälp av olika brusreducerande metoder. Vi kunde se att det finns stor potential för att få bättre signal, men också för att kunna förbättra upplösningen i bilderna framöver. Det stora målet är att patienterna i framtiden ska kunna få en mer skräddarsydd behandling med så små biverkningar som möjligt. Detta skulle kunna förbättra patientens sista tid i livet och kan kanske köpa värdefull extra tid tillsammans med nära och kära.

För att sammanfatta det här avhandlingsarbetet har en ny metod för strålbehandling, baserad på endast MR-bilder, utvecklats och utvärderats för patienter med hjärntumörer. Slutsatsen var att metoden uppfyller våra krav på noggrannhet i både dos och positionering. Dessutom har metoden införts i klinisk rutin sedan november 2023 för patienter med aggressiva hjärntumörer, där vi nu har behandlat runt 80 patienter sedan start. Vad gäller arbetet kring diffusions-MR och hjärnmetastasers behandlingssvar har forskningen inom detta avhandlingsarbete skapat en plattform för att kunna genomföra avancerad biologisk bildtagning på vår strålbehandlingsanpassade MR-kamera. Utvärderingen av bilderna och de olika egenskaperna som kan beräknas är lovande, men kräver ett större patientunderlag för att säkert kunna säga hur och om vi kan använda dessa för att utvärdera behandlingssvar. Ett sätt att komma vidare i den avancerade bildtagningen är att använda nya metoder för att minska bruset i bilderna och på så sätt uppnå en högre upplösning och mer precisa parametrar i framtida studier. Men en sak är säker, och det är att MR-baserad strålbehandling av hjärntumörer är här för att stanna.

List of papers

This thesis is based on the research presented in the following papers. They will be referred to in the text by their roman numerals. The papers are appended at the end of the thesis, see *Part II: Research papers*.

I. **Clinical validation of a commercially available deep learning software for synthetic CT generation for brain**
Minna Lerner, Joakim Medin, Christian Jamtheim Gustafsson, Sara Alkner, Carl Siversson and Lars E. Olsson
Radiation Oncology 2021 Apr 7;16(1):66

II. **Prospective clinical feasibility study for MRI-only brain radiotherapy**
Minna Lerner, Joakim Medin, Christian Jamtheim Gustafsson, Sara Alkner and Lars E. Olsson
*Frontiers in Oncol*ogy 2022 Jan 10;11:812643

III. **Tensor-valued diffusion magnetic resonance imaging in a radiotherapy setting**
Patrik Brynolfsson*, Minna Lerner*, Pia C. Sundgren, Christian Jamtheim Gustafsson, Markus Nilsson, Filip Szczepankiewicz and Lars E. Olsson (*Shared first authorship)
Physics and Imaging in Radiation Oncology 2022 Nov 10;24:144-151

IV. **Exploring imaging biomarkers from tensor-valued diffusion MRI for predicting treatment response in brain metastases during stereotactic radiotherapy**
Minna Lerner, Patrik Brynolfsson, Filip Szczepankiewicz, Pia C. Sundgren, Lars E. Olsson and Sara Alkner
Manuscript

V. **Denoising for high-resolution tensor-valued brain diffusion MRI**
Ivan A. Rashid, Minna Lerner, Lars E. Olsson and Patrik Brynolfsson
Manuscript

Preliminary reports

Below is a list of selected preliminary reports, related to this work.

Validation of synthetic CTs of the brain generated with a commercially available deep learning software
Minna Lerner, Joakim Medin, Christian Gustafsson, Sara Alkner, Carl Siversson and Lars E Olsson, *Öresund Workshop,* Helsingborg, Sweden, 2020

MRI-only based treatment with a commercial deep-learning generation method for synthetic CT of brain
Minna Lerner, Joakim Medin, Christian Jamtheim Gustafsson Sara Alkner and Lars E Olsson, *8th Annual Symposium on Magnetic Resonance Imaging in Radiation Therapy,* Heidelberg, Germany, 2021

MRI-only radiotherapy of gliomas – a prospective implementation study
Minna Lerner, Joakim Medin, Christian Jamtheim Gustafsson Sara Alkner and Lars E Olsson, *ESTRO 41,* Copenhagen, Denmark, 2022

Intracranial MRI-CT registration uncertainties: A motivation for MRI-only radiotherapy or not?
Minna Lerner, Joakim Medin, Sara Alkner, Lars E Olsson and Emilia Persson, *ESTRO 43***,** Glasgow, United Kingdom, 2024

Exploring imaging biomarkers from tensor-valued diffusion-MRI for predicting treatment response in brain metastases during stereotactic radiotherapy
Minna Lerner, Patrik Brynolfsson, Filip Szczepankiewicz, Joakim Medin, Pia C. Sundgren, Lars E Olsson and Sara Alkner, *11th Annual Symposium on Magnetic Resonance Imaging in Radiation Therapy*, New York, USA, 2025

Advanced denoising enables high-resolution diffusion MRI in radiotherapy
Ivan A. Rashid, Minna Lerner, Lars E. Olsson and Patrik Brynolfsson, *11th Annual Symposium on Magnetic Resonance Imaging in Radiation Therapy*, New York, USA, 2025

Abbreviations

ADC	Apparent diffusion coefficient
AI	Artificial intelligence
ARDL	AIR Recon DL
CBCT	Cone beam computed tomography
CNS	Central nervous system
CSF	Cerebrospinal fluid
CT	Computed tomography
CTV	Clinical target volume
DIVIDE	Diffusional variance decomposition
DL	Deep learning
DTI	Diffusion tensor imaging
DSC	Dice similarity coefficient
DVH	Dose volume histogram
ED	Electron density
ETD	ExacTrac Dynamic
FA	Fractional anisotropy
GTV	Gross tumour volume
HU	Hounsfield units
IGRT	Image guided radiotherapy
LTE	Linear tensor encoding
MAE	Mean absolute error
ME	Mean error
MKA	Anisotropic diffusional variance
MKI	Isotropic diffusional variance
MD	Mean diffusivity
MPPCA	Marchenko-Pastur principal component analysis
MR	Magnetic resonance
MRI	Magnetic resonance imaging
OAR	Organs at risk
PCA	Principal component analysis
PTV	Planning target volume
QA	Quality assurance
QTI	Q-space trajectory imaging
RT	Radiotherapy
sCT	Synthetic computed tomography
SGRT	Surface guided radiotherapy
SNR	Signal to noise ratio

SRS	Stereotactic radiosurgery
SRT	Stereotactic radiotherapy
STE	Spherical tensor encoding
SUS	Skåne University Hospital
TMZ	Temozolomide
TPS	Treatment planning system
µFA	Microscopic fractional anisotropy
VMAT	Volumetric modulated arc therapy
WBRT	Whole brain radiotherapy

Declaration of generative AI usage

Generative AI tools (GPT-4 by OpenAI) were used on individual sentences to improve language, grammar, and flow in parts of this thesis. The use was limited to improving clarity and did not influence the originality or intellectual content of the thesis.

Table of contents

Part I: Research context

Part II: Research papers

Part I

Research context

1 Introduction

External radiotherapy is one of the cornerstones in the treatment of most brain cancer patients. The purpose of radiotherapy is to deliver a high absorbed dose of ionising radiation to the tumour, while sparing the surrounding healthy tissue to minimise side effects. To achieve this, precision and accuracy of radiation delivery are crucial. Therefore, imaging is an important part of the preparations to determine the exact position of the tumour in the brain. Traditionally, computed tomography (CT) in combination with magnetic resonance imaging (MRI) have been used as clinical standard for brain tumours. One of the major advantages of MRI compared to CT, is the improved soft tissue contrast, especially important in the brain.

To optimise the dose to be delivered, an individual treatment plan is created for each patient. The CT images, containing Hounsfield Units (HU) which reflect the electron density (ED) of the tissues, hold the data for the dose calculation. The MR images are the foundation for delineating the tumour and nearby organs. The combined workflow of CT and MR images requires an image registration between the two modalities to transfer the delineations from the MRI frame of reference to the CT for dose optimisation and calculation. However, this registration introduces a geometric uncertainty which persists throughout the entire treatment workflow. One way to eliminate this uncertainty is to use an MRI-only radiotherapy (RT) workflow, in which synthetic CT (sCT) images are created from the MR images. The sCT may be used for dose optimisation and calculation, and later, for patient positioning during treatment. The first part of this thesis focuses on the development, validation, and implementation of MRI-only RT of brain tumours.

Despite treatment, the prognosis for patients with glioblastoma or brain metastases is poor (Mohammed et al., 2022, Sperduto et al., 2020). Although the variations in survival for patients with brain metastases depends on various factors, such as primary diagnosis and overall health performance, not all patients respond to treatment. Currently, there is no way to differentiate the responders from non-responders prior to treatment using existing imaging methods. Furthermore, there is a need for improved and faster follow-up after treatment. Today, follow-up includes measuring the change in tumour volume, from which it takes several weeks or months to determine

responders from non-responders. Diffusion MRI has the potential to provide parameters that could serve as imaging biomarkers, both for prediction of treatment outcome and early treatment response assessment. The second part of this thesis aims to explore imaging biomarkers derived from advanced diffusion MRI, focusing on technical implementation and clinical feasibility.

In summary, patients with brain cancer are often profoundly affected by their disease and face a poor prognosis. Therefore, it is crucial to continue to optimise and further individualise the treatment workflows for these patients. The research presented in this thesis aims to contribute to the future of brain cancer treatments, offering a meaningful step towards improving patient care with the aid of MRI-based radiotherapy. More specifically, this thesis addresses the clinical need for more precise and efficient cancer treatment and follow-up, by implementing MRI-only RT, and by utilising advanced diffusion MRI techniques to enable enhanced follow-up after treatment.

2 Aims

The overall aim of this thesis was to optimise radiotherapy of brain tumours by developing, validating, and implementing MRI-only RT, and to implement and explore advanced diffusion MRI methods to investigate new potential imaging biomarkers for early response assessment.

The specific aims of this work were as follows:

- retrospectively evaluate geometric and dosimetric criteria of deep-learning generated sCT images for MRI-only RT of brain tumours (**Paper I**).
- prospectively investigate the feasibility of implementing an MRI-only RT workflow for glioma patients, including the evaluation of dosimetric criteria and patient positioning (**Paper II**).
- implement tensor-valued diffusion MRI in a radiotherapy setting by optimising imaging parameters and setup (**Paper III**).
- investigate parameters derived from tensor-valued diffusion MRI as potential predictive imaging biomarkers for treatment response during stereotactic radiotherapy of brain metastases (**Paper IV**).
- evaluate the potential of open-source and vendor-provided denoising methods to enhance the resolution of tensor-valued diffusion MRI in the brain on a radiotherapy dedicated MRI scanner (**Paper V**).

3 Cancer in the brain

The incidence of brain tumours is increasing worldwide (Ilic and Ilic, 2023) and in Sweden 1400 people are diagnosed with primary tumours in the central nervous system (CNS) each year (Socialstyrelsen, 2023). Curative treatment of these lesions is generally challenging, and in many cases not possible.

This thesis investigates how to implement MRI methods to optimise the radiotherapy of brain tumours. Patients of focus are those with the most common types of primary and secondary brain malignancies. Prior to exploring the details of this thesis, a brief overview is provided of the different tumour types, their respective treatment options, and a summary of the patient cohorts included in the individual papers.

3.1 Primary brain tumours

The most common type of primary CNS tumour is glioma, accounting for approximately 80% of all malignant cases (Goodenberger and Jenkins, 2012). The tumour cells derive from the glial cells (astrocytes and oligodendrocytes), originally protecting and supporting the neurons in the brain. Most primary brain tumours, including gliomas, arise without known cause, though cancer-causing mutations are mainly due to internal factors rather than external ones (van den Bent et al., 2023).

3.1.1 Glioblastoma

Glioblastoma is the most common type of glioma. It is a grade four diffuse astrocytoma, which is highly aggressive and fast-growing, making it the most lethal form of primary cancer in the CNS. Without treatment, expected survival is limited to 3-4.5 months. If maximal treatment regimens are tolerated, median survival may improve to 15-16 months (McKinnon et al., 2021). The most common tumour occurrence is in the cerebral hemispheres, especially in the frontal and temporal lobes. Typical properties of the glioblastoma tumours are high cell density, a liquidised central necrosis, and a

heterogenic structure, including bleeding. Median age of diagnosis is 64 years with a male predominance (Tamimi, 2017).

3.1.2 Treatment options for glioblastoma

Glioblastoma is difficult to treat due to the inherent characteristics of the tumour with rapid and invasive growth. The aim of the treatment is to limit tumour growth, relieve clinical symptoms, prolong overall survival, and improve quality of life.

The first step of treatment is to fully or partially remove the tumour volume by surgery (Weller et al., 2021). For glioblastoma, a full resection (>98% of the tumour volume removed) yields significant survival advantage compared to partial removal of the tumour (Lacroix et al., 2001). Within 48 hours of the surgery, a post-operative MRI is performed to assess if there is any remaining tumour tissue. The result may serve as the baseline for continued oncological treatment.

In line with national guidelines, standard post-operative therapy for glioblastoma patients is radiotherapy in combination with chemotherapy. Typical radiation dose prescription is 60 Gy, delivered in 30 treatment sessions, five days a week, with concomitant chemotherapy of Temozolomide (TMZ) (Regionala Cancercentrum i Samverkan, 2024). This combined treatment is followed by six cycles of adjuvant TMZ. This regimen quickly became standard of care after 2005 when Stupp et al. presented a randomised, multicentre study of 573 glioblastoma patients, demonstrating an improved two-year survival rate from 10.4% with radiotherapy alone to 26.5% for radiotherapy and TMZ combined (Stupp et al., 2005). Ideally, radiotherapy should commence as soon as possible once the surgical scar has adequately healed, which is usually within four weeks. The final radiation dose and number of treatment sessions may be reduced depending on the patients age and overall performance status (Regionala Cancercentrum i Samverkan, 2024). Hypofractionation may be considered in one of the following combinations:

- Prescribed dose of 40.05 Gy given in 15 fractions of 2.67 Gy.
- Prescribed dose of 34 Gy given in 10 fractions of 3.4 Gy.
- Prescribed dose of 25 Gy given in 5 fractions of 5 Gy.

The most recent breakthrough in glioblastoma treatment is the introduction of tumour treating fields (TTFields) (Stupp et al., 2017), prolonging survival up to 5 months post radiotherapy compared to TMZ alone. With this technique, intermediate-frequency (200 kHz) electric fields are applied through transducer arrays on the shaved scalp of the patient for more than 18 hours a day. The treatment is gentle and free from serious

side effects but at the same time expensive and tend to interfere with the everyday life of the patient (Kinhult et al., 2023).

Finally, an important choice of treatment for glioblastoma, is the symptomatic therapy. Symptomatic therapy in brain cancer includes treating brain swelling (oedema), epilepsy, rehabilitation, and psychological discomfort, such as insomnia and mood disorders (Roth et al., 2021).With poor prognosis and a life expectancy reduced to only a few months or years, the quality of life should be in focus in all stages of therapy planning. In some cases, the best treatment option might be to refrain from demanding treatments and instead focus on other palliative options during the time left.

3.2 Brain metastases

A brain metastasis is a tumour that originates from a primary cancer elsewhere in the body. The most common source is lung cancer, followed by breast cancer, malignant melanoma, and colon cancer. Brain metastases are the overall most common type of intracranial neoplasms, with an incidence higher than all primary brain tumours combined (Brenner and Patel, 2022). The metastases can occur as single or multiple lesions. At the time of diagnosis, up to 85% of patients already have multiple intracranial metastases (Fox et al., 2011). Survival varies depending on number of lesions, primary cancer type, and overall health status. However, similarly to glioblastoma, prognosis is poor. In a cohort of patients where the majority had more than ten brain metastases, the median overall survival was less than six months (Estermann et al., 2024), while overall survival of 12 months has been reported for patients with less than four metastases (Brown et al., 2017).

Brain metastases are increasingly common as a result of improved efficacy in systemic cancer treatment, and thereby a longer life expectancy. One example is the increase in HER2-positive breast cancer survivors after the introduction of the targeting drug trastuzumab, leading to increased incidence of brain metastasis as the patients live longer with their systemic disease (Miller et al., 2003).

The appearance of brain metastases tends to be more confined and focal than for primary brain cancer. The metastases preserve the histology of their primary pathology and therefore differ depending on main diagnosis. Approximately 85% of brain metastases are located in the cerebrum, 10-15% in the cerebellum and less than 5% in the brainstem.

3.2.1 Treatment options for brain metastases

Patients with brain metastases most often receive palliative treatment due to the cancer already being spread from the primary tumour location. The intent of the treatment aligns with that of glioblastoma: to prolong overall survival and improve quality of life during the patient's remaining lifespan. The preferred treatment options are highly individual, but in general surgery and radiotherapy are the cornerstones (Vogelbaum et al., 2021).

In brain metastases, surgery is considered standard of care. It is also a way to diagnose the lesion based on histology, which is not possible through only imaging. However, patient selection for surgery requires consideration of age, performance status and extent of primary disease. Furthermore, not all locations are possible to resect. For example, tumours located in deep nuclei or white matter tracts are considered too high risk of morbidity and are therefore not resected (Brenner and Patel, 2022).

Radiotherapy treatment regimens for brain metastases tend to be more aggressive than for primary brain tumours. This is possible since they are often small, clearly defined lesions, enabling high doses in few fractions (Guckenberger et al., 2020). Stereotactic radiosurgery (SRS), i.e. a single fraction of 18 or 24 Gy, or stereotactic radiotherapy (SRT), 3-5 fractions of 27-35 Gy, have proven to yield one-year local tumour control above 80% (Redmond et al., 2021). A stereotactic dose distribution has an inhomogeneous dose intensity across the tumour, with its peak intensity in the centre which radially decreases to the prescribed dose at the tumour edges.

In cases of multiple brain metastases or patients with relatively shorter life expectancy, whole brain radiotherapy (WBRT) is the preferred option. It may also be used as adjuvant therapy after surgery. Although it does not improve survival, it may reduce the risk of local recurrence and distant metastases (Brenner and Patel, 2022).

Finally, an important treatment option is symptomatic therapy. The aim of this treatment is to focus on alleviating symptoms and improving quality of life. Depending on the number, and location, of the tumours, common symptoms may be headaches, nausea, seizures, and anxiety (Roth et al., 2021).

3.3 Study cohorts

All studies included in this thesis involved human research subjects. Some were healthy adults (**Paper III and V**), but the majority were patients with brain tumours (**Paper I, II, III** and **IV**). All subjects were prospectively included with informed consent, in accordance with the ethical permits (details in chapter 7). In the MRI-only RT validation study (**Paper I**), both glioma (n=10) and brain metastases (n=10) were included. Mean age was 68 years (range: 42-81 years). All treatments were planned and delivered using modern, state-of-the-art techniques. Prescribed total absorbed doses were between 25 to 60 Gy, according to local clinical routines. The second part of the MRI-only RT project (**Paper II**) focused on high-grade glioma patients (n=21). Mean age was 62 years (range: 46-85 years). Treatments were prescribed with doses of 34, 40.05 or 60 Gy in 10, 15 or 30 fractions, again according to clinical routine.

For the tensor-valued diffusion MRI projects (**Paper III** and **IV**), adult patients with brain metastases were included. One of the inclusion criteria was a solid tumour volume of at least 1cm^3, which essentially excluded surgically resected patients. The included patients had different primary diagnoses (lung cancer, breast cancer, colon cancer, malignant melanoma, renal cancer, testis cancer and unknown primary), however, all patients were referred to radiotherapy of their brain metastases. Mean age was 64 years (range: 44-85 years). All patients were treated using high-precision, state-of-the-art radiotherapy with initially prescribed dose of 30 Gy in 3 fractions. Some patients had reduced doses down to 21 or 24 Gy due to large tumour volumes or close proximity to critical organs at risk (OAR) and/or previously irradiated regions.

4 Radiotherapy and magnetic resonance imaging

4.1 Radiotherapy of brain tumours

Brain tumours have been treated using ionising radiation for over 70 years (Chao et al., 1954), initially via WBRT with two opposing lateral fields. As medical imaging improved, 3-dimensional (3D) conformal radiotherapy became widely used during the 1970-80s. Adding 3D information about the tumour and surrounding OAR allowed shaping of the radiation with higher doses to the tumour while sparing the critical organs nearby. Dose distribution and conformity was further improved with technical developments of the linear accelerators and treatment planning systems (TPS). Intensity modulated radiotherapy (IMRT) was introduced in the late 1990s, followed by volumetric modulated arc therapy (VMAT) in 2007, which soon became standard for many cancer types. During VMAT, the gantry of the linear accelerator rotates around the patient while thin metal multi leaf collimators (MLC) continuously move to optimise the dose intensity and field shape (Teoh et al., 2011). Today, VMAT is considered state-of-the-art radiotherapy for brain tumours. The VMAT treatment may be delivered using several half- or full arcs, allowing for precise optimisation of the dose and enabling a high conformal dose distribution to the tumour.

A requirement for all advanced radiotherapy techniques is accurate patient positioning by image guidance before delivering the treatment. Image guided radiotherapy (IGRT) is made possible through integrated 2-dimensional (2D) and 3D imaging systems on the linear accelerators, allowing for positioning of the patient with adjustments in up to six dimensions (including rotations). Recent advancement also allows for imaging during treatment (intra-fractional). With daily images, the aim is to reduce positional errors and ensure a safe delivery of the treatment (Scaringi et al., 2018).

4.2 Imaging in radiotherapy of brain tumours

Medical imaging is crucial in cancer care, and radiotherapy in particular. In addition to the integrated image guidance for daily positioning during treatment, imaging is used in diagnostics, treatment planning, and follow-up. Several imaging modalities are often combined pre- and post-treatment, as they may provide complementary information and quality. The main imaging modalities in brain tumour radiotherapy are CT and MRI, where MRI can be either the secondary or primary imaging modality.

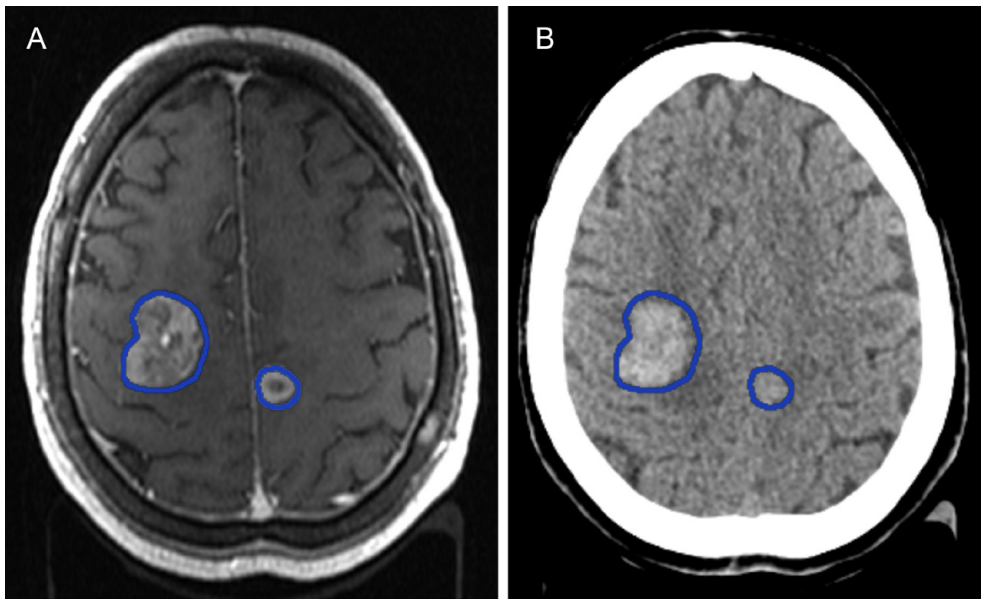

Figure 1. A patient with two brain metastases (outlined in blue) imaged with **A)** MRI (T1w + Gadolinium-based contrast agent) and **B)** CT (window level -20 to 100 HU).

For precise target definitions, the International Commission on Radiation Units and Measurements (ICRU) has established standardised terminology in radiotherapy treatment planning. The visible tumour is defined as the gross tumour volume (GTV), the total volume including potential microscopic disease as the clinical target volume (CTV) while the planning target volume (PTV) also considers geometric uncertainties due to technical and biological factors (ICRU, 1993).

4.2.1 MRI as a secondary imaging modality

Computed tomography has long been the foundation for imaging in radiotherapy. The CT images have high geometric accuracy, and each voxel contains values expressed in HU. The HU provide information about the radiation attenuation of the tissues, which can be converted to ED essential for radiation dose calculations during treatment planning (Gardner et al., 2019). During treatment, the CT images serve as the reference to position the patient correctly in the IGRT workflow, ensuring accurate delivery of the prescribed dose (Scaringi et al., 2018). In the case of brain tumours, a limitation to the CT images is the image contrast, which poorly separates soft tissue variations.

Compared to CT, MRI provides superior soft-tissue contrast (Figure 1), which was the original motivation to introduce MRI as the secondary imaging modality in radiotherapy (Datta et al., 2008). The use of MRI in radiotherapy was mentioned already in 1987 (Fraass et al., 1987), and has in the last few decades become a standard complement to CT in radiotherapy planning (Niyazi et al., 2023, Brenner and Patel, 2022, Srinivasan et al., 2022). MRI does not use ionising radiation. Instead, the image is generated using a strong magnetic field and radio waves that excites the hydrogen atoms in the body. A set of radiofrequency coils collects the signal from the tissue, from which a 3D image is reconstructed. Magnetic field gradients are used for spatial encoding, allowing precise localisation of the signal's origin within the body (McRobbie et al., 2009).

In the conventional radiotherapy workflow (Figure 2), MRI primarily serves to delineate the target and OAR during treatment planning. A critical requirement in this combined CT-MR, or dual-modality, workflow is the registration of images from the two modalities. This registration can be achieved using either rigid or deformable methods. Typically, registration algorithms rely on mutual information to align the images accurately (Speight, 2019). Regardless, this may be a process prone to errors and could introduce errors up to a few millimetres (Ulin et al., 2010, Owrangi et al., 2018, Lerner et al., 2024), that persist throughout the treatment chain.

Finally, MRI offers a significant advantage by providing not only a variety of contrasts in anatomical images, but also functional and quantitative information, such as tissue perfusion and diffusion (Goodburn et al., 2022). This may be useful both during treatment planning (Aldawsari et al., 2023) and in response assessment (Shah et al., 2021). A highly active research field within MRI is imaging biomarkers, which potentially could help predict treatment response during or soon after radiotherapy. The exploration of technical implementation and clinical feasibility regarding new predictive imaging biomarkers is the focus of chapter 6.

4.2.2 MRI as a primary imaging modality

In recent years, MRI as the primary imaging modality, excluding the CT, has become a realistic option in radiotherapy for certain patient groups. In this way, the full potential of MRI can be reached while the image registration uncertainty from the dual-modality workflow is eliminated. The new workflow is referred to as MRI-only RT. The MR images replace the CT in all steps of the workflow (Figure 2), which includes providing HU to be used in the dose calculation process. The HU maps derived from MRI data, so called sCT images, can be generated using various methods (described in chapter 5.2).

MRI-only RT has gained increasing interest in the research community with main advantages proposed as streamlined workflows, reduced radiation exposure to the patient and mitigated registration uncertainties (Jonsson et al., 2019). However, due to absent guidelines and lack of general consensus, MRI-only RT is not yet standard clinical practice (Villegas et al., 2024). The concept, development, and implementation of MRI-only RT for brain tumours is the focus of chapter 5.

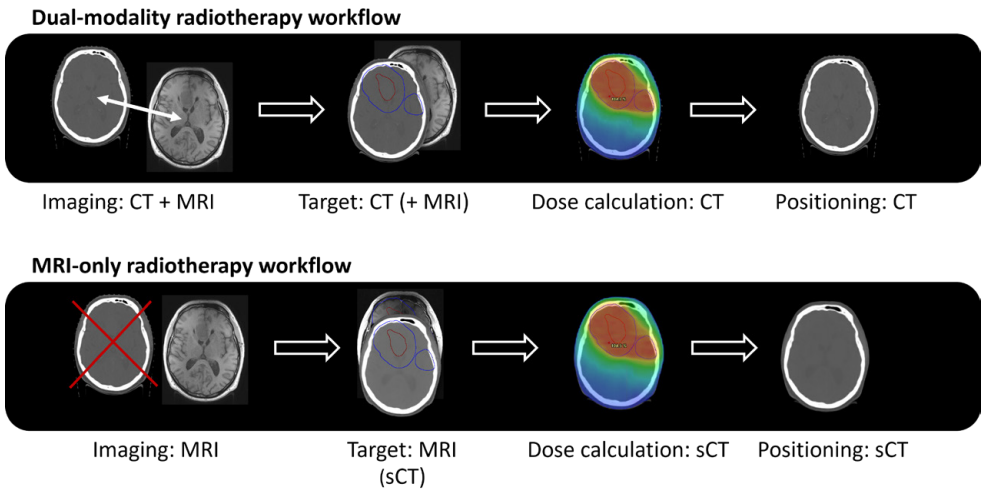

Figure 2. Overview of the radiotherapy workflows in which MRI may be used as the secondary or primary imaging modality. The conventional, dual-modality radiotherapy workflow (upper row) rely on CT images, with complementary MR images registered for target and OAR delineations. The MRI-only RT workflow (lower row) completely excludes the CT and relies only on MR images. Synthetic CT images are generated from the MR images and are used for dose calculation and patient positioning during treatment.

5 MRI-only radiotherapy of brain tumours

This chapter of the thesis primarily relates to **Paper I** and **Paper II**. At the time when this work was initiated, the research field mainly consisted of in-house developed sCT generation methods for brain, with no overall demonstration of clinical implementation strategies. The general focus of this work was to develop and implement an MRI-only RT workflow for brain tumours. We contributed to the development of the sCT generation software MRI Planner (Spectronic Medical AB, Helsingborg, Sweden), which became commercially available during the process. Utilising a commercial product increases the potential of a widespread clinical implementation.

In **Paper I**, the quality of the sCT images was evaluated based on geometric and dosimetric criteria, investigating both primary and secondary brain tumours. The patient cohort also comprised patients with anatomical anomalies due to bone resection, a group which has been excluded in many previous studies on the subject. In **Paper II**, a prospective evaluation of the workflow was conducted for high-grade glioma patients. Acceptance criteria regarding geometric properties, dose accuracy and patient positioning were investigated. The last section of this chapter presents initial experiences from the clinical implementation of the MRI-only RT workflow developed during this thesis work. Building on the studies presented here, MRI-only RT of glioblastoma has become clinical routine at the radiotherapy department at Skåne University Hospital (SUS) in Lund as of November 2023.

5.1 The motivation

As a medical physicist, or any researcher within the field of radiotherapy, our purpose is to improve and optimise methods and treatments, for the individual patient as well as for the whole population. With MRI becoming a standard part of the radiotherapy workflow, it is only natural to question whether we really need the CT? Relying only

on the MR images offers several advantages, which encourages the MRI-only RT approach.

The most obvious advantage with MRI compared to CT images is the superior soft tissue contrast, as already mentioned in chapter 4.2.1. Another advantage that is generally mentioned in this context is the elimination of the CT-MR image registration, which can otherwise introduce systematic errors that persist throughout the treatment workflow. The use of two imaging modalities introduces uncertainties due to the time between imaging sessions, re-positioning of the patient, possible anatomical changes between the scans and inherently different properties of the images such as resolution and image contrasts.

On the topic of brain image registration uncertainties, a study by Ulin et al has been frequently referenced (Ulin et al., 2010). The study evaluated the CT-MR image registration based on a single paediatric patient, used as a benchmark case. 45 institutions with a total of 11 different software performed the registration according to their local routines. Registration errors up to 6 mm and an average inherent uncertainty of approximately 2 mm were reported. Considering the limited material of the study, and the technical improvements made since 2010, we initiated a local study as part of our MRI-only RT investigation. The aim was to evaluate the uncertainty related to the image registration between CT and MR images of the brain using a clinical registration method (Lerner et al., 2024). Our study compared registration results from clinical routine to those of an observer, based on 45 patients with intracranial lesions. As expected, the deviations were small, with a median translational difference vector of 0.6 mm. However, upon further investigation, an outlier case was identified, where the resulting centre of mass shift was more than 4 mm between registrations. Although the registration uncertainty was demonstrated to be of minor concern for the majority of patients, our results highlight that there is motivation to exclude the CT-MR image registration, especially as we move towards smaller margins and higher doses. Based on the aspect of reduced geometric uncertainties from excluding the CT-MR image registration, our results imply that treatments such as stereotactic radiotherapy of small brain metastases may benefit most from the MRI-only RT approach.

When discussing the motivation for MRI-only RT in general, it is important to also consider the patient experience. To our patients, the preparatory phase of radiotherapy involves long days of various examinations and appointments. Excluding the CT examination and the waiting time associated with it, can improve patient comfort and convenience. Excluding the CT also reduces the overall imaging dose from ionising radiation to the patient. The absorbed dose from this type of CT examination is small in comparison to the total dose of the radiotherapy treatment. However, in the field of

ionising radiation, we are always embracing the principle of ALARA (As Low As Reasonably Achievable), enhancing patient safety by minimising radiation exposure.

Furthermore, the use of a single imaging modality streamlines the radiotherapy workflow. Potentially, this can save time for the clinic and make the process less prone to errors (Owrangi et al., 2018). Implementation of MRI-only RT workflows may also come with long-term economic benefits, depending on potential margin reductions, number of annually treated patients and the total cost of the sCT generation, as previously demonstrated for prostate cancer (Persson et al., 2023, Keyriläinen et al., 2021).

Finally, the introduction of MRI-only RT may also become a bridge to MRI-guided radiotherapy, where daily treatment adaptation is possible based on MR images (Guerini et al., 2023).

5.2 Synthetic CT generation

One of the first challenges encountered in MRI-only RT is the lack of HU information in the MR images. The absorbed dose calculation carried out for each treatment plan requires tissue specific ED. In a CT image, the HU in each voxel inherently correlate to the ED. However, this is not the case for the MRI signal, which instead mainly relates to the proton density and relaxation times of the tissue. Therefore, different methods to generate HU from MR images have been developed. An sCT is created completely based on MRI data but resembles a CT image in appearance and information content, including HU values. Other commonly used expressions for images containing HU generated from MRI data are pseudo-CT or substitute CT. In this thesis, the term synthetic CT will be used throughout. The most common sCT generation method today is through deep learning (DL) algorithms, available as both commercial products and in-house-developed research software (Autret et al., 2023, Boulanger et al., 2021).

Since the sCT is a map of HU values, it may be used for both dose calculations during treatment planning and as a reference for patient positioning during treatment. Figure 3 shows a comparison of CT and sCT images for a patient from **Paper II**.

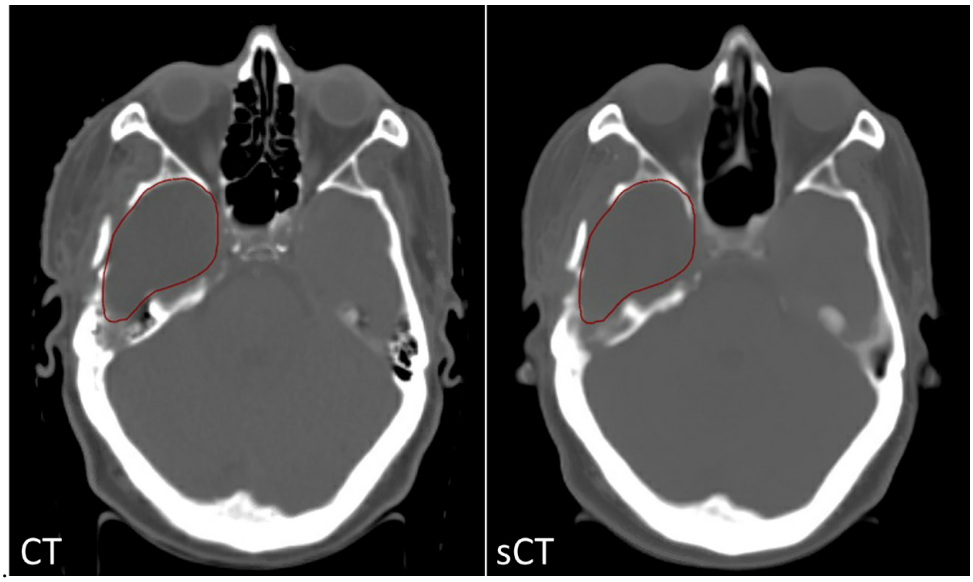

Figure 3. Comparison of CT and sCT images for a patient case from **Paper II**, showing excellent visual agreement in soft tissue as well as bone structures. The tumour is outlined in red.

5.2.1 Available sCT generation methods

Bulk density methods

Methods for sCT generation from MRI data were first presented in the 1990's. This first and most simple method is called bulk density assignment. In its most trivial form, the entire patient volume is assigned water equivalent ED (HU=0) (Schad et al., 1994). Bulk density methods may also include tissue classifications, such as soft tissue, bone, and air. Initially, the delineations and segmentations were manually performed (Jonsson et al., 2010), making it both time-consuming and operator dependent. With regards to the sparse tissue classification, dose accuracy and patient positioning was initially not optimal for clinical use, as it neglects the real tissue heterogeneity (Johnstone et al., 2018). However, more recent commercially available software, based on bulk density, has demonstrated clinically acceptable performance (Autret et al., 2023).

Atlas-based methods

The next generation of sCT methods were atlas-based, introduced in the 2010's. This conversion typically uses a single MRI sequence, often part of the standard protocol, to produce the sCT. Employing standard MRI sequences enhances the implementation

of the method, while keeping the total scan time to a minimum (Demol et al., 2016). Atlas-based methods can be either single-atlas or multi-atlas, both using a database of registered MRI and CT images. An average patient anatomy represents the single atlas, which uses deformable image registration of the input MRI to find the best fit of CT to generate an estimated sCT for the individual patient. The multi-atlas technique includes, as the name implies, several atlases from which the best match can be found based on registration metrics. Increasing the number of atlases has been shown to improve performance (Uh et al., 2014). However the generalisability of the method is limited to the material included in the databases, which may constitute a problem for patients with anatomical anomalies (Uh et al., 2014).

Voxel-based methods

Statistical methods may be used to develop voxel-based techniques for sCT generation (Edmund et al., 2014). Typically, these methods require several standard and/or some specialised MRI sequences (Zheng et al., 2015). Voxel-based methods primarily use voxel intensities in MRI images to assign the HU. Compared to bulk density and atlas-based methods, the voxel-based approach is better equipped at handling large variations between patient anatomies (Jonsson et al., 2013). However, the need for several sequences is a limitation, as it prolongs the total acquisition time.

Deep learning-based methods

The most recent category for sCT generation emerged around 2017 and is based on DL (Han, 2017, Spadea et al., 2021). There has been a rapid evolvement of the technique, from the first publication to international sCT generation competitions (Huijben et al., 2024). DL-based models are a subset of machine learning, a subgroup to artificial intelligence (AI), utilising neural networks and large patient datasets. The DL-based models may be viewed as an extension of the voxel-based method, being trained to model the relationship between HU and MRI intensities. Training of the network is performed on large sets of paired or unpaired CT and MR images to estimate optimal neural net parameters, generating its corresponding sCT.

A recent review summarises the latest advancements in techniques and trends for sCT generation, with its main focus on AI-based models (Bahloul et al., 2024). With current methods and technology, it is possible to generate high quality sCT images from MRI data, regardless of the type of architecture (Huijben et al., 2024). Despite the fast, realistic, and accurate generation of sCT, DL-based models still have some limitations. The first is the data quality sensitivity, which limits quality of the possible output. It is crucial that the training data consists of high quality, correctly registered CT and MR images. This can be handled to some extent by extensive data augmentation during the

training process. Another limitation is its generalisability. The particular training data contains all the features that the model can output, and if the clinical test data that the model is applied to differs significantly from the training data, this may cause inaccurate sCT images. Thus, this highlights the importance of large training datasets, with a variety of anatomical features to improve robustness and avoid bias.

Commercial solutions

In recent years, several commercial sCT generation software for radiotherapy purposes have emerged on the market. Some are specific to the MRI vendor, while others can transform MR images from multiple vendors to sCT images. The currently available commercial software all offer solutions based on AI. An overview is provided in Table 1. In this thesis, MRI Planner (Spectronic Medical AB, Helsingborg, Sweden) was used for sCT generation (Cronholm et al., 2020).

Clinical implementation of MRI-only RT using DL-based methods for sCT requires knowledge regarding the model and its limitations. To use a commercial product for sCT generation, the vendor must provide enough details about the underlying training data set and/or provide suggested patient inclusion and exclusion criteria. For instance, the model input must be restricted to the relevant MRI sequence for sCT generation. For brain applications, most commercial software use Dixon images as MRI input.

Table 1. Currently CE/FDA approved commercial software for sCT generation (February 2025).

Product name	MRI Planner	MRCAT	Syngo.via RT Image Suite	MR-box by ART-plan
Company	Spectronic Medical AB, Helsingborg, Sweden	Philips Healthcare, Cleveland, OH, USA	Siemens Healthcare, Erlangen, Germany	Therapanacea, Paris, France
sCT generation method	AI-based	AI-based	AI-based	AI-based
Availability	Non vendor specific	Philips only	Siemens only	Non vendor specific
MRI-sequence	Dixon (brain), T2w (pelvic)	Dixon	Dixon	T1 + Gd (brain), T2 (pelvic)
Anatomical sites	Brain, head-neck, pelvic	Brain, pelvic	Brain, pelvic	Brain, pelvic
CE approval	Yes	Yes	Yes	Yes
FDA approval	Yes	Yes	Yes	Yes

5.2.2 MRI acquisition sequence for sCT generation

The first version of MRI Planner for brain was developed in collaboration with two Swedish hospitals, including our department at SUS, Lund and Sahlgrenska University Hospital in Gothenburg. The project was part of a research agreement within a national consortium called Gentle Radiotherapy (VINNOVA (Sweden's innovation agency), reference number 2016-03847). Part of the data used for training of the DL model for brain and head-neck anatomies in MRI Planner, was obtained from a pre-study of **Paper I** and **II.** There was no overlap between the training data and the study participants.

MRI using a Dixon acquisition sequence for sCT was agreed upon within the collaboration. A three-point Dixon acquisition sequence was therefore optimised at our site for the purpose of sCT generation. In general, a Dixon sequence uses two or, as in this case, three echoes, designed such that the water and fat magnetisation vectors are at -180, 0 and 180 degrees opposed to each other. The carefully chosen echo times enable calculation and automatic generation of separate in-phase, out-of-phase, water-only and fat-only images for each image slice (Low et al., 2011). The human head contains complex air-bone-tissue interfaces, which makes the conversion from MR signal to HU more complex than in regions such as the pelvis, containing mainly soft tissue. The combination of the four Dixon output images provides more information compared to a single input (Florkow et al., 2020), which may explain why it has become the preferred single-sequence choice for sCT generation of the brain. A patient example of Dixon, sCT and CT images is provided in Figure 4.

In the process of optimising the Dixon sequence for sCT generation, there are several important parameters to consider. The total scan time is important to keep to a minimum, primarily for patient convenience due to uncomfortable immobilisation equipment. A two-point Dixon is faster in total acquisition time but is more prone to artefacts due to undesired fat-water swaps (Kirchgesner et al., 2020). A three-point Dixon is more robust but at the expense of a slightly longer acquisition time. The final sequence developed during the pre-study of this work was a three-point Dixon, with a total acquisition time of 4.5 minutes. The additional scan time of 4.5 minutes (total scan time of 25 minutes) was tolerable for all patients in **Paper I** and **II**. No cases of fat-water swaps were observed.

Another important aspect in the sequence optimisation is to minimise geometric distortions. To mitigate these effects, we enabled the vendor-provided 3D geometry correction, reducing the geometric distortions due to non-linearity in the encoding gradients. Patient specific geometric distortions can be mitigated using a high bandwidth (Weygand et al., 2016), which was set to 744 Hz/pixel.

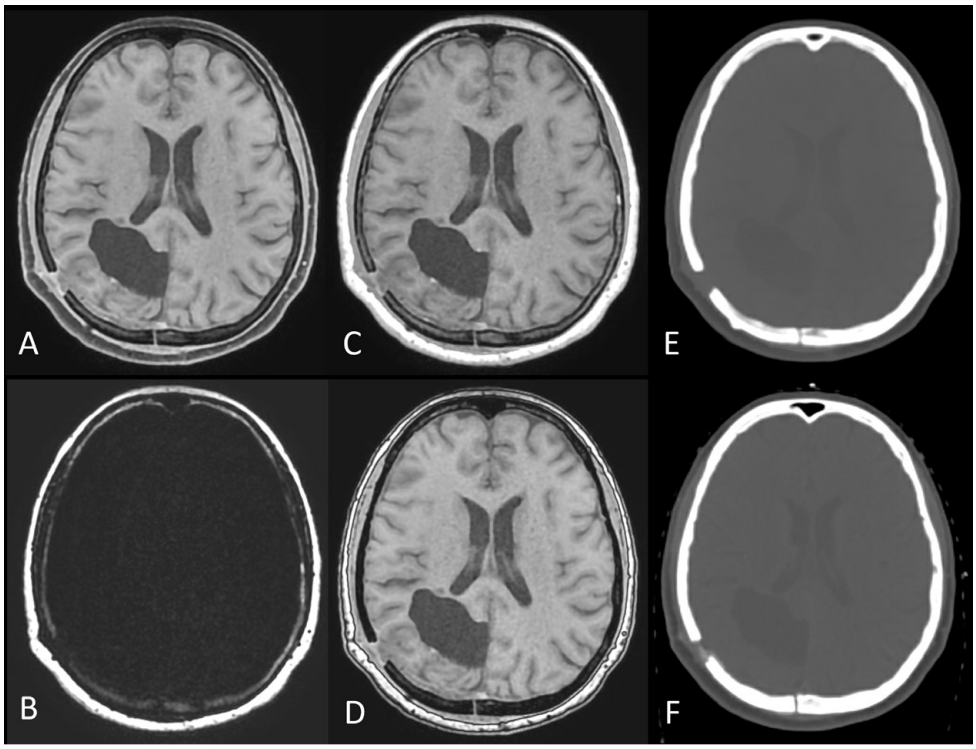

Figure 4. All four Dixon output images are used for sCT generation in the software MRI Planner; (A) water-only, (B) fat-only, (C) in-phase and (D) out-of-phase. The resulting sCT image (E) is automatically returned to the treatment planning system. (F) Corresponding CT image is included for comparison.

The geometric distortions in the Dixon images were evaluated in **Paper I** through phantom measurements, using the GRADE phantom (Spectronic Medical AB, Helsingborg, Sweden), and by generating individual B0-maps for each patient. The system dependent geometric distortions from the phantom measurements were evaluated within 15 cm of the MRI isocentre, a geometry relevant for the head anatomy. They were found to be on average 0.3 mm. The maximum geometric distortion in the patient specific B0-maps was 0.9 mm or less within the 99th percentile for all patients and regions (air, bone and soft tissue). This corresponds to less than one pixel width. Hence, the geometric integrity of the Dixon images used for sCT generations fulfilled the requirements for radiotherapy applications (Weygand et al., 2016).

5.3 MRI-only RT workflow

To use the sCT images as a substitute for conventional CT images in an MRI-only RT workflow, some adjustments are required compared to the dual-modality workflow. For instance, the delineations of targets and OAR must be performed using MR images in complete absence of the CT. The intention in **Paper I** and **II** was to introduce as few changes as possible, to preserve the properties and routines of the conventional clinical workflow. With that said, several factors must be considered in the transition from a dual-modality workflow to an MRI-only RT workflow, including HU to ED conversions, identifying the user origin of the image, missing image information about the fixation mask, and localisation of the treatment couch.

5.3.1 Treatment planning

Modern treatment planning is performed in advanced TPS. Dose constraints are used for optimisation and dose calculation algorithms model the complex interactions of radiation with tissues in the VMAT planning. The aim is to ensure that the radiation dose is precisely delivered to the tumour while sparing healthy tissue. Commercially available TPS expect CT images as the input for dose calculations. MRI-guided delineations of target (tumour volume) and OAR form the basis of objectives in the dose optimisation, enabling individually optimal treatment plans for each patient. In **Paper I** and **II**, all steps of the treatment planning were performed in Eclipse TPS (Varian Medical Systems, Palo Alto, CA, USA). Dose calculation was performed using the anisotropic analytical algorithm. The sCT images, generated through MRI Planner, were automatically exported to the TPS via a cloud-based solution. All treatment plans were optimised by experienced dosimetrists, generating clinical-standard plans delivered using VMAT technique.

5.3.2 Target delineation

In radiotherapy, accurate target delineation is crucial for effective treatment planning and delivery. Regardless of a conventional dual-modality workflow or an MRI-only RT workflow, guidelines for glioblastoma target delineations recommend using MR images, more specifically contrast enhanced 3D T1-weighted and T2/FLAIR sequences (Niyazi et al., 2023). Also, for other primary and secondary brain tumours, guidelines are based on using MRI for target delineation (Vellayappan et al., 2020, Soliman et al., 2018, Martz et al., 2023). In the interventional **Paper II**, tumour targets were successfully delineated using only MR images, in the absence of CT data. This

approach, in principle, differed very little from the standard clinical delineations performed with MRI as guidance in **Paper I**. All delineated targets were approved in peer-reviewed chart rounds.

Although the absence of CT data, with target delineations entirely based on MR images, may introduce discrepancies in other anatomical regions (Gunnlaugsson et al., 2019), it is less of a concern for brain radiotherapy. Excellent agreement between target delineations from the different workflows was recently demonstrated for glioblastoma patients (Rossi et al., 2024). As the MRI-only RT workflow follows the same guidelines for target delineation, it implies that there are no introduced uncertainties in this step of the process.

5.3.3 Organs at risk delineations

Recommendations for OAR delineations are less standardised than guidelines for tumour delineations (Vogin et al., 2021). As CT and MRI data have been the standard image basis during the last decades, both have commonly been used for OAR delineations (Eekers et al., 2018). In contrast to the MRI-based delineation recommendations of tumours, some OAR are better visualised on CT. Organs such as the lacrimal gland, the lens of the eyes and the brain are all easily delineated manually or semi-automatically on the CT. Since sCT lacks sufficient detail for diagnostic purposes, it should not replace the CT for delineating OAR. Consequently, MR images serves as the sole delineation material in the MRI-only RT workflow, which may lead to a slight increase in processing time. In **Paper II**, this was not reported as a problem by the radiation oncologists. However, automatic segmentation of the brain, based on HU threshold in the sCT, does require additional validation against the MR images and sometimes manual adjustments. Situations where this becomes increasingly important are discussed in chapter 5.6.

More recently, automatic segmentation-tools for OAR have become a standard implementation in many radiotherapy clinics, reforming the way of work and allowing for great time savings. The commercially available models today are all based on CT images, which of course pose limitations to the MRI-only RT workflows. However, current research suggests that MRI-based models are demonstrating excellent results and should be available in the near future (Alzahrani et al., 2023).

5.3.4 Electron density

To enable dose calculations, conversion from HU in each voxel of the CT or sCT to its corresponding ED value is made through energy dependent conversion curves. In **Paper I** and **II**, the same conversion curve as for conventional CT, provided in the TPS, was employed. Most sCT vendors provide a specific calibration curve, but it is optional to use (Autret et al., 2023). Although identified as one of the confounding factors for dosimetric comparisons between CT and sCT (Maspero et al., 2017), the difference in calibration curves for modern software seems to be clinically insignificant (Emin et al., 2024). Nevertheless, using the same conversion for CT and sCT in a study setting, provides a fairer comparison of the evaluated dose distributions.

5.3.5 User origin

The user origin in the image is set to spatially correlate the isocentre of the planned dose to the patient's anatomy. This relation is required for geometrically accurate delivery of the treatment, if positioning is based on tattoos or skin markers. In the CT-based workflow, small metal spheres can be placed on the patient's immobilisation mask according to the laser intersection. The intersection of these markers inside the patient then indicates the user origin when the images are imported to the TPS. In the MRI-only RT workflow, liquid markers (Beekly Medical, Bristol, CT, United States) may be used for the same purpose. This was the approach in **Paper I** and **II**. However, in the final clinical implementation these were replaced by only using the isocentre coordinates from the MR images (the DICOM zero position), since this yields a simpler method.

5.3.6 Treatment couch

The position of the treatment couch in relation to the patient must be known to account for radiation attenuation, ensuring accurate dose calculations. For this purpose, a virtual structure of the couch is manually inserted in the TPS. In a CT, its position is easily identified with a large field of view and clear image signal of the couch. However, the corresponding information is not available in standard MR images. In a Dixon sequence (**Paper I** and **II**), the treatment couch does not yield any useful signal due to the short relaxation time of the material. Another restriction lies in selecting a more constrained FOV compared to CT, only including the relevant patient anatomy. The solution suggested in **Paper I** was to implement a large FOV zero echo time sequence, only adding 21 seconds to the imaging protocol. This allowed for accurate identification of the treatment couch, which was easily incorporated in the workflow

(**Paper II**). Another option is to use a standard sequence with a large FOV and place liquid markers on either side of the patient onto the treatment couch surface (Emin et al., 2024). This enables a similar identification procedure, but with the additional manual step of placing the liquid markers.

5.3.7 Fixation mask

Patients treated for brain tumours are generally fixated using an immobilisation mask. The mask ensures reproducible positioning of the patient between preparational imaging and each treatment session. During irradiation, the mask attenuates the radiation in the order of 0.5% for photon energies between 6-15 MV (Orfit Industries NV, Wijnegem, Belgium).

In a CT image, the thermoplastic mask is clearly visible. However, it does not yield any substantial signal in the MR images. Consequently, there is no visualisation of the mask in the sCT images. In **Paper I** and **II**, this did not constitute a problem when comparing sCT to CT images since the dose calculation only included voxels within the patient's body contour. Others have used the same approach to avoid the introduction of errors in the absence of mask signal in the MRI and sCT images (Masitho et al., 2022). Clinics should therefore consider their strategy for defining spatial dose calculation limits prior to MRI-only RT implementation.

5.4 Quality assurance during implementation

Clinical implementations of new technology or methods should always be preceded by commissioning with rigorous validations to ensure a safe transition into clinical routine. In this thesis work, quality assurance (QA) was performed in several steps, as described in the following chapter. The first step was to validate the sCT (**Paper I**), ensuring at least equal quality as to performing treatment planning based on conventional CT images. This evaluation was performed in a retrospective, non-interventional manner. The second step was to do a structured implementation (**Paper II**), using prospective acceptance criteria and keeping the CT as a ground truth evaluation in the background. Here, sCT was used for treatment planning, treatment positioning and delivery in an interventional approach. Finally, QA program during clinical routine will be discussed. But first, a short note about MRI-related QA in an MRI-only RT workflow.

5.4.1 MRI-related QA

Regular quality controls of the MRI scanner in an MRI-only RT workflow does not differ significantly from standard QA of an MRI scanner for radiotherapy in the dual-modality workflow. Image quality should always comply with recommendations for MRI in radiotherapy (Speight et al., 2021). Specific QA should be performed on the acquisition sequence for sCT generation with emphasis on geometric distortions, as these may vary over time.

Regarding the export of the MR images for sCT generation, a verification to ensure that the correct images are exported to the generation software can be simple but effective. In **Paper I** and **II**, this was solved by a user setting selecting the correct DICOM tag containing the MRI series description. In the case of vendor-specific sCT generation methods, this should not be an issue since the sCT is automatically generated on the console.

5.4.2 Validation of sCT

As part of the commissioning and implementation of MRI-only RT, the sCT images should be validated based on geometric and dosimetric criteria. In **Paper I**, the CT images were considered as ground truth and sCT images were resampled and registered to the CT prior to evaluation**.** The quality and feasibility of using the sCT for treatment planning were evaluated. The patients received their treatment according to clinical routine in the conventional dual-modality workflow.

Geometric evaluation of sCT

When evaluating sCT images, the first step is to assure geometric accuracy and correct HU assignment. A number of studies have previously investigated sCT images generated from in-house developed software, with a range of different evaluation metrics (Johnstone et al., 2018). The most common metric for investigating the HU agreement between the CT and sCT is the mean absolute error (MAE) (Edmund and Nyholm, 2017, Vandewinckele et al., 2020).

The MAE describes the voxel-wise difference in HU in absolute values according to the following equation:

$$MAE = \frac{1}{N}\sum_{i=1}^{N}|sCT_i - CT_i| \qquad \text{(Equation 1)}$$

where N is the number of voxels, CT is the conventional CT (reference) and sCT is the synthetic CT.

The MAE indicates the overall error magnitude of HU discrepancies but may overestimate the clinical relevance by only considering magnitude values. An alternative metric describing the voxel-wise agreement is the mean error (ME) which estimates the signed differences in HU. By not only relying on absolute values, the ME provides information about under- and over-estimation of the HU assigned to the tissue. The ME is calculated according to:

$$ME = \frac{1}{N}\sum_{i=1}^{N}(sCT_i - CT_i) \qquad \text{(Equation 2)}$$

Using only the ME as a metric to evaluate HU could underestimate the discrepancy, as positive and negative errors may balance out in the results. Thus, both MAE and ME were used to evaluate the sCT images in **Paper I**.

One of the most commonly used geometric evaluations of the sCT is the dice similarity coefficient (DSC). For sCT evaluations, the DSC can be used to evaluate the overlap in bone structures compared to the reference CT. DSC is calculated according to:

$$DSC_{bone} = \frac{2(V_{CT} \cap V_{sCT})}{V_{CT} + V_{sCT}} \qquad \text{(Equation 3)}$$

where V is the volume of the segmented bone structures in the CT and sCT, respectively. A DSC value of 1 corresponds to complete overlap between the two datasets, while a value of 0 corresponds to no overlap at all. Here, it is important to report the threshold value for the bone segmentation as this may influences the result.

In **Paper I**, evaluation of HU demonstrated excellent agreement between CT and sCT. The average patient specific MAE in the brain tissue was found to be between 8 and 11 HU for all patients and the average ME was between -3 and 5 HU for all patients. This indicates accurate HU assignment of the soft tissue without bias. Bone structures, on the other hand, were slightly underestimated in the sCT images with a ME of -42 HU for the whole cohort. Bone segmentation was performed with a lower threshold of 250 HU.

Previously reported MAE including all voxels within the body contour were between 34-150 HU for in-house developed voxel-based (Price et al., 2016) and DL-based methods (Han, 2017, Dinkla et al., 2018, Emami et al., 2018, Liu et al., 2019), compared to 62 HU in **Paper I**. Later, as other commercial products became available, studies have demonstrated similar performances, with reported voxel-wise MAE of 136 HU for the Siemens product (Masitho et al., 2022) and 38-52 HU for the Philips product (Yip et al., 2025). An overall (not voxel-wise) MAE of 22-40 HU for software from Spectronic, Siemens and Therapanacea were reported in another study (Autret et

al., 2023). Comparing MRI Planner to the sCT generation software from Siemens and Therapanacea, Autret et al. reported overall best performance using MRI Planner.

Comparing bone structures in CT to sCT, the overlap in the patient cohort from **Paper I** was similar or better (DSC=0.90-0.94) compared to previously reported voxel-based methods (DSC=0.8-0.9) (Jonsson et al., 2015). Correct representation of bone structures is relevant to dose accuracy, but also for patient setup, where the image registration generally is based on bony anatomy.

In general, the performance of sCT generation methods for patients with anatomical anomalies, such as bone resection due to surgery prior to radiotherapy, has been given less attention. In **Paper I** and **II** it was demonstrated that the use of MRI Planner is feasible also for patients with anatomical anomalies. While no statistically significant differences from normal anatomies were observed in the evaluated metrics, minor local deviations without clinical relevance may occur in individual cases. Earlier work on atlas-based methods reported unacceptable sCT representations in the area where patient anatomy differed from the atlas material (Demol et al., 2016). Since surgery is often the initial treatment for brain cancer patients, this group represents a large fraction of the total brain tumour patients and should not be discriminated from MRI-only RT options. In the cohorts examined in this thesis, the majority of patients underwent surgery prior to radiotherapy. This relates back to the need for comprehensive, including, and relevant training data in the development of sCT generation models.

To summarise the obtained results, we can conclude that sCT of the brain were generated with accurate HU and good geometric accuracy using MRI Planner for the patients included in this work.

Dosimetric evaluation

In addition to validating the geometric properties of the sCT images, it is important to commission and validate the sCT from a dosimetric point of view. The two evaluations are not unrelated, as the HU are converted to EDs, which subsequently determines the amount of radiation attenuation in the dose calculation. Nevertheless, it is crucial to also validate the dosimetric accuracy from treatment plans calculated using sCT images compared to conventional CT-based calculations.

Some of the most commonly used metrics for dosimetric evaluations are the relative dose difference, dose-volume histogram (DVH) comparisons, and the gamma pass rate (Edmund and Nyholm, 2017, Vandewinckele et al., 2020). The relative dose difference is usually reported as the percentage difference in a point or a volume, such as the target

or an OAR. The gamma evaluation considers both the magnitude and spatial shift of the dose difference between each point in the two distributions.

Dosimetrically, most generation methods seem to provide accurate sCT images. Bulk density methods were originally inadequate, especially the most simple versions which produced dose differences between 3-5% depending on the intracranial location of the target (Wang et al., 2008). However, by adding bone segmentations to the images, clinically acceptable dose deviations were achieved (Kristensen et al., 2008). Dosimetric accuracy improved further with the introduction of atlas-based methods compared to bulk density methods, with dose deviations between sCT and CT based calculations below 1% (Andreasen et al., 2015). Voxel-based methods also demonstrate good dosimetric performance with mean dose differences below 1% (Paradis et al., 2015) and 100% gamma pass rates (1%,1mm) within the tumour target volume (Jonsson et al., 2015). In-house developed DL-based methods demonstrate consistently good results with many studies reporting mean dose differences on sub-percentage levels (Dinkla et al., 2018, Kazemifar et al., 2020, Boulanger et al., 2021).

The excellent agreement in dose calculated on sCT compared to conventional CT was further supported by the results in **Paper I**. The mean dose difference in the tumour target volume was 0.1% with corresponding gamma pass rates of 100% (1%, 1mm). Dose deviations in brainstem and chiasma were evaluated using the relevant DVH parameter $D_{2\%}$ (corresponding to the near maximum dose) and demonstrated differences between -0.7 to +0.3%. Thus, all dose differences were clinically insignificant.

Treatment plans with beams passing through internal air cavities, such as the sinuses, have previously demonstrated unacceptable dosimetric deviations (Johnstone et al., 2018, Tyagi, 2019). This inspired a separate evaluation of patients with complex targets, i.e. located in the close proximity of air cavities, in the cohort of **Paper I**. Results demonstrated, despite the complexity of the target location and anatomy, excellent dosimetric performance of the sCT and no statistically significant deviations in calculated absorbed dose compared to CT. This highlights the robustness and clinical applicability of the MRI Planner, which is compatible with anatomical anomalies as well as complex regions in brain tumour patients.

After the publication of **Paper I** and **II**, there has been additional reports using commercially available sCT generation software. The dosimetric performance across all represented vendors fulfils the requirements for clinical application, with mean dose differences remaining below 1% (Autret et al., 2023, Emin et al., 2024, Masitho et al., 2022, Ranta et al., 2023, Yip et al., 2025).

Patient positioning

The last step of the workflow concerns the treatment situation where it is crucial that the patient is accurately positioned in a reproducible way at every treatment fraction. When the CT is substituted for sCT, the sCT becomes the reference to which the daily X-ray images on the linear accelerator are matched. Hence, the final step of the sCT validation was to ensure equal performance when registering a 2D or 3D X-ray image of the patient in treatment position using the sCT compared to the conventional CT.

In **Paper I**, cone-beam CT (CBCT) images for positioning brain tumour patients were acquired the first three fractions and then once a week, or more often when needed. Patient set-up verification was evaluated retrospectively in **Paper I,** one fraction for each patient, using rigid image registrations in six degrees of freedom. The CBCT images were registered to the CT and sCT images respectively, and the resulting registrations were compared. Equally accurate performances using sCT and CT as reference images were observed for all patients, with maximum absolute deviations being 0.5 mm and 0.3 degrees.

Anatomical anomalies are often used as landmarks in evaluating the resulting registration, putting high demands on the accuracy of these areas. In-depth investigation of patients with anatomical anomalies revealed no significant difference in registration accuracy compared to non-resected patients.

There are other studies reporting similar results of reliable registrations with errors less than 1 mm using sCT from both voxel-based sCT generation methods and DL-based methods (Yang et al., 2016, Price et al., 2016, Gupta et al., 2019, Liu et al., 2021, Ranta et al., 2023). A prerequisite for accurate image registration and reliable sCT images for patient positioning is MR imaging in treatment position, using identical immobilisation equipment (Masitho et al., 2022, Yip et al., 2025).

5.4.3 QA during MRI-only RT workflow implementation

After validating the sCT images, assuring quality equal to conventional CT images for the purpose of MRI-only RT planning, the implementation of the workflow was initiated. Implementation was performed in a controlled study setting, where **Paper II** was a prospective, interventional study. Twenty high-grade glioma patients received treatment following the suggested MRI-only RT workflow. One patient was excluded (further discussed in chapter 5.6).

The sCT was the foundation in all steps and was used for treatment planning, dose calculation, and patient positioning prior to treatment delivery. While corresponding CT images were still acquired during the prospective study, they were strictly used for

QA and were not available during target delineation or treatment planning. Since the publication of **Paper I**, MRI Planner for brain anatomy had received CE-approval, a vital step to enable widespread clinical implementations.

To assess each step of the workflow in **Paper II**, a prospective QA program was developed. As there were no general guidelines available, the acceptance criteria were determined based on the results from **Paper I**. Each QA step is summarised in Table 2. Despite the interventional study design, a safe implementation was ensured by integrating digital check points in the workflow. This ensured that all steps of the QA were approved in consecutive order prior to the treatment delivery. A similar approach had previously been used in the implementation of a prostate MRI-only RT workflow (Persson et al., 2020).

Table 2. Quality assurance during the implementation phase. The method of each QA step is summarised along with the corresponding results from the clinical study in **Paper II**.

QA step	Method	Result
MRI Dixon acquisition parameters for sCT generation Automatic control of esstenial acquisition parameters compared to a predefined template	Automatic parameter script	Identical to template for all 21 patients
Visual inspection Alignment verification between MR images and artefact inspection of sCT and MR images	Manual inspection, special attention to the target region 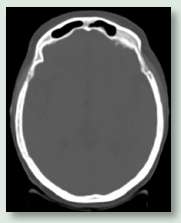	Fullfilled for 20 patients, 1 failure (the patient was excluded from the MRI-only RT workflow due to abnormal bone in the sCT, related to an area of remaining gel from previous surgery, see chapter 5.6 for details)
Accuracy of sCT HU General comparison of HU between sCT and CT, manually performed in the TPS	Qualitative comparison of line profiles 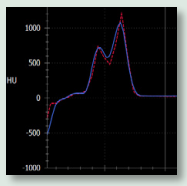	Acceptable for 20 patients

QA step	Method	Result
Bone evaluation Inspection of bone structures, additional evaluation in areas of bone resection. Bone edges should agree within 1.5 mm (diameters within 3 mm) compared to CT	Manual inspection and comparison of bone edge measurements 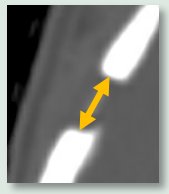	Fulfilled for 20 patients
Evaluation of planned dose distribution Prospective evaluation in TPS comparing dose optimised and calculated on sCT to CT-recalculated dose (rotations not included) Dose differences in target and relevant OARs should be within ±1% or OAR absolute dose should be at least 10% below clinical DVH criteria Additional retrospective evaluation of the dose distribution, including rotation correction of the dose distributions	Quantitative comparison of DVH parameters for target and OAR Retrospective gamma analysis and rotation-corrected comparison of dose distributions 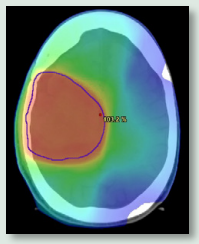	All target doses were within 1% of the CT-calculated dose. All OAR doses were at least below 10% of the clinical dose restriction or within 1% of the CT-calculated dose. After rotational correction, all OAR dose differences were within 1%.
Patient setup Retrospective evaluation of patient setup through image registration results comparing sCT and CT as the reference. All translational differences should be within ±1 mm and all rotational differences within ±1 degree.	Quantitative evaluation of CBCT image registation 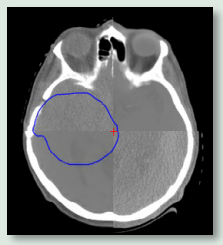	Fulfilled for all patients

5.5 Clinical experience of MRI-only RT for glioblastoma

Over the last years, there has been several publications from prostate MRI-only RT implementations (Greer et al., 2019, Tyagi et al., 2020, Persson et al., 2020, Keyriläinen et al., 2021). Our clinical implementation study (**Paper II**) was the first report of MRI-only glioma RT with a commercially available software for sCT generation. Since then, there has been two other publications on MRI-only RT implementations of brain radiotherapy (Emin et al., 2024, Ranta et al., 2023), and one published protocol for an ongoing study (Grigo et al., 2024). The field is still growing, and it is important to continuously publish results and experiences to build a solid foundation for general guidelines (Villegas et al., 2024).

At the radiotherapy department at SUS, Lund, glioblastoma patients have been treated using MRI-only RT in clinical routine since November 2023. At the time of writing this thesis, approximately 80 glioblastoma patients have successfully completed MRI-only RT.

A recommissioning of the workflow building up to clinical routine was performed due to upgrades of MRI hardware and software, as well as a new release of MRI planner since the implementation study (**Paper II**). During this phase, a back-up CT was acquired for the first 16 patients, enabling a comparison to CT-based dose calculations and image qualities. One patient was transitioned to the dual-modality workflow due to an initial decision based on rotational discrepancies between the CT and MRI scans. This discrepancy initially appeared as a deviation in the dose comparison. However, additional retrospective evaluation, accounting for the rotations, demonstrated excellent dosimetric agreement. Thus, after confidently confirming the quality of the sCT and workflow for all 16 patients, the CT could be omitted for all consecutive patients. If needed, individual patients can still be scheduled for a CT and the treatment can be transferred to the dual-modality workflow. Patients with MRI contraindications are always excluded from the MRI-only RT workflow.

The routine for daily setup of the patient during treatment had also been upgraded, compared to the workflow investigated in **Paper I** and **II.** In addition to initial and weekly CBCT images, patient positioning is in the new workflow based on non-coplanar kV X-ray images pre- and intra-fractionally, in combination with surface guidance, using the ExacTrac Dynamic (ETD) (Brainlab AG, Munich, Germany). Using this imaging regime, patient positioning in 6 degrees of freedom is utilised, including both translations and rotations.

Based on **Paper I** and **II**, CBCT-based setup using the sCT as a reference instead of the CT differed less than 1 mm and 1 degree for all patients. A similar evaluation was

performed for the patients during recommissioning, confirming that all absolute translational differences, comparing sCT and CT references, were less than 1 mm.

To evaluate the performance of sCT in combination with ETD, an additional registration study was conducted, this time comparing setup results from CBCT and ETD. Due to restrictions in the ETD software, it was not possible to import two reference images to the system to compare sCT to CT-based registrations. Setup was therefore evaluated based on CBCT-sCT registrations compared to ETD-sCT. Given that these registrations make use of two different imaging modalities, 2D versus 3D, it is expected that the results differ more than when comparing the same modality with different reference images. However, the evaluation of the 16 patients demonstrated equally accurate results, with all absolute differences in translations and rotations within 1 mm (Figure 5) and 1 degree (Figure 6), respectively.

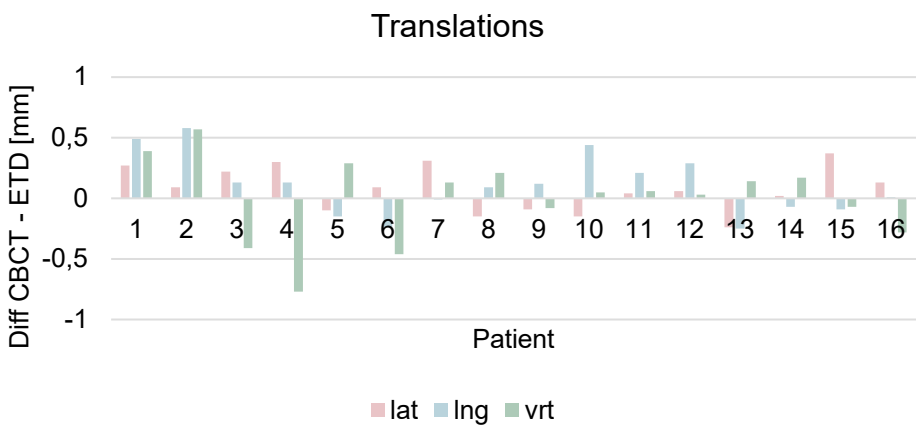

Figure 5. Translational differences when comparing image registrations between sCT and 3D CBCT or 2D ETD imaging for the 16 glioblastoma patients during recommissioning prior to clinical routine.

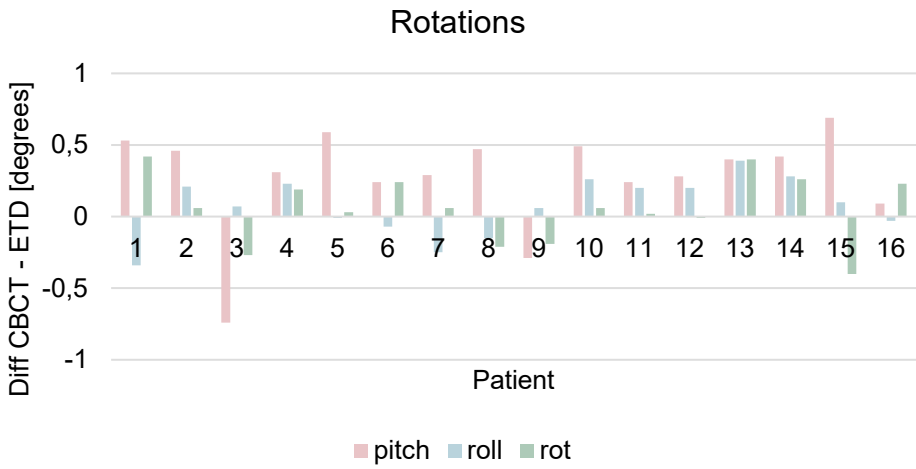

Figure 6. Rotational differences when comparing image registrations between sCT and 3D CBCT or 2D ETD imaging for the 16 glioblastoma patients during recommissioning prior to clinical routine.

In conclusion, MRI-only RT for glioblastoma is feasible in clinical routine. Both 3D (CBCT) and 2D (ETD) imaging is compatible with sCT as the reference for daily setup. Some patients have required additional attention due to minor artefacts in the sCT. These are discussed in more detail in chapter 5.6. However, none of these patients required a transition to the dual-modality workflow. Even with the high success rate demonstrated in the work presented within this thesis, the combined dual-modality or CT-only workflow cannot be completely phased out, as it may still be needed for patients with MRI contraindications or if sCT generation fails.

5.5.1 QA in clinical routine

As with all processes in radiotherapy, a continuous QA program is required to ensure safe treatment delivery to all patients in clinical routine. MRI-only RT is still a relatively new field and so far, has no long-term clinical experience to build solid QA recommendations on. Until such recommendations are in place, each clinic must evaluate their own process and build QA programs to support the use of sCT images for radiotherapy in their own clinical setting. Evaluation metrics described in chapter 5.4.2-3, may also be used as QA tools after software or hardware upgrades, as well as for consistency checks of the sCT generation performance over time. During implementation of MRI-only RT, the CT is the optimal verification reference, since it is the gold standard imaging modality for radiotherapy historically. It is geometrically

accurate and contains established HU. However, after the transition to clinical routine the CT is no longer available and a different approach to QA must be obtained.

Patient specific QA

Every patient anatomy is unique, which is why individual, case specific QA is recommended (Vandewinckele et al., 2020). Despite general exclusion criteria for MRI-only RT, related to MRI contraindications, there may be cases less well handled in the sCT generation model. To detect these cases, patient specific QA should be implemented. The simplest approach is to carefully check the sCT output images, where each generated sCT is visually inspected after import to the TPS. Other alternatives include independent sCT generation models and CBCT to verify the quality of the sCT (Vandewinckele et al., 2020). Independent sCT generations models for comparison should be used with care as the results strongly depends on the metrics evaluated during the QA process (Levardon et al., 2024). Given that the CBCT is available from the first treatment fraction onwards through daily patient setup, this approach is appealing to convey. Successful QA-approaches using CBCT comparison to the sCT have been demonstrated for both prostate (Palmer et al., 2018) and brain (Irmak et al., 2021). This was also the approach employed for the clinical implementation at the radiotherapy department at SUS, Lund.

In our local clinical routine, the CBCT is used as a visual control of the sCT geometric properties, including correctly represented bone structures. Any deviations are reported to the medical physicists team for further assessment. If the inconsistency between the CBCT and sCT is located far from the treatment area and assessed to have no impact on the image registration for patient setup, no further actions are required. The patient may continue its MRI-only RT course. If the inconsistency interferes with the radiation path or is in proximity to the target, dose calculation may be performed on the CBCT. Note that the dose can only be recalculated on the CBCT if it is acquired without any rotations of the treatment couch, as required by the Eclipse TPS. To manage this, the CBCT may be acquired without couch rotations to be used specifically for dose calculation when needed.

The dose calculated on CBCT was found to be a reliable substitute for dose comparison in absence of CT data, based on the evaluation of the 15 patients during recommissioning. Following calibration of the HU to ED conversion curve, using a CIRS phantom (Computerized Imaging Reference Systems, INC., Virginia, USA), the dose difference between CBCT- and CT-based dose calculations was less than 1% for $D_{98\%}$ in the target volumes GTV, CTV and PTV. Also, all relevant dose differences were within 1% for the clinical OAR criteria.

Routine model QA

General QA in the MRI-only RT workflow includes QA of the MRI (as mentioned in chapter 5.4.1) and the sCT generation model. The sCT generation model could undergo regularly scheduled QA, for example monthly or annually. One method to perform this QA is by utilising a set of paired MR and CT images. In this approach, the MRI data can be used to regenerate an sCT, which can be validated for consistency against the original CT as well as previously generated sCT. Any disturbances in the model or defective sCT images in between the routine model QA are likely to be found during the case specific QA, performed for each patient.

New sets of paired CT and MRI data could preferably be acquired as a recommissioning related to major changes to the workflow, such as a new or upgraded MRI scanner or substantial changes to the acquisition protocol (Vandewinckele et al., 2020). This precaution was used during the recommissioning, prior to clinical MRI-only RT routine at the radiotherapy department at SUS, Lund, as already discussed.

5.6 Case studies: Addressing potential artefacts

While the evaluations of sCT and MRI-only RT workflow presented in this thesis, as well as in other studies, have demonstrated successful results, occasional deviations and artefacts must still be considered. This section provides a summary of selected cases that were encountered during the course of this thesis work, and how they were addressed.

5.6.1 MRI software upgrade

After any upgrades on the MRI system, hardware or software, additional sCT generation QA should be performed. Even minor changes can affect the sCT output. This was the case during the work of **Paper II**, where there was a software upgrade on the MRI scanner. Routine QA, evaluating the performance of the MRI, revealed no concerns. The vendor-provided report also did not specify any significant changes that would affect the Dixon acquisition sequence used for sCT generation. However, there was a slight change to how the homogeneity correction during MR image reconstruction operated. The deviation in training data (in the DL model) and new input data (study patients), resulted in artefacts in the sCT images, manifested as streaks of increased HU (Figure 7). The artefacts appeared in the soft tissue, with a magnitude of about 40-50 HU higher than expected. Evaluation showed no dosimetric impact from the higher HU values and in the particular cases observed in this study, the artefact did not overlap with the image slices containing the target volume.

The deviation was reported back to the sCT vendor, who updated the DL model based on the new characteristics of the Dixon images. Note that no changes were made to the MRI acquisition protocol or parameters to cause the artefact. This highlights the demand for continuous QA procedures combined with patient specific QA of the sCT images in a routine MRI-only RT workflow.

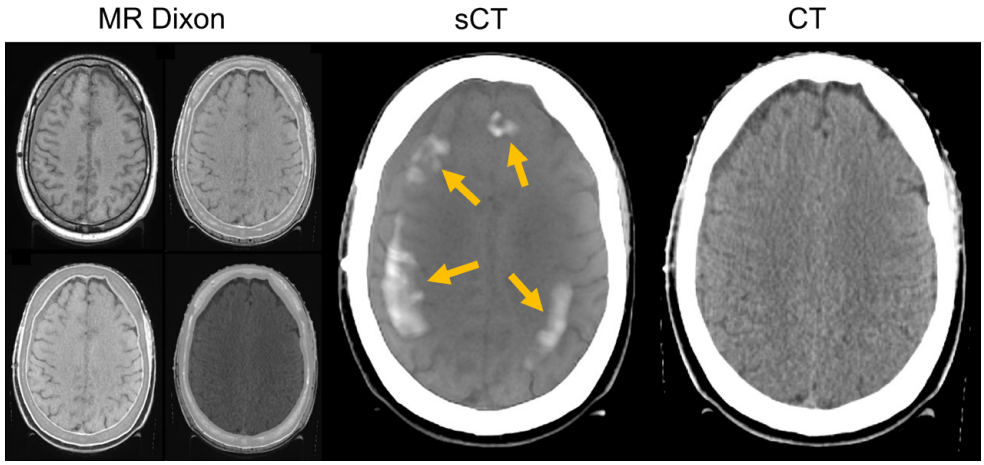

Figure 7. Example case of streak artefacts in sCT (middle). The corresponding MR Dixon images (all four outputs) used for sCT generation are presented on the left and the conventional CT of the same image slice on the right. The artefacts appeared due to minor changes in the image reconstruction after a software upgrade on the MRI scanner but did not have any clinically significant dosimetric impact. The sCT and CT images are both applied with a -20 to 100 HU window setting to highlight the artefact.

5.6.2 Remaining impact from surgery

The majority of brain tumour patients that undergo surgery prior to radiotherapy are generally well handled in the MRI-only RT workflow. However, in **Paper II**, a single patient was excluded due to thicker bone in a region near the target (Figure 8). During the investigation following the exclusion, the surgical report revealed that the patient had bleedings during the surgery prior to radiotherapy, and a haemostatic gel had been injected. This gel is normally absorbed by the body within a few weeks but in this case, it caused severe signal loss in the MR images. As this was new information to the sCT generation model, the signal void was interpreted as bone, resulting in a thicker bone in the sCT compared to the CT. The patient was successfully transferred to the dual-modality workflow with no delay in treatment delivery. Retrospective evaluation of this patient demonstrated no clinically significant deviations in dose distribution nor patient set-up compared to CT. Hence, the recommendation in **Paper II** was that

similar cases in the future should be individually investigated based on the extent and location of the artefact relative to the target.

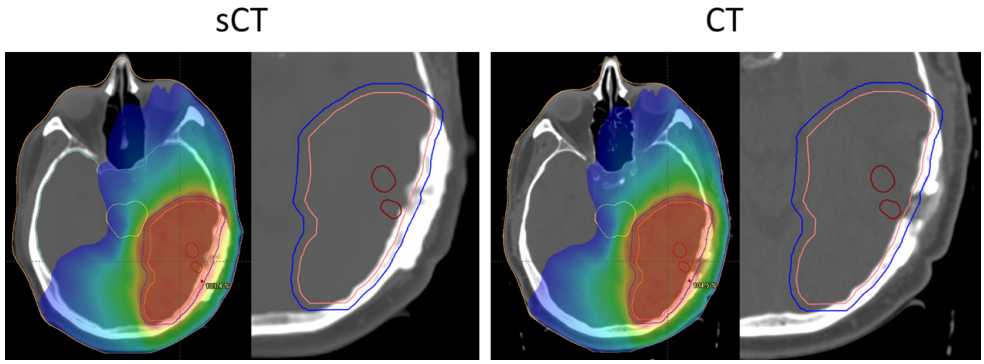

Figure 8. Patient excluded in **Paper II** due to bone artefact caused by remaining hemoestatic gel injected during surgery due to bleeding. Dose distribution and close-up of the target and bone is shown for sCT (left) and CT (right). Despite the thicker bone on sCT, all dose differences were within 1%.

As MRI-only RT was implemented for glioblastoma in clinical routine, one of the first patients appeared to be a similar case, with remaining haemostatic gel from pre-radiotherapy surgery causing increased thickness of the bone in the sCT. Conveniently, the CT was acquired for additional QA for the first patients during recommissioning. This allowed for easy gold standard comparison of the dose distribution calculated on the sCT and conventional CT. The comparison showed no clinically relevant dose deviations, and the patient was approved for MRI-only RT. The image registration for setup during the first treatment session was carefully reviewed, ensuring accurate image registration between the sCT and CBCT images. The artefact's effect on image registration was limited because the incorrect thicker bone constituted only a small part of the entire volume used for the image registration. Thus, the treatment staff were instructed to follow their clinical routines, and the patient successfully completed their treatment course. During clinical routine, with no CT available, the CBCT may be used for dose evaluation after the first treatment fraction.

5.6.3 Metal clips near target

Another impact that can remain from surgery is metal clips used to fixate the bone. These cause signal loss in the MR images, which can be interpreted as bone in the sCT generation. As the surgical resection area is generally adjacent to the target, the metal artefact may cause errors if the target delineation is cropped to the automatically generated brain structure. However, precise methods and careful review of the

delineated target volumes, including target modifications when necessary, can mitigate this problem. A recent study investigated the impact from these types of artefacts in sCT images generated by MRCAT (Philips OY, Vantaa, Finland), suggesting that the effect from such metal clips on glioblastoma targets and the corresponding dose coverage is negligible if the target (CTV) is cropped to the bone instead of the brain structure (Rossi et al., 2024).

5.6.4 Other sCT artefacts

There can be different reasons behind sCT artefacts, most stemming from the fact that the data in the input MRI differs from the training data of the DL model or simply that there is a signal void in the MR images. Artefacts in the MR images are likely to be transferred to the sCT, such as metal artefacts causing signal loss in its surrounding area. One such case was encountered during clinical routine, where a 2 cm signal void in the MRI resulted in a void in the corresponding sCT (Figure 9). The metal-like artefact was not noticed during the MRI examination and as it was not present in the CBCT at treatment start, the cause of it remains unknown. Careful investigation after the first treatment fraction revealed no dosimetric impact due to the artefact, as well as accurate image registration and patient positioning. No further action was required, and the patient continued their treatment in the MRI-only RT workflow.

Non-typical air cavities in the brain may be incorrectly generated as bone, either as an individual volume or as an extension of the skull (Figure 10). Based on the experiences from this work, such artefacts will most likely have little effect during dose calculations and be of clinical insignificance, when treating large brain tumours with photon VMAT. However, automatic cropping of target structures based on bone should be done with care and may require manual adjustment, as demonstrated in Figure 10.

As previously emphasised, it is crucial to investigate each occasional deviation and artefact in sCT images individually because each case is unique. Although none of the deviations or artefacts encountered in this work have been of clinical concern, it is important to be aware of the potential limitations of DL-based models for sCT generation. To conclude, based on the collective experience from **Paper I**, **Paper II**, and the patients treated in clinical routine, MRI-only RT with sCT images from MRI Planner is a robust and safe treatment option for glioblastoma patients.

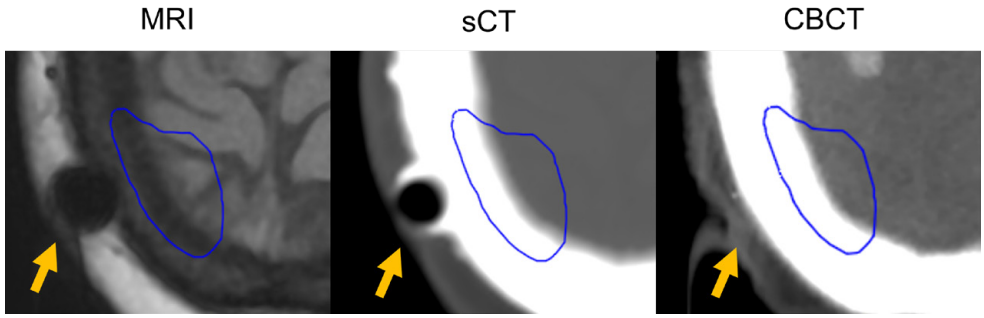

Figure 9. Patient with MRI artefact of unknown origin, causing a void in the sCT which was not present in the CBCT images. Dosimetric investigation showed no clinically significant impact. PTV is outlined in blue.

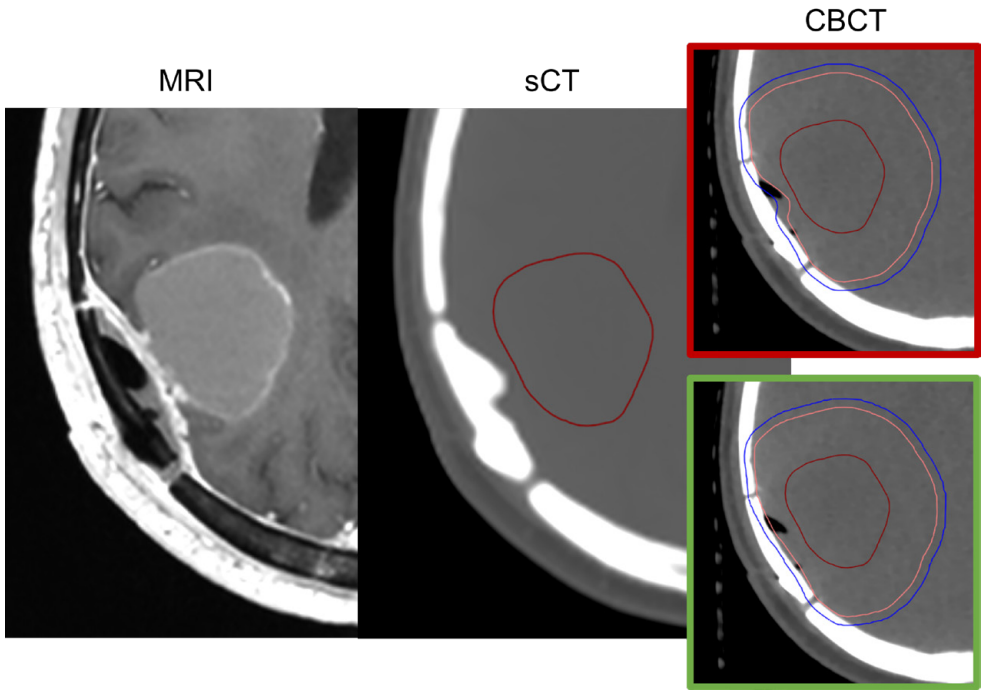

Figure 10. Patient with air cavity inside the skull bone illustrated in a transversal image slice from MRI, sCT and CBCT, respectively. The GTV is delineated in red, CTV in pink and PTV in blue. Two versions of target delineations overlayed on CBCT are framed in red (top image - incorrect) and green (bottom image - correct) to emphasise the importance of manual inspection and potential adjustments of autogenerated structures to crop target based on sCT bone.

6 Exploring diffusion MRI-based imaging biomarkers

This chapter of the thesis primarily relates to **Paper III**, **IV** and **V**. In the search for new imaging biomarkers to predict or assess early radiotherapy treatment response, advanced diffusion parameters could be potential candidates. Tensor-valued diffusion MRI was implemented on our radiotherapy dedicated MRI scanner to explore this capability (**Paper III)**. Diffusion parameters were derived from healthy adults and evaluations of setup, image quality, and parameter repeatability were performed. The implemented tensor-valued diffusion sequence was evaluated in a patient cohort (**Paper IV**), comprised of adults with brain metastases receiving SRT at our department. The potential of the diffusion parameters as imaging biomarkers to predict treatment outcome was exploratory assessed through the prospective, longitudinal study design. Finally, technical challenges encountered in **Paper III** and **IV** served as the motivation for **Paper V**, where denoising methods to improve image quality and parameter reliability were investigated in phantom and in healthy brain.

6.1 Imaging biomarkers

A quantifiable characteristic in a medical image can become an imaging biomarker if it represents a normal or pathological process, or response to an intervention, such as radiotherapy. In contrast to conventional biomarkers, which are often retrieved by blood samples or biopsies, imaging biomarkers provide information non-invasively. Additionally, the information is spatially resolved instead of just systemic or local. Imaging biomarkers derived from quantitative MRI therefore holds the potential to further personalise radiotherapy during treatment planning, delivery, and follow-up. Metrics for radiotherapy response may be derived from physiological response. These can present earlier than anatomical changes, which is one of the promising features of MRI-based imaging biomarkers (Das et al., 2019).

A biomarker is “a defined characteristic that is measured as an indicator of normal biological processes, pathogenic processes or responses to an exposure or intervention, including therapeutic interventions” (Biomarkers Definitions Working, 2001).

Accordingly, an *imaging biomarker* is such a measurement derived from one or more medical images (O'Connor et al., 2017).

An imaging biomarker can be either prognostic or predictive. *Prognostic* biomarkers provide information about the patient’s outcome, while *predictive* biomarkers relate to the response of a specific treatment (Oldenhuis et al., 2008).

Although extensive research has been carried out over the last decades, the status of imaging biomarkers in radiotherapy is still “promising” (Gurney-Champion et al., 2020). To bring the “promising” to clinical routine, a certain imaging biomarker roadmap for oncology has been proposed (O'Connor et al., 2017). The three paths suggested in the comprehensive guide provided by O’Conner et al., are i) Technical validation, ii) Biological and clinical validation, and iii) Cost effectiveness.

The technical validation is required to assure accuracy, repeatability, and reproducibility of the imaging biomarker. This facilitates that the imaging biomarker is reliable throughout the course of the study in repeated measurements, as well as providing equal outputs on different scanners and centres.

Biological and clinical validation investigates the imaging biomarkers’ correlation to tumour biology, outcome variables and what value it presents in terms of guiding treatment decisions. It is important to know that the dedicated biomarker reflects a relevant property of the characteristics of interest, e.g. treatment response. Evidence of correlation between imaging and biology can also guide the use of imaging biomarkers in clinical trials.

To eventually reach clinical translation, the imaging biomarker must be cost effective. An imaging biomarker proving greater value than the actual cost required performing a study in a research setting, is not enough to guarantee clinical adaptation. This third path will not be further discussed within the scope of this thesis.

The intention of the guidelines by O’Connor et al. was to provide a formalisation of the process to establish new imaging biomarkers and thereby aid the acceleration of clinical translation. **Papers III-V** are studies exploring the first and second paths, i.e.

technical and clinical validations of new imaging biomarkers within the application of tensor-valued diffusion MRI.

6.2 Diffusion MRI

The concept of diffusion MRI is based on measuring the random motion of water molecules in the body, caused by thermal energy, known as Brownian motion. Diffusion MRI enables assessment of how the molecules move through free, hindered, and restricted diffusion, revealing insights into tissue microstructure (Le Bihan, 2006, White et al., 2014).

Free diffusion (Figure 11A) is most likely to be found in areas with low complexity and few barriers, such as the cerebrospinal fluid (CSF). In the extracellular space, motion may be hindered by cell membranes but is less restricted in less dense regions (Figure 11B), or in regions of breached cell membranes. Restricted diffusion occurs in the intracellular space or if the molecules are restricted by microscopic structures in the tissue, such as nerve tracks (Figure 11C). When the diffusion has a certain preferred direction, it is referred to as anisotropic, while diffusion which is equally distributed in all direction is referred to as isotropic.

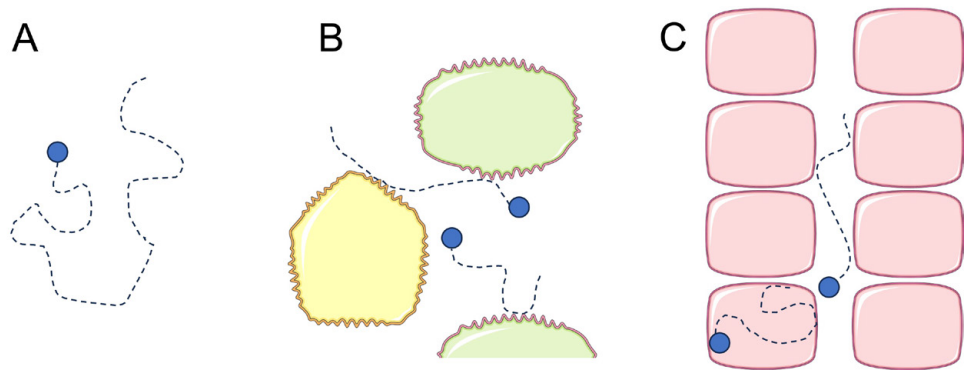

Figure 11. Schematic illustration of diffusion. A) free, isotropic diffusion (such as in the CSF). B) hindered diffusion in the extracellular space, in less cell dense areas, or areas of defective cell membranes. C) restricted diffusion in the intracellular space, in cell dense volumes (such as tumours), or in areas of a certain preferred (anisotropic) direction (such as nerve tracks). Blue circles illustrate the water molecules. This figure was partly created using Servier Medical Art, provided by Servies, licensed under CC BY 4.0 (https://creativecommons.org/licenses/by/4.0/).

A key distinction between diffusion MRI and morphologic MRI sequences is the scale of information obtained. Morphological MRI images the tissue on a millimetre scale, while diffusion MRI can provide information on a micrometre scale. Generally, high water motion corresponds to a low diffusion signal, whereas low motion yields a high signal. By exploiting these signals, diffusion MRI provides valuable insight into the underlying tissue and its microstructural properties (Le Bihan, 2013).

6.2.1 Conventional diffusion encoding

The majority of diffusion MRI studies are based on single diffusion encoding as proposed by Stejskal and Tanner (1965). This simple form of diffusion encoding is often referred to as linear or conventional diffusion, consisting of two symmetrical diffusion gradients applied in one direction. The degree of diffusion weighting can be controlled, where the measured signal depends on the diffusion gradient amplitude (G), the duration of the gradient application (δ) and the temporal spacing between repeated gradients (Δ) described by the b-value:

$$b = \gamma^2 G^2 \delta^2 \left(\Delta - \frac{\delta}{3}\right) \qquad \text{(Equation 4)}$$

where γ is the gyromagnetic ratio.

As the estimated displacement of a water molecule during a diffusion measurement is comparable to the scale of human cell sizes, diffusion weighted imaging is a good tool for tumour microenvironment investigations (Koh and Collins, 2007).

The signal can be mathematically expressed as:

$$S(b) = S(0)\exp\left(-bD\right) \qquad \text{(Equation 5)}$$

where *S(b)* is the signal for a particular *b*-value, b is the diffusion weighting (from equation 4), *S(0)* is the signal at *b=0 s/mm*^{2}, and *D* is the self-diffusion constant of the tissue. Factors such as temperature and viscosity of the tissue affect D.

The diffusion is measured in one direction at a time (e.g. x, y, or z), providing the average diffusion of the tissue in that specific direction. By acquiring images based on at least two b-values, typically one low (e.g. b=0 s/mm^2) and one higher b-value (e.g. b=1000 s/mm^2), the apparent diffusion coefficient (ADC) can be calculated:

$$ADC = -\frac{1}{b} ln \left(\frac{S(b)}{S(0)}\right) \qquad \text{(Equation 6)}$$

The ADC is inversely related to the diffusion signal, meaning that a high value of ADC corresponds to greater water motion, which yields a low signal in the diffusion weighted image. If multiple diffusion directions are measured, the total ADC is the arithmetic mean of all directions:

$$ADC = \frac{ADC_x + ADC_y + ADC_z}{3} \qquad \text{(Equation 7)}$$

An intrinsic limitation of conventional, single diffusion encoding is the fact that it is only able to apply diffusion encoding in one direction per signal readout. The only diffusion property provided by single diffusion encoding is therefore the magnitude of the average diffusivity within a voxel. However, microscopic diffusion can vary in speed and direction, with different rates in different directions and regions, even when there is no preferred direction. Combining several linear encoding directions, known as diffusion tensor imaging (DTI), allows additional features to be estimated (Le Bihan et al., 2001). For instance, the fractional anisotropy (FA) is derived from DTI. FA describes the directional properties of the tissue (Alexander et al., 2007), enabling for example white matter tractography. Additionally, there are other more advanced encoding methods such as double diffusion encoding, oscillating gradients and free gradient waveforms, which may unlock additional properties of the tissue diffusivity in different ways (Alexander et al., 2019). The diffusion method which is further discussed in this work is tensor-valued diffusion encoding, based on free gradient waveforms (Westin et al., 2016).

6.2.2 Tensor-valued diffusion encoding

Tensor-valued diffusion encoding is a new and more advanced method for probing the diffusion process, allowing estimation of various tissue properties that are not accessible by conventional means. It is based on free gradient waveforms and includes all simpler waveform designs but adds more intricate, multi-directional diffusion encoding (Szczepankiewicz et al., 2021). A b-tensor mathematically represents how diffusion measurements can simultaneously probe multiple directions. For instance, tensor-valued diffusion encoding can encode for diffusion in the x-y-plane in a single shot, rather than being restricted to a single direction. Unlike vectors, which describe only magnitude and direction, tensors also carry information about the shape of the diffusion encoding. The shape is quantified by its eigenvalues and can be described as linear tensor encoding (LTE), which is a conventional one-directional measurement, planar tensor encoding (PTE), which encodes the diffusion in a plane, or spherical tensor encoding (STE), which encodes the diffusion in three dimensions (Westin et al.,

2016). The tensor-valued diffusion MRI may consist of one of the three encoding types or a combination thereof (Szczepankiewicz, 2016).

Diffusional variance decomposition (DIVIDE) (Lasič et al., 2014, Szczepankiewicz et al., 2015), and later q-space trajectory imaging (QTI) (Westin et al., 2016), are related methods that exploit tensor-valued diffusion encoding to probe features of tissue microstructure. Using DIVIDE or QTI, several tissue characteristics may be obtained by estimating their corresponding diffusion parameters based on the diffusion measurement: mean diffusivity (MD), fractional anisotropy (FA), microscopic FA (μFA) and diffusional variance caused by isotropic (MKI) and anisotropic diffusion (MKA). The relation between diffusion characteristics and tensor estimation is illustrated in Figure 12.

The signal equation for tensor-valued encoding can be approximated in terms of conventional b-value and b-tensor shape (b_Δ) as:

$$S(b) \approx S_0 \exp\left(-b\mathrm{MD} + \frac{1}{6}b^2\mathrm{MD}^2\left(\mathrm{MKI} + b_\Delta^2\mathrm{MKA}\right)\right) \text{ (Equation 8)}$$

The b-tensor anisotropy shape describes the encoding according to b_Δ=1 for linear, b_Δ=-1/2 for planar and b_Δ=0 for spherical. Further details regarding the signal equation are beyond this thesis but is described in the references (Sjölund et al., 2015, Szczepankiewicz et al., 2016, Nilsson et al., 2020, Teh et al., 2023).

Like the ADC obtained through conventional diffusion encoding, MD can be estimated from tensor-valued encoding and describes the mean diffusivity of the tissue (Basser and Pierpaoli, 1996). Furthermore, each voxel may contain several microenvironments with distinct diffusivities, referred to as diffusional variance. The degree of directional dependence of the brain tissue diffusivity is described by FA, as already mentioned in chapter 6.2.1. However, the FA quantifies the diffusion anisotropy on a voxel level, meaning that it may be confounded by e.g. crossing fibres, where the directional dependence is distinctly separate (Alexander et al., 2007). The microscopic FA (μFA) is an extension to the FA, which disentangles the directional properties within a voxel and thereby offers a solution to the confounding effect of crossing fibres (Szczepankiewicz et al., 2015).

The mean kurtosis estimates the deviation from Gaussian diffusion, which is assumed for conventional diffusion encoding. The kurtosis can be interpreted as the variance of the diffusivity related to the heterogeneity of the tissue microstructure or a tissue's degree of structure (Jensen et al., 2005). Tensor-valued diffusion allows the unspecific total mean kurtosis to be calculated but also disentanglement of its individual components, correlating to isotropic and anisotropic contributions (Szczepankiewicz et

al., 2016), as described by Equation 8. The variance in isotropic diffusivities in the microenvironments within the voxel is estimated by MKI, while the anisotropic contribution, i.e. the degree of directional dependence of diffusion at a microscopic level, is estimated by MKA.

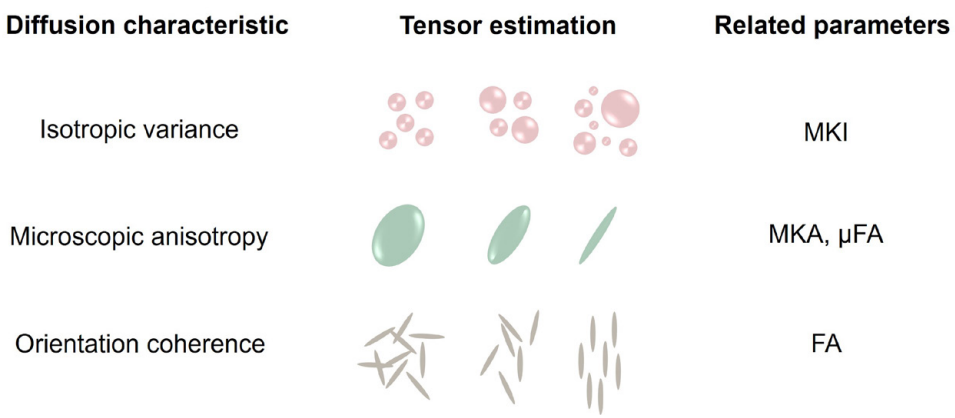

Figure 12. In addition to mean diffusivity (MD), tensor-valued diffusion MRI allows separation of parameters related to the isotropic variance (MKI), microscopic anisotropy (MKA and μFA) and orientation coherence (FA). Assuming that the diffusion occurs within the volumes, the image illustrates a simplified approximation of how the tensor distribution changes with the parameter value, from low (left) to high (right).

The technique has previously been applied in studies of diagnostic applications in intracranial tumours. The first study by Szczepankiewicz et al compared QTI parameters with histology samples of glioma and meningioma (Szczepankiewicz et al., 2016). They found a correlation between MKA and cell shapes, and MKI and cell density variations within each voxel, through which they could also identify each tumour type. Nilsson et al presented an overview of QTI parameters in different intracranial tumours, including brain metastases, with an estimation based on a 3-minute diffusion sequence (Nilsson et al., 2020). In a third study, Brabec et al. showed that QTI parameters could facilitate the prediction of meningioma grading, by comparing histopathological tumour classification and histogram-analysis of the diffusion parameters within each lesion (Brabec et al., 2022).

6.3 Technical feasibility in a radiotherapy setting

The technical validation is a way to ensure that the biomarker has potential as a useful tool for the intended medical research (Nilsson et al., 2018). In the initial phase, phantoms may replace patients to assess feasibility of ADC, MD, and FA. One example is to use an asparagus phantom to simulate nerve fibres (Jokivuolle et al., 2024). However, no phantom to date is complex enough to mimic the advanced physiology and microstructures related to MKI and MKA, leaving a healthy brain as the best substitute during the feasibility investigation. Tensor-valued diffusion encoding has previously been demonstrated clinically feasible in healthy tissue on a range of diagnostic scanners between 1.5-7 T using head coil arrays (Szczepankiewicz et al., 2019a). However, the technique has not been previously explored for assessing tumour radiosensitivity or predicting treatment outcome of radiotherapy.

To enable exploration of imaging biomarkers derived from tensor-valued diffusion parameters, the technique was for the first time implemented on a radiotherapy-dedicated MRI scanner (**Paper III**). The validation, as part of implementing the new sequence, is an important initial step as the requirements and challenges for radiotherapy examinations differs compared to the diagnostic setting. For instance, the use of fixation equipment for radiotherapy limits the use of high-performing receiver coils and potentially increases the distance between the patient and the coil (Gurney-Champion et al., 2020). Another limitation is the gradient performance on MRI scanners for radiotherapy, which is generally weaker than on diagnostic scanners. These limitations have a negative effect on the SNR, which is further impaired by the wide-bore design of the scanners. Therefore, one of the aims was to compare the diagnostic setup, using a head coil, to the radiotherapy setup, including a fixation mask and flexible receiver coils.

The implemented MRI sequence contained optimised waveforms combining LTE and STE. The waveforms had been numerically optimised for the specific MRI system (Sjölund et al., 2015), with a randomised acquisition order of the b-tensor shapes and b-values, to reduce effects of heating and systematic signal bias (Szczepankiewicz et al., 2021). To limit vibrations of the system due to gradient switching, the maximum strength and slew rate were restricted to 31 mT/m and 50 T/m/s in the waveform optimisation.

Technical feasibility was investigated in five healthy individuals to ensure sufficient image quality and stability of the sequence.

6.3.1 Evaluation of SNR

Diffusion images have lower SNR than morphological MR images by nature, due to the strong diffusion gradients (high b-values) and long echo times required to collect the diffusion signal (Jones, 2010). However, sufficient SNR is important to avoid bias in the estimated QTI parameters (Szczepankiewicz et al., 2019b).

The SNR was estimated using the ratio of the mean and standard deviation of the signal for the repeated measurements of the highest b-value (STE). As a quality measure, we applied the methodology of estimating the fraction of voxels with SNR higher than 3 and 6 at the highest b-value (Szczepankiewicz et al., 2019b). The results demonstrated sufficient SNR in both setups if a resolution of 3x3x3 mm^3 was used (Figure 13).

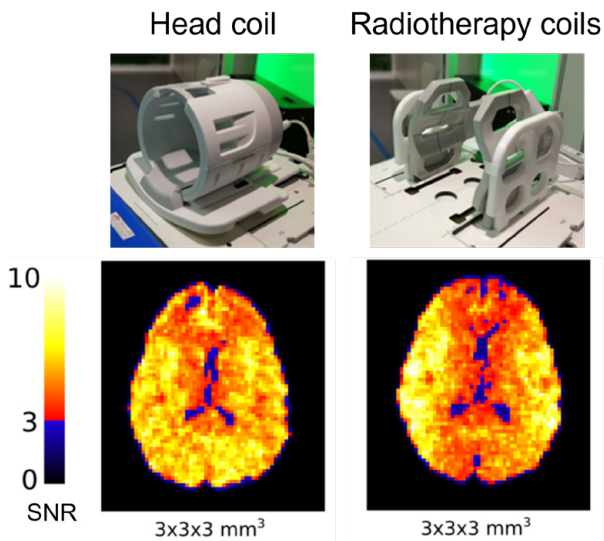

Figure 13. The head coil was the reference coil in the technical feasibility study (left), as commoly used in diagnostics. In the radiotherapy setting, flexible coils (right) with less elements are used to enable simultaneous use of fixation equipement, which ensures that the patient position is identical during preparational imaging and subsequent treatment sessions. Signal-to-noise ratios (SNR) were comparable using a 3 mm isotropic resolution for both coil setups. The figure is adapted from **Paper III**.

6.3.2 Evaluation of QTI parameters

The distributions of QTI parameters within a white matter mask generated for each patient were compared between the head coil and the flexible coil for radiotherapy setup. The estimated parameters were very similar between the two coil configurations, with the best agreement seen in MD (Figure 14). Minor variations were observed in

the other QTI parameters, but with no pattern or bias between cases. However, this highlights the importance of using the same coil throughout a longitudinal quantitative study, to avoid the introduction of coil bias.

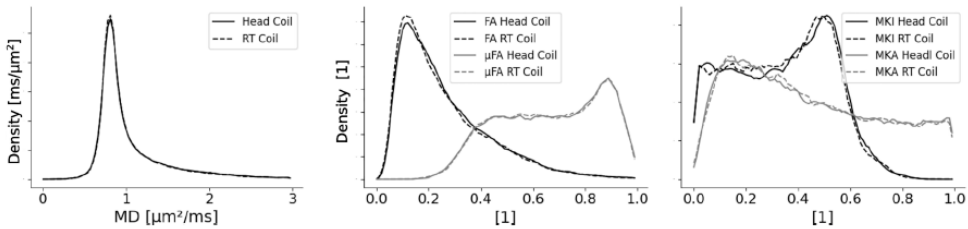

Figure 14. Histograms comparing the QTI parameter distributions from one subject. The solid and dashed lines represent the estimates from the head coil and flexible coil, respectively. The three plots show the mean diffusivity (MD), the macrocopic and microscopic fractional anisotropy (FA and μFA), and the distributions of isotropic and anisotropic diffusivities (MKI and MKA). The figure is adapted from **Paper III**.

Further, we investigated the bias and variance of the estimated QTI parameters using Bland-Altman-plots for different conditions. Intra- and inter-exam repeatability were tested in the radiotherapy setup, while reproducibility was compared to the result from the conventional head coil setup. The resulting bias and variance were negligible in all test conditions and across cases, demonstrating sequence stability which is a condition for further studies.

In summary, we demonstrated that advanced diffusion methods can be used with the flexible coils utilised in radiotherapy applications, but with lower resolution than that achieved with the head coil.

6.4 Diffusion MRI for assessment of treatment response

The most common evaluation of treatment response following radiotherapy involves standard radiological examinations, often using MRI. The changes in tumour size are measured in at least one or two dimensions and are compared to pre-treatment images to assess the response in brain metastases (Lin et al., 2015). However, the visible changes in tumour response occur gradually and take several weeks or months to appear in the images. Hence, the recommended time interval for follow-up examinations is 6-12 weeks post completion of radiotherapy. This prevents treatment adaptations and potentially delays necessary changes to the individual treatment plan, which motivates

the need for earlier treatment assessment through imaging biomarkers. Ideally, these could predict the treatment outcome before or during radiotherapy. At the radiotherapy department at SUS, Lund today, all patients with brain metastases are prescribed 30 Gy in 3 fractions, unless the tumour is too large or located near critical structures (e.g. the brainstem), in which case the dose is reduced to limit side effects. Early imaging biomarkers to predict or identify treatment response (and failure) would be advantageous as they could enable personalised treatment schemes by adjusting the dose during radiotherapy or initiate further treatment within a more efficient timeframe.

Studies utilising conventional diffusion encoding have demonstrated that increasing ADC between baseline and timepoints during or after radiotherapy, correlate with better treatment response in brain metastases (Zhao et al., 2021, Mahmood et al., 2020, Chen et al., 2017, Lee et al., 2014). A numerically higher ADC value has also been predictive for responders compared to non-responders at both baseline (Zhao et al., 2021), and post treatment (Chen et al., 2017). The higher ADC in responders may be explained by lower cell-densities which may relate to less aggressive tumours (Miloushev et al., 2015, Hayashida et al., 2006). On the contrary, other studies have shown that low pre-treatment ADC correlate with better treatment response (Mardor et al., 2004, Mahmood et al., 2020). The suggested explanation in this case is that low ADC indicates a higher tumour viability which relates to better treatment response than tumours with higher ADC, which may indicate the presence of necrotic regions. Furthermore, there are also examples of contradictions regarding the change in ADC over time, as one study found that responders demonstrated a decrease in ADC at timepoints of 1 week and 1 months after radiotherapy (Jakubovic et al., 2016), rather than an ADC increase, as previously suggested. Given the inconsistent results between different studies, ADC alone may be a too simplistic metric to capture the complexity of microstructural changes related to radiotherapy treatment response in brain tumours. This motivates the investigation of more advanced diffusion parameters for early response assessment.

In **Paper IV**, the same tensor-valued diffusion encoding as in **Paper III** was utilised to derive advanced diffusion parameters, using QTI, to investigate the relation between treatment response and diffusivity. Each patient was scheduled for four MRI examinations: before radiotherapy, during radiotherapy (adjacent to the last treatment fraction) and 3- and 6-months after completed treatment (Figure 15). The study sequence was added to the clinical MRI protocol, resulting in a total scan time of 30 minutes. The morphological images were used for target delineation for treatment planning (MRI 1) and for conventional radiological follow-up after treatment (MRI 3 and 4). MRI 2 was unique to the study to enable early response assessment.

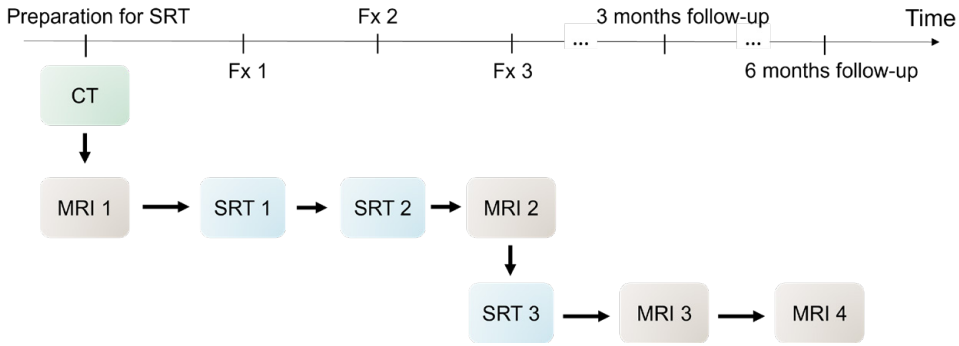

Figure 15. Each study participant in **Paper IV** was scheduled for four MRI examinations. The first (MRI 1) was part of the preparatory scans, including CT and MRI, as routinely performed for all patients referred to SRT. The second examination (MRI 2) was scheduled adjacent to the last treatment fraction and was unique to the study. Finally, follow-up examinations were performed at three and six months post SRT (MRI 3 and MRI 4, respectively). At each MRI examination, a tensor-valued diffusion sequence was added to the clinical MRI protocol, resulting in a total scan time of 30 minutes.

Patient selection for QTI analysis is outlined in Figure 16, with thirteen patients who fulfilled the criteria, thereof ten responders and three non-responders. In this work, responders were defined as patients with partial or complete response, with at least 30% decrease in tumour volume at 3 months follow-up. Patients with stable or progressive disease were classified as non-responders. Nine patients had to be excluded from further analysis due to missing MRI examinations or unavailable response data due to the following reasons. Five patients died before their 3-months follow-up. Two patients withdrew from study participation on their own initiative after MRI 1. Technical issues due to a faulty receiver coil or unavailable study sequence due to a system upgrade, caused two exclusions. Thus, seventeen patients had complete data sets defined as MRI 1, MRI 2 and either MRI 3 or response data from medical records. Quality assuring the data prior to QTI analysis resulted in four exclusions. Three patients had insufficient SNR in the diffusion images while one patient had a cystic tumour. Finally, the thirteen remaining patients were included in the QTI analysis.

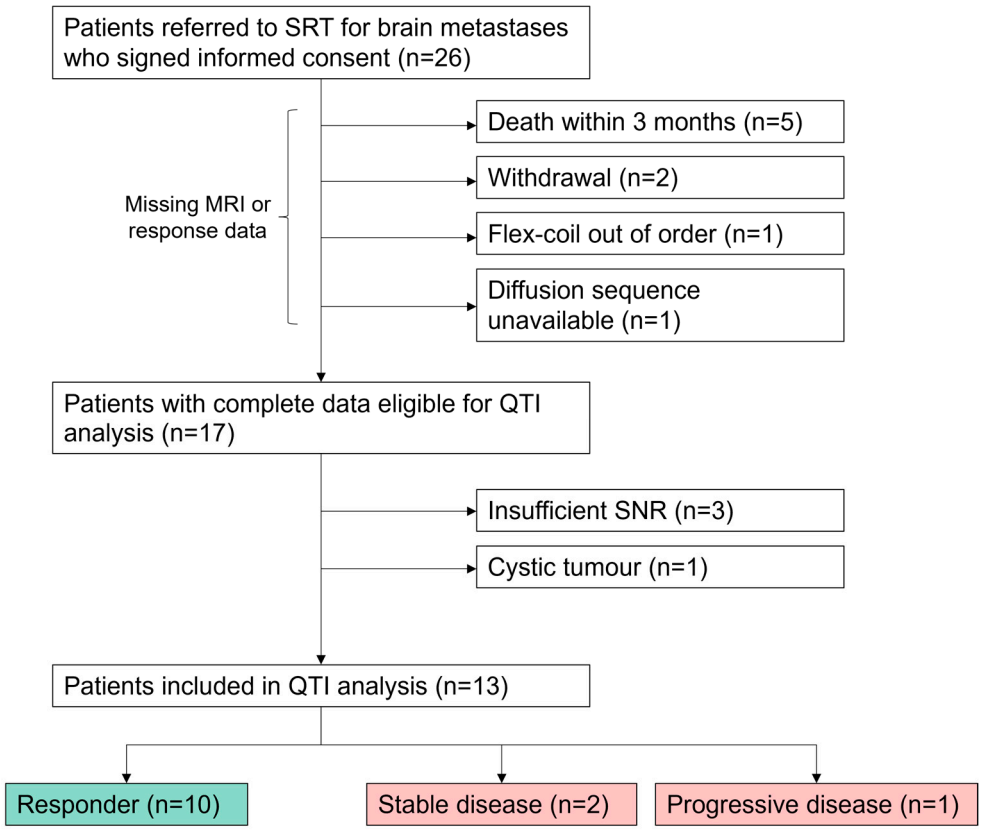

Figure 16. Flow chart of patient selection for QTI analysis and response assessment in **Paper IV**.

The QTI analysis was implemented in Hero (Hero Imaging AB, Umeå, Sweden), based on a method applying positivity constraints for increased noise-robustness (Herberthson et al., 2021). A pipeline to generate the QTI parameters was developed and applied to all patient data. Basic statistics was calculated, and maps were generated for each parameter.

Individual patients demonstrated changes in parameter maps between time points for all QTI parameters. Parameter maps for a patient identified as a responder, with primary breast cancer, is presented in Figure 17. The metastasis demonstrated a reduction in MKI over time, while μFA and MKA were partially enhanced at the tumour edge before and during SRT but reduced after treatment. The high intensity region in the MD map corresponds to the necrotic region observed centrally in the T1w + Gd images in the left column. Such voxels were excluded from the quantitative evaluation, to ensure that only solid tumour tissue was compared.

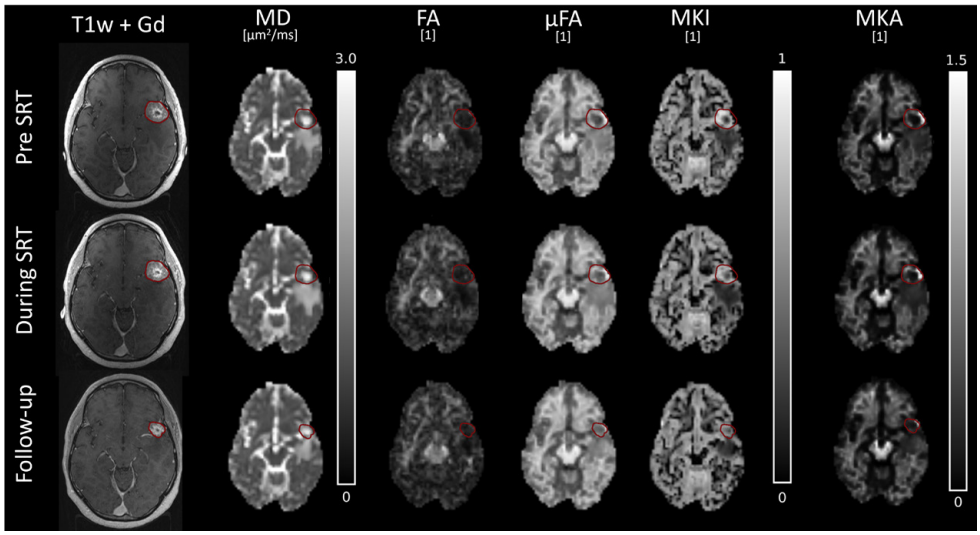

Figure 17. Parameter maps before, during and after SRT of a patient identified as a responder at 3 months follow-up.The red outline represents the contrast-enhanced region in the T1w+Gd image at each time point. Figure from **Paper IV**.

Median QTI parameter values calculated based on the voxels within GTV were statistically tested but revealed no significant differences between responders and non-responders at the individual time points. Additionally, no statistically significant differences were observed between time points within each response group. However, numerically, the trend indicated that MD was higher in responders than non-responders, while the other parameters generally showed overall lower values in responders than non-responders. The variance between patients within each parameter was rather large, and the number of samples was small (10 responders and 3 non-responders). Therefore, we continued with a pooled voxel analysis, to increase the sample numbers and potentially increase the statistical power. In this analysis, all voxels within the GTV were pooled for responders and non-responders, respectively (Figure 18).

The fraction of anisotropic diffusion, FA, was found to be significantly lower in responding than in non-responding tissue. This indicates less orientation coherent microstructures in the responding tissue compared to the non-responding lesions. Yet, both responding and non-responding tissue had lower FA than for example white matter (Ciccarelli et al., 2008).

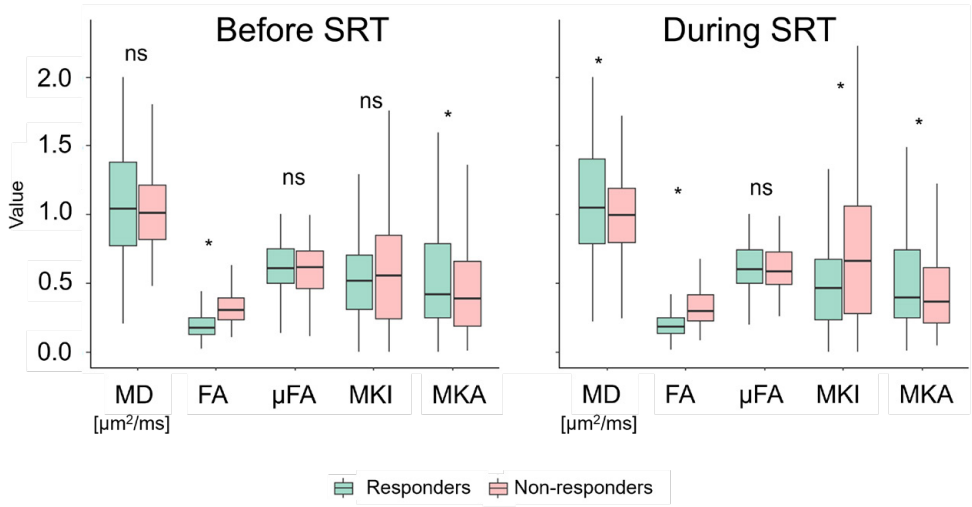

Figure 18. QTI parameters from the pooled voxel analysis presented in a boxplot for responders and non-responders before SRT (left) and during SRT (right). Statistical significance between responders and non-responders is indicated by an asterisk (*), while non-significance is indicated by *ns*. Data from **Paper IV**.

The difference in the parameter describing microscopic diffusion anisotropy, MKA, was also statistically significant, with higher MKA in responders than non-responders. Both FA and MKA differed significantly before and during SRT, while MD and MKI demonstrated statistical significance during SRT only. A higher MD was observed in responding tissue, which is in line with ADC correlations reported in earlier studies (Chen et al., 2017, Zhao et al., 2021). MKI relates to the microscopic diffusion heterogeneity, suggesting that non-responding tissue is more heterogeneous than responding tissue after 20 Gy.

Our findings demonstrate important trends and in the pooled-voxel analysis, the statistical significance indicates that there are changes in the microstructure of responding and non-responding tumour tissue, possible to detect using tensor-valued diffusion MRI. However, the clinical and histological relevance of these findings require further investigation in larger studies. Furthermore, the variability in treatment response and disease progression, with a significant part of the cohort passing away within six months, complicates data analysis and underscores the necessity for personalised treatment approaches.

In summary, this pilot study of imaging biomarkers based on tensor-valued diffusion encoding highlights the potential of QTI parameters for predicting treatment response in brain metastases during SRT. Assuming that the analysis is comprised of

representative tumour tissue, the trends observed in this work may pave the way for further studies with larger patient cohorts. In addition, multi-centre studies are crucial to bring imaging biomarkers toward clinical applications and is something that is generally lacking within the research field (Goodburn et al., 2022).

6.5 Denoising to enhance clinical applicability

In the radiotherapy setup described in **Paper III**, the required resolution was a limiting factor in maintaining an adequate SNR compared to the diagnostic setup. Despite using the same setup and acquisition parameters in **Paper IV**, insufficient SNR led to the exclusion of several cases from further analysis, highlighting a fundamental challenge in diffusion MRI. While SNR-related limitations can be partially mitigated by acquiring the data in larger voxels, which increases the signal intensity, this comes at the cost of reduced spatial resolution and potential partial volume effects. This trade-off is critical when imaging small volumes, such as brain metastases, where high spatial resolution provides a more representative analysis. Although achieving both high resolution and sufficient SNR remains challenging, recent developments in denoising techniques may help overcome these limitations.

The threshold below which the MRI signal becomes indistinguishable from the noise is referred to as the noise floor. While denoising reconstructed diffusion images, or magnitude data, preserves the noise floor, denoising of complex data enables signal below the noise floor to be retrieved (Manzano Patron et al., 2024). Denoising in the complex domain may be resource-intensive and, at this point, mainly at a research stage, but it has the potential to significantly improve the quality of diffusion images.

To enhance feasibility of parameters derived from tensor-valued diffusion MRI, we investigated four different denoising methods, both open-source and vendor-provided. The aim was to explore the potential of maximising image resolution without compromising SNR (**Paper V**). Denoising was applied to both conventional and tensor-valued diffusion data collected from a spherical phantom and a healthy brain in a radiotherapy-dedicated MRI scanner. Image acquisition was performed using the diagnostic head coil and the radiotherapy flex coil setup, respectively.

The denoising methods were selected based on availability and current standard for diffusion MRI specifically, using Principal Component Analysis (PCA) (Tax et al., 2022). Three versions of patch-based denoising methods were compared: two versions of Marchenko-Pastur PCA (MPPCA) and Noise Reduction with Distribution Corrected PCA (NORDIC). These methods were applied to manually reconstructed

magnitude and complex signal data. The vendor-provided solution, available at the scanner was AirReconDL (ARDL) (Peters and Lawson, 2021), which was also applied to patient data in **Paper IV**. ARDL is an AI-based technique developed by GE Healthcare, which processes the complex data directly on the scanner.

All results were compared to the baseline SNR established in **Paper III**, without denoising, at an isotropic resolution of 3x3x3 mm^3. Using complex-valued denoising, the noise floor effects were reduced, demonstrated by reduced parameter bias in both conventional and QTI parameters. Specifically, quantitative phantom measurements of ADC demonstrated improved accuracy with complex denoising whereas denoising of magnitude data increased the parameter bias compared to no denoising.

One of the MPPCA implementations applied to complex-valued data was the overall best performing denoising method and enabled improved resolutions with both coil setups. The QTI parameter maps at higher resolutions were visually comparable to the baseline resolution for all parameters, except MKI. This is expected as MKI is known to be the most noise-sensitive parameter (Szczepankiewicz et al., 2019a), with potentially unreliable estimation at low SNR. Nonetheless, appropriate denoising on complex-valued diffusion data in general has the potential to enhance clinical feasibility and precision of diffusion MRI methods in a radiotherapy setting, which may bring such imaging biomarkers closer to clinical applications.

7 Ethical considerations

The aim of medical research involving human subjects is to gain new knowledge. To protect the research subjects, being either patients or healthy individuals, medical research is subject to ethical standards. It is always the duty and responsibility of the medical researcher to protect the life, health, dignity, integrity, right to self-determination, privacy and confidentiality of personal information of research subjects (World Medical Association, 2013). All studies in this thesis were performed in accordance with both the World Medical Association's Declaration of Helsinki ethical principles for medical research involving human subjects, and the Swedish law (2003:460) regarding ethical approval for research involving humans. **Paper I** and **II** were ethically approved by the Regional ethical review board, Lund, Sweden (2018/445). **Paper III**, **IV and V** were approved by the National ethical review board, Sweden (2020-01495 and 2020–06389). Participation in the studies was voluntary and written informed consent was obtained from all participants. The participants could at any time terminate their study participation, without stating the cause.

The study participants in the papers presented in this thesis, consisting of adult cancer patients, can be considered vulnerable individuals. Since brain tumours can cause cognitive difficulties, the responsible physician assessed the suitability of each participant for inclusion, ensuring they could make an informed decision regarding study participation.

After an initial oral briefing, participants were given time to independently read the written materials. To ensure comprehensive understanding, a subsequent discussion was held where participants could ask questions or express any concerns. Most patients were in company of a relative, who also received the same information.

Study participation did not pose significant risk to the subject but did involve a longer examination time in the MRI scanner. There is no ionising radiation in MRI. In rare cases, patients may react to contrast agents which are used in clinical examinations, as well as in the study protocols used in this work. However, all study participants had previously undergone MRI examinations and any known contraindications to contrast agents would exclude them from inclusion.

The study participants did not receive any direct benefits from study participation, as the aim of the project was to improve radiotherapy for future patients. The absence of risk and benefit for the individual participant was clarified during the inclusion process and in the written patient information. In a dialogue with the patient, we emphasised that the study was entirely voluntary and that they could withdraw at any times, even during an on-going MRI examination. Withdrawal did not affect or delay their intended treatment.

Paper II was interventional, as the patients were treated in the MRI-only RT workflow incorporating a CE-approved software. Even so, treatment quality was ensured through rigorous quality assurance, comparing to the corresponding conventional treatment for each individual. Participation did therefore not pose any relevant risk. In **Paper IV**, participation involved one additional MRI examination and follow-up scans in Lund, which could result in extra travelling compared to having the examination at their home clinic. Follow-up exams within the study were potentially more formalised than in clinical routine, but all patients would have had at least one MRI within the next six months for treatment response assessment regardless of study participation. Participation in the studies did not restrict participants from undergoing additional radiological exams outside the study, if needed.

Reports from the experience of MRI-only RT in clinical routine (chapter 5.5) was done under ethical permit for retrospective studies (2013/742). All data were pseudo anonymised and due to the retrospective nature of the report, there were no risks or benefits to the patients included.

A key consideration regarding healthy individuals in MRI studies is the risk of incidental findings, i.e. unexpected abnormalities. Thus, there was a formalised procedure for image review by a qualified physician. If a potentially significant abnormality was to be found, the participant would be informed in accordance with ethical guidelines, and referral options would be provided.

8 General discussion and future perspectives

The ambition of our research in MRI-only RT has always been to use it to treat patients, a goal that was defined even before the first validation study. Perhaps that was one of the keys to why we are now having MRI-only RT for glioblastoma clinically implemented at the radiotherapy department at SUS, Lund. The studies presented in this thesis, paving the way for this implementation, demonstrated a safe and accurate use of sCT for treatment planning and patient positioning. We made early contributions to the rapidly evolving field of MRI-only RT for brain tumours, by demonstrating feasibility and adding valuable data to future guidelines through the results presented.

The utilised software has demonstrated compatibility with various MRI vendors in the brain, head and neck and pelvic regions (Palmer et al., 2021, Autret et al., 2023, Persson et al., 2020). Although our clinical routine of MRI-only RT currently focuses on glioblastoma, the workflow is likely transferable to other brain diagnoses, such as low-grade gliomas. To include stereotactic brain tumour treatments in MRI-only RT, further validation is necessary due to the 1 mm MRI slice thickness recommended for such treatment planning (Paulson et al., 2016). Furthermore, the sCT software and suggested workflow is currently restricted to adult patients. Others have shown feasibility of MRI-only RT also for paediatric patients (Maspero et al., 2020), where the reduction of ionising radiation is important as children are more radiosensitive and expected to live longer than adult patients, with increased risk to develop secondary cancers.

Radiotherapy treatment integrates various techniques and vendors routinely. One that has been less investigated in the context of MRI-only RT is using sCT as the image reference in surface scanning or surface guided radiotherapy (SGRT). During our implementation, two different systems (Catalyst by C-RAD AB, Uppsala, Sweden and ExacTrac by Brainlab AG, Munich, Germany) have been indirectly verified, but their exact performance was outside the scope of this work. As SGRT is clinical routine in our department, the same procedures were applied to the MRI-only patients. The final

positioning is always based on X-ray images, while monitoring during treatment is based primarily on surface scanning. An in-house investigation showed no increased positional deviations or treatment interruptions in the MRI-only patients compared to those with comparable anatomical locations treated on CT-based images. Studies investigating this in more detail are warranted to determine the accuracy and precision of surface scanning combined with sCT.

Another area that needs further research and development is QA for sCT and MRI-only RT, specifically in clinical routine and in the patient-specific cases. There are options, as already mentioned, with evaluations based on CBCT, bulk density or independent sCT generations. What these QA methods have in common is that they are time consuming and tend to require manual input. For MRI-only RT to reach its full potential and a wider clinical implementation, these shortcomings must be addressed, and automatic procedures would be preferred.

Introducing a new method into the clinic, in this case MRI-only RT, is time and resource consuming. We have learned, through the rigorous project of developing and implementing MRI-only RT for brain tumours, that the way to a successful implementation is based on solid methods, thorough evaluations, structured education, and good communication. By incorporating these aspects, it is possible to build trust, confidence, and experience to finally be able to take a research project all the way into clinical routine. With time, the long-term benefits of MRI-only RT will show - or not. The health-economic benefits presented for prostate cancer may not be exceedingly convincing but must be individually assessed for each diagnosis and anatomy (Persson et al., 2023). Such studies are warranted for brain cancer patients to enable clinics to make informed decisions regarding the investment in MRI-only RT. Furthermore, as we move towards smaller margins and fewer fractions, the spatial accuracy becomes increasingly important, and potentially, MRI-only RT will be the leading choice for some of these treatments.

In addition to applications directly related to the treatment situation, MRI is an important tool for assessing treatment response. While current follow-up primarily relies on volumetric changes, the image-focused modern radiotherapy workflow could provide new possibilities to explore imaging biomarkers, for early response assessment and treatment adaptation.

In the studies presented within this thesis, we explored the potential of imaging biomarkers based on tensor-valued diffusion MRI. Our findings indicate that the method is worth further investigation, as the derived parameters provide information beyond conventional diffusion MRI, which may help us stratify patients in the future and identify non-responders earlier than today. However, there is still a need for

standardisation of both image acquisition and image processing. Moreover, the field will benefit from the continued technical development, such as improved coils, to enable improved SNR in advanced diffusion MRI. Another significant advancement lies in the development of enhanced denoising methods, which can bring the imaging biomarkers based on diffusion MRI closer to clinical applicability through improved image resolution and parameter precision.

Current analysis procedures in imaging biomarker studies tend to be time consuming and require substantial manual input. Potentially AI could be integrated in imaging biomarker studies to enable an automated and objective segmentation of solid tumour tissue, avoiding necrotic, cystic and haemorrhagic regions. AI integration could also aid the development of predictive models, combining diffusion image features and other clinical data for early response assessment. Another general challenge in response assessment is the differentiation between true tumour progression and radionecrosis or pseudo progression. Perhaps diffusion MRI imaging biomarkers in combination with AI could help advance the development of such methods.

An interesting aspect where MRI-only RT and imaging biomarker research may be combined is through MR-linacs. The benefits of MRI-only RT may further increase in a workflow with repeated imaging, such as the one enabled with the MR-linac. The primary benefit for patients with brain tumours is the possibility to detect target volume changes and adapt the treatment accordingly on a fraction-to-fraction basis (Guerini et al., 2023). There has been limited advancement in the treatment of high-grade gliomas in the past twenty years, but a promising progress was presented in a preliminary report at ASTRO 2024. The trial from the group at Sunnybrook, Toronto, Canada had evaluated weekly online MR-linac adaptive radiotherapy with reduced margins for 108 high-grade glioma patients. They demonstrated a low risk of marginal failure (recurrence) of 4% while maintaining progression free and overall survival outcomes (Detsky et al., 2024).

Furthermore, with the opportunity of daily MR images, imaging biomarkers can be explored longitudinally throughout the treatment and optimal timepoints for correlations with early response predictions may be identified. The technical feasibility of diffusion MRI in the MR-linac setting has been demonstrated (Lawrence et al., 2021), and future efforts should continue to focus on the clinical and biological aspects of such imaging biomarkers.

As a final reflection, combining the worlds of radiotherapy and MRI is not trivial but very exciting. The MRI-based radiotherapy of brain tumours offers a potential to further improve treatment precision and patient care in the future.

9 Conclusions

This thesis added new knowledge to the field of MRI-based radiotherapy of brain tumours by demonstrating the following:

- A commercial, DL-based sCT generation software was validated. Feasibility was demonstrated in treatment planning of brain malignancies, with and without anatomical anomalies in the skull due to surgery (**Paper I**).
- Excellent agreement between CT and sCT was observed for dosimetric and geometric endpoints as well as for CBCT image registration used for patient positioning (**Paper I** and **II**).
- The first prospective clinical MRI-only RT implementation study was presented for primary brain tumours, including a set of acceptance criteria. Twenty glioma patients successfully completed their treatments in the new workflow (**Paper II**).
- The combined results from **Paper I** and **II** led to a full implementation of the MRI-only RT workflow for glioblastoma patients, which is now clinical routine at the radiotherapy department at SUS, Lund with 80+ treated patients.
- Feasible implementation of tensor-valued diffusion-MRI on a radiotherapy dedicated MRI scanner. Results demonstrated sufficient SNR and reproducible advanced diffusion parameter maps in healthy individuals, as well as in tumour tissue (**Paper III**).
- QTI parameters demonstrated potential to differentiate between responders and non-responders before and during stereotactic radiotherapy (**Paper IV**).
- Advanced denoising methods on complex diffusion data allow for improved image resolution, enhancing clinical feasibility of imaging biomarkers based on tensor-valued diffusion MRI (**Paper V**).
- The combined results from **Paper III-V** have contributed to a platform for research using tensor-valued diffusion MRI in a radiotherapy setting.

Acknowledgements

First of all, I would like to thank all the **brave patients**, who participated and contributed so selflessly to the studies making up this thesis. Without you there would be no data to analyse, and although I wish with all my heart that none of you would have to go through the horrible reality of brain cancer, you have all made a lasting impact on the treatment of future cancer patients. So, thank you for that.

During the journey that has finally led to this thesis, many people have contributed in one way or another. I am very grateful to all of you, but there are some who deserve special thanks.

I would like to start by thanking my supervisors for believing in me. Firstly, thank you to my main supervisor, **Lars E. Olsson**, whose guidance has been invaluable. Thank you for providing me with both freedom and responsibility, offering honest opinions, and sharing your impressive research experience. Secondly, thank you to my physics supervisor, **Joakim Medin**, for your expertise in dosimetry, your valuable input on various research and clinic-related issues, and your sense of humour. Thirdly, thank you to my oncology supervisor, **Sara Alkner**, for sharing all your medical expertise, teaching me about patient recruitment, and always providing quick and constructive feedback. Finally, **Patrik Brynolfsson**, my co-author and unofficial supervisor. Thank you for always making time, for analysis support and for providing your expertise in MRI as well as Hero. Because that's who you are (i.e. a hero!).

A sincere thank you to **Sven Bäck, Per Munck Af Rosenschöld**, and **Silke Engelholm** for the opportunity to combine my PhD studies with clinical work, and for supporting me through both clinical and academic questions. Thanks to **Andrej Tomaszewicz**, **Sacha Af Wetterstedt**, and **Jonas Scherman** for their invaluable support in managing the clinical schedule throughout the years, allowing me the necessary time to focus on my research.

A special mention to my co-authors **Filip Szczepankiewicz**, **Markus Nilsson** and **Pia Sundgren**. Thank you for fruitful collaborations and valuable input. Thank you to everyone who has helped with the practical aspects of the studies: the MRI staff **Senada Kapetanovic, Sveinung Groven, Urban Alkhed** and **Anna Lippe**;

Martin Södergren and his excellent team at "bokningen"; **Victor Pham** and **Marie Tärnhuvud** for treatment planning; and **Linda Wennberg**, for an excellent collaboration regarding follow-up exams and optimising the logistics.

Next, I would like to give a special mention to a few special colleagues. **Emilia Persson**, thanks for your friendship and for sticking by my side since the very start. Thank you for paving the way in MRI-only RT, for always taking time to listen and for your never-ending support (including invaluable proofreading of this thesis!). **Christian Jamtheim-Gustafsson**, thanks for guiding me through the world of MR in RT and for your wise words about research in general. It's not the topic that makes the researcher! **Annika Mannerberg**, thank you for becoming my office roomie, for supporting both cravings and research discussions. This final year was so much better thanks to you. I would also like to thank **Ivan Rashid** for an excellent collaboration during the final project, for your bright mind, and for loving bag pipes even more than I do.

Thank you to all my colleagues at Radiation Physics in Lund for supporting me throughout my PhD studies, covering in the clinic or just discussing different aspects of radiotherapy. Thank you to all my colleagues at MSF Malmö and Lund, for always making me feel welcome.

Thank you, **Spectronic Medical AB**, **GE Healthcare** and **Hero Imaging AB** for excellent collaborations and research support.

I would also like to take this opportunity to thank some of my teachers over the years. Those who sparked my joy for learning from the very beginning: **Lena Malmqvist** and **Ann-Christin Aspegren**, and those who sparked my curiosity and interest in physics: **Hans Rosengren** and **Boel Holmqvist**. You are all part of my scientific journey.

Finally, I would like to thank the people who really mean the world to me. My friends and family! Thank you to all my friends, for keeping me sane and for making each day that little bit better, just by being there. Thank you, **Mamma** and **Pappa**, for your unwavering love and for always supporting me to go my own way. Thank you for encouraging my scientific interest in every way possible, even though you both preferred rugby over maths (I do too). Thank you to my soulmate and sister, **Nora**, simply for being who you are, and for always inspiring me to do my best. Thank you, **Tim**, for always cheering on me, at least pretending to read my work, and for loving us as if we were your own. Thank you to my extended **Lerner**-family for being the best in-laws anyone could wish for. And **Nils**, my love, thank you for everything that we have. You always believe in me and raise me up (sometimes more than I deserve). For us, forever.

And last, but definitely not least – my boys, **Elliot** and **Aston**. The best outcome from these years is not actually the thesis, but rather the two of you! Tack för att ni påminner mig om det som verkligen är viktigt i livet. Tack för skratt, bus och kärlek varje dag. Ni är bäst! Och vet ni vad? *Jag älskar er mest i hela världen!*

Funding

This work was supported by:

- Allmänna sjukhusets i Malmö Stiftelse för bekämpande av cancer
- Fru Berta Kamprads stiftelse för utforskning och bekämpning av cancersjukdomar
- Skåne University Hospital, Lund, Sweden
- Skånes universitetssjukhus stiftelser och donationer
- Stiftelsen för cancerforskning vid Onkologiska kliniken vid Universitets-sjukhuset MAS
- Södra sjukvårdsregionens doktorandanslag
- VINNOVA: Gentle Radiotherapy project (2016-02529 and 2016-03847)

References

Aldawsari, A. M., Al-Qaisieh, B., Broadbent, D. A., Bird, D., Murray, L. & Speight, R. 2023. The role and potential of using quantitative MRI biomarkers for imaging guidance in brain cancer radiotherapy treatment planning: A systematic review. *Phys Imaging Radiat Oncol,* 27**,** 100476.

Alexander, A. L., Lee, J. E., Lazar, M. & Field, A. S. 2007. Diffusion Tensor Imaging of the Brain. *Neurotherapeutics,* 4**,** 316-329.

Alexander, D. C., Dyrby, T. B., Nilsson, M. & Zhang, H. 2019. Imaging brain microstructure with diffusion MRI: practicality and applications. *NMR Biomed,* 32**,** e3841.

Alzahrani, N., Henry, A., Clark, A., Murray, L., Nix, M. & Al-Qaisieh, B. 2023. Geometric evaluations of CT and MRI based deep learning segmentation for brain OARs in radiotherapy. *Phys Med Biol,* 68.

Andreasen, D., Van Leemput, K., Hansen, R. H., Andersen, J. A. & Edmund, J. M. 2015. Patch-based generation of a pseudo CT from conventional MRI sequences for MRI-only radiotherapy of the brain. *Med Phys,* 42**,** 1596-605.

Autret, D., Guillerminet, C., Roussel, A., Cossec-Kerloc'h, E. & Dufreneix, S. 2023. Comparison of four synthetic CT generators for brain and prostate MR-only workflow in radiotherapy. *Radiat Oncol,* 18**,** 146.

Bahloul, M. A., Jabeen, S., Benoumhani, S., Alsaleh, H. A., Belkhatir, Z. & Al-Wabil, A. 2024. Advancements in synthetic CT generation from MRI: A review of techniques, and trends in radiation therapy planning. *J Appl Clin Med Phys***,** e14499.

Basser, P. J. & Pierpaoli, C. 1996. Microstructural and physiological features of tissues elucidated by quantitative-diffusion-tensor MRI. *J Magn Reson B,* 111**,** 209-19.

Biomarkers Definitions Working, G. 2001. Biomarkers and surrogate endpoints: preferred definitions and conceptual framework. *Clin Pharmacol Ther,* 69**,** 89-95.

Boulanger, M., Nunes, J. C., Chourak, H., Largent, A., Tahri, S., Acosta, O., De Crevoisier, R., Lafond, C. & Barateau, A. 2021. Deep learning methods to generate synthetic CT from MRI in radiotherapy: A literature review. *Phys Med,* 89**,** 265-281.

Brabec, J., Szczepankiewicz, F., Lennartsson, F., Englund, E., Pebdani, H., Bengzon, J., Knutsson, L., Westin, C. F., Sundgren, P. C. & Nilsson, M. 2022. Histogram analysis of tensor-valued diffusion MRI in meningiomas: Relation to consistency, histological grade and type. *Neuroimage Clin,* 33**,** 102912.

Brenner, A. W. & Patel, A. J. 2022. Review of Current Principles of the Diagnosis and Management of Brain Metastases. *Front Oncol,* 12**,** 857622.

Brown, P. D., Ballman, K. V., Cerhan, J. H., Anderson, S. K., Carrero, X. W., Whitton, A. C., Greenspoon, J., Parney, I. F., Laack, N. N. I., Ashman, J. B., Bahary, J. P., Hadjipanayis, C. G., Urbanic, J. J., Barker, F. G., 2nd, Farace, E., Khuntia, D., Giannini, C., Buckner, J. C., Galanis, E. & Roberge, D. 2017. Postoperative stereotactic radiosurgery compared with whole brain radiotherapy for resected metastatic brain disease (NCCTG N107C/CEC·3): a multicentre, randomised, controlled, phase 3 trial. *Lancet Oncol,* 18**,** 1049-1060.

Chao, J. H., Phillips, R. & Nickson, J. J. 1954. Roentgen-ray therapy of cerebral metastases. *Cancer,* 7**,** 682-9.

Chen, Z., Zu, J., Li, L., Lu, X., Ni, J. & Xu, J. 2017. Assessment of stereotactic radiosurgery treatment response for brain metastases using MRI based diffusion index. *Eur J Radiol Open,* 4**,** 84-88.

Ciccarelli, O., Catani, M., Johansen-Berg, H., Clark, C. & Thompson, A. 2008. Diffusion-based tractography in neurological disorders: concepts, applications, and future developments. *Lancet Neurol,* 7**,** 715-27.

Cronholm, R. O., Karlsson, A. & Siversson, C. 2020. Whitepaper: MRI only radiotherapy planning using the transfer function estimation algorithm.

Das, I. J., McGee, K. P., Tyagi, N. & Wang, H. 2019. Role and future of MRI in radiation oncology. *Br J Radiol,* 92**,** 1094.

Datta, N. R., David, R., Gupta, R. K. & Lal, P. 2008. Implications of contrast-enhanced CT-based and MRI-based target volume delineations in radiotherapy treatment planning for brain tumors. *J Cancer Res Ther,* 4**,** 9-13.

Demol, B., Boydev, C., Korhonen, J. & Reynaert, N. 2016. Dosimetric characterization of MRI-only treatment planning for brain tumors in atlas-based pseudo-CT images generated from standard T1-weighted MR images. *Med Phys,* 43**,** 6557.

Detsky, J., Chan, A. W., Palhares, D. M., Hudson, J. M., Stewart, J., Chen, H., Das, S., Lipsman, N., Lim-Fat, M. J., Perry, J., Ruschin, M. E., Myrehaug, S. D., Soliman, H., Tseng, C. L. & Sahgal, A. 2024. MR-Linac On-Line Weekly Adaptive Radiotherapy for High Grade Glioma (HGG): Results from the UNITED Single Arm Phase II Trial. *International Journal of Radiation Oncology, Biology, Physics,* 120**,** S4.

Dinkla, A. M., Wolterink, J. M., Maspero, M., Savenije, M. H. F., Verhoeff, J. J. C., Seravalli, E., Isgum, I., Seevinck, P. R. & van den Berg, C. A. T. 2018. MR-Only Brain Radiation Therapy: Dosimetric Evaluation of Synthetic CTs Generated by a Dilated Convolutional Neural Network. *Int J Radiat Oncol Biol Phys,* 102**,** 801-812.

Edmund, J. M., Kjer, H. M., Van Leemput, K., Hansen, R. H., Andersen, J. A. & Andreasen, D. 2014. A voxel-based investigation for MRI-only radiotherapy of the brain using ultra short echo times. *Phys Med Biol,* 59**,** 7501-19.

Edmund, J. M. & Nyholm, T. 2017. A review of substitute CT generation for MRI-only radiation therapy. *Radiat Oncol,* 12**,** 28.

Eekers, D. B., In 't Ven, L., Roelofs, E., Postma, A., Alapetite, C., Burnet, N. G., Calugaru, V., Compter, I., Coremans, I. E. M., Hoyer, M., Lambrecht, M., Nystrom, P. W., Mendez Romero, A., Paulsen, F., Perpar, A., de Ruysscher, D., Renard, L., Timmermann, B., Vitek, P., Weber, D. C., van der Weide, H. L., Whitfield, G. A., Wiggenraad, R., Troost, E. G. C. & European Particle Therapy Network" of, E. 2018. The EPTN consensus-based atlas for CT- and MR-based contouring in neuro-oncology. *Radiother Oncol,* 128**,** 37-43.

Emami, H., Dong, M., Nejad-Davarani, S. P. & Glide-Hurst, C. K. 2018. Generating synthetic CTs from magnetic resonance images using generative adversarial networks. *Med Phys*.

Emin, S., Rossi, E., Myrvold Rooth, E., Dorniok, T., Hedman, M., Gagliardi, G. & Villegas, F. 2024. Clinical implementation of a commercial synthetic computed tomography solution for radiotherapy treatment of glioblastoma. *Physics and Imaging in Radiation Oncology,* 30**,** 100589.

Estermann, A., Schneider, C., Zimmermann, F., Papachristofilou, A. & Finazzi, T. 2024. Whole brain radiation therapy for patients with brain metastases: survival outcomes and prognostic factors in a contemporary institutional series. *Strahlentherapie und Onkologie,* 200**,** 942-948.

Florkow, M. C., Zijlstra, F., Willemsen, K., Maspero, M., van den Berg, C. A. T., Kerkmeijer, L. G. W., Castelein, R. M., Weinans, H., Viergever, M. A., van Stralen, M. & Seevinck, P. R. 2020. Deep learning–based MR-to-CT synthesis: The influence of varying gradient echo–based MR images as input channels. *Magnetic Resonance in Medicine,* 83**,** 1429-1441.

Fox, B. D., Cheung, V. J., Patel, A. J., Suki, D. & Rao, G. 2011. Epidemiology of metastatic brain tumors. *Neurosurg Clin N Am,* 22**,** 1-6, v.

Fraass, B. A., McShan, D. L., Diaz, R. F., Ten Haken, R. K., Aisen, A., Gebarski, S., Glazer, G. & Lichter, A. S. 1987. Integration of magnetic resonance imaging into radiation therapy treatment planning: I. Technical considerations. *Int J Radiat Oncol Biol Phys,* 13**,** 1897-908.

Gardner, S. J., Kim, J. & Chetty, I. J. 2019. Modern Radiation Therapy Planning and Delivery. *Hematol Oncol Clin North Am,* 33**,** 947-962.

Goodburn, R. J., Philippens, M. E. P., Lefebvre, T. L., Khalifa, A., Bruijnen, T., Freedman, J. N., Waddington, D. E. J., Younus, E., Aliotta, E., Meliado, G., Stanescu, T., Bano, W., Fatemi-Ardekani, A., Wetscherek, A., Oelfke, U., van den Berg, N., Mason, R. P., van Houdt, P. J., Balter, J. M. & Gurney-Champion, O. J. 2022. The future of MRI in radiation therapy: Challenges and opportunities for the MR community. *Magn Reson Med,* 88**,** 2592-2608.

Goodenberger, M. L. & Jenkins, R. B. 2012. Genetics of adult glioma. *Cancer Genet,* 205**,** 613-21.

Greer, P., Martin, J., Sidhom, M., Hunter, P., Pichler, P., Choi, J. H., Best, L., Smart, J., Young, T., Jameson, M., Afinidad, T., Wratten, C., Denham, J., Holloway, L., Sridharan, S., Rai, R., Liney, G., Raniga, P. & Dowling, J. 2019. A Multi-center Prospective Study for Implementation of an MRI-Only Prostate Treatment Planning Workflow. *Front Oncol,* 9**,** 826.

Grigo, J., Szkitsak, J., Höfler, D., Fietkau, R., Putz, F. & Bert, C. 2024. "sCT-Feasibility" - a feasibility study for deep learning-based MRI-only brain radiotherapy. *Radiation Oncology,* 19**,** 33.

Guckenberger, M., Baus, W. W., Blanck, O., Combs, S. E., Debus, J., Engenhart-Cabillic, R., Gauer, T., Grosu, A. L., Schmitt, D., Tanadini-Lang, S. & Moustakis, C. 2020. Definition and quality requirements for stereotactic radiotherapy: consensus statement from the DEGRO/DGMP Working Group Stereotactic Radiotherapy and Radiosurgery. *Strahlenther Onkol,* 196**,** 417-420.

Guerini, A. E., Nici, S., Magrini, S. M., Riga, S., Toraci, C., Pegurri, L., Facheris, G., Cozzaglio, C., Farina, D., Liserre, R., Gasparotti, R., Ravanelli, M., Rondi, P., Spiazzi, L. & Buglione, M. 2023. Adoption of Hybrid MRI-Linac Systems for the Treatment of Brain Tumors: A Systematic Review of the Current Literature Regarding Clinical and Technical Features. *Technol Cancer Res Treat,* 22**,** 15330338231199286.

Gunnlaugsson, A., Persson, E., Gustafsson, C., Kjellén, E., Ambolt, P., Engelholm, S., Nilsson, P. & Olsson, L. E. 2019. Target definition in radiotherapy of prostate cancer using magnetic resonance imaging only workflow. *Phys Imaging Radiat Oncol,* 9**,** 89-91.

Gupta, D., Kim, M., Vineberg, K. A. & Balter, J. M. 2019. Generation of Synthetic CT Images From MRI for Treatment Planning and Patient Positioning Using a 3-Channel U-Net Trained on Sagittal Images. *Front Oncol,* 9**,** 964.

Gurney-Champion, O. J., Mahmood, F., van Schie, M., Julian, R., George, B., Philippens, M. E. P., van der Heide, U. A., Thorwarth, D. & Redalen, K. R. 2020. Quantitative imaging for radiotherapy purposes. *Radiother Oncol,* 146**,** 66-75.

Han, X. 2017. MR-based synthetic CT generation using a deep convolutional neural network method. *Med Phys,* 44**,** 1408-1419.

Hayashida, Y., Hirai, T., Morishita, S., Kitajima, M., Murakami, R., Korogi, Y., Makino, K., Nakamura, H., Ikushima, I., Yamura, M., Kochi, M., Kuratsu, J. I. & Yamashita, Y. 2006. Diffusion-weighted imaging of metastatic brain tumors: comparison with histologic type and tumor cellularity. *AJNR Am J Neuroradiol,* 27**,** 1419-25.

Herberthson, M., Boito, D., Haije, T. D., Feragen, A., Westin, C. F. & Özarslan, E. 2021. (Q-)(s)(pace trajectory imaging with positivity constraints (QTI+)). *Neuroimage,* 238**,** 118198.

Huijben, E. M. C., Terpstra, M. L., Galapon, A., Jr., Pai, S., Thummerer, A., Koopmans, P., Afonso, M., van Eijnatten, M., Gurney-Champion, O., Chen, Z., Zhang, Y., Zheng, K., Li, C., Pang, H., Ye, C., Wang, R., Song, T., Fan, F., Qiu, J., Huang, Y., Ha, J., Sung Park, J., Alain-Beaudoin, A., Bériault, S., Yu, P., Guo, H., Huang, Z., Li, G., Zhang, X., Fan, Y., Liu, H., Xin, B., Nicolson, A., Zhong, L., Deng, Z., Müller-Franzes, G., Khader, F., Li, X., Zhang, Y., Hémon, C., Boussot, V., Zhang, Z., Wang, L., Bai, L., Wang, S., Mus, D., Kooiman, B., Sargeant, C. A. H., Henderson, E. G. A., Kondo, S., Kasai, S., Karimzadeh, R., Ibragimov, B., Helfer, T., Dafflon, J., Chen, Z., Wang, E., Perko, Z. & Maspero, M. 2024. Generating synthetic computed tomography for radiotherapy: SynthRAD2023 challenge report. *Medical Image Analysis,* 97**,** 103276.

ICRU 1993. Prescribing, Recording, and Reporting Photon Beam Therapy. Bethesda, MD, USA: International Commission on Radiation Units and Measurements (ICRU).

Ilic, I. & Ilic, M. 2023. International patterns and trends in the brain cancer incidence and mortality: An observational study based on the global burden of disease. *Heliyon,* 9**,** e18222.

Irmak, S., Zimmermann, L., Georg, D., Kuess, P. & Lechner, W. 2021. Cone beam CT based validation of neural network generated synthetic CTs for radiotherapy in the head region. *Medical Physics,* 48**,** 4560-4571.

Jakubovic, R., Zhou, S., Heyn, C., Soliman, H., Zhang, L., Aviv, R. & Sahgal, A. 2016. The predictive capacity of apparent diffusion coefficient (ADC) in response assessment of brain metastases following radiation. *Clin Exp Metastasis,* 33**,** 277-84.

Jensen, J. H., Helpern, J. A., Ramani, A., Lu, H. & Kaczynski, K. 2005. Diffusional kurtosis imaging: the quantification of non-gaussian water diffusion by means of magnetic resonance imaging. *Magn Reson Med,* 53**,** 1432-40.

Johnstone, E., Wyatt, J. J., Henry, A. M., Short, S. C., Sebag-Montefiore, D., Murray, L., Kelly, C. G., McCallum, H. M. & Speight, R. 2018. Systematic Review of Synthetic Computed Tomography Generation Methodologies for Use in Magnetic Resonance Imaging-Only Radiation Therapy. *Int J Radiat Oncol Biol Phys,* 100**,** 199-217.

Jokivuolle, M., Mahmood, F., Madsen, K. H., Harbo, F. S. G., Johnsen, L. & Lundell, H. 2024. Assessing tumor microstructure with time-dependent diffusion imaging: Considerations and feasibility on clinical MRI and MRI-Linac. *Med Phys*.

Jones, D. K. 2010. Precision and Accuracy in Diffusion Tensor Magnetic Resonance Imaging. *Topics in Magnetic Resonance Imaging,* 21**,** 87-99.

Jonsson, J., Nyholm, T. & Soderkvist, K. 2019. The rationale for MR-only treatment planning for external radiotherapy. *Clin Transl Radiat Oncol,* 18**,** 60-65.

Jonsson, J. H., Akhtari, M. M., Karlsson, M. G., Johansson, A., Asklund, T. & Nyholm, T. 2015. Accuracy of inverse treatment planning on substitute CT images derived from MR data for brain lesions. *Radiat Oncol,* 10**,** 13.

Jonsson, J. H., Johansson, A., Soderstrom, K., Asklund, T. & Nyholm, T. 2013. Treatment planning of intracranial targets on MRI derived substitute CT data. *Radiother Oncol,* 108**,** 118-22.

Jonsson, J. H., Karlsson, M. G., Karlsson, M. & Nyholm, T. 2010. Treatment planning using MRI data: an analysis of the dose calculation accuracy for different treatment regions. *Radiation Oncology,* 5**,** 62.

Kazemifar, S., Barragan Montero, A. M., Souris, K., Rivas, S. T., Timmerman, R., Park, Y. K., Jiang, S., Geets, X., Sterpin, E. & Owrangi, A. 2020. Dosimetric evaluation of synthetic CT generated with GANs for MRI-only proton therapy treatment planning of brain tumors. *J Appl Clin Med Phys,* 21**,** 76-86.

Keyriläinen, J., Sjöblom, O., Turnbull-Smith, S., Hovirinta, T. & Minn, H. 2021. Clinical experience and cost evaluation of magnetic resonance imaging -only workflow in radiation therapy planning of prostate cancer. *Physics and Imaging in Radiation Oncology,* 19**,** 66-71.

Kinhult, S., Tavelin, B., Löfgren, D., Rosenlund, L., Strandeus, M. & Henriksson, R. 2023. Regional variation i användningen av TTF vid glioblastombehandling. *Läkartidningen,* 120.

Kirchgesner, T., Acid, S., Perlepe, V., Lecouvet, F. & Vande Berg, B. 2020. Two-point Dixon fat-water swapping artifact: lesion mimicker at musculoskeletal T2-weighted MRI. *Skeletal Radiology,* 49**,** 2081-2086.

Koh, D. M. & Collins, D. J. 2007. Diffusion-weighted MRI in the body: applications and challenges in oncology. *AJR Am J Roentgenol,* 188**,** 1622-35.

Kristensen, B. H., Laursen, F. J., Løgager, V., Geertsen, P. F. & Krarup-Hansen, A. 2008. Dosimetric and geometric evaluation of an open low-field magnetic resonance simulator for radiotherapy treatment planning of brain tumours. *Radiother Oncol,* 87**,** 100-9.

Lacroix, M., Abi-Said, D., Fourney, D. R., Gokaslan, Z. L., Shi, W., DeMonte, F., Lang, F. F., McCutcheon, I. E., Hassenbusch, S. J., Holland, E., Hess, K., Michael, C., Miller, D. & Sawaya, R. 2001. A multivariate analysis of 416 patients with glioblastoma multiforme: prognosis, extent of resection, and survival. *J Neurosurg,* 95**,** 190-8.

Lasič, S., Szczepankiewicz, F., Eriksson, S., Nilsson, M. & Topgaard, D. 2014. Microanisotropy imaging: quantification of microscopic diffusion anisotropy and orientational order parameter by diffusion MRI with magic-angle spinning of the q-vector. *Front. Phys.,* 2.

Lawrence, L. S. P., Chan, R. W., Chen, H., Keller, B., Stewart, J., Ruschin, M., Chugh, B., Campbell, M., Theriault, A., Stanisz, G. J., MacKenzie, S., Myrehaug, S., Detsky, J., Maralani, P. J., Tseng, C. L., Czarnota, G. J., Sahgal, A. & Lau, A. Z. 2021. Accuracy and precision of apparent diffusion coefficient measurements on a 1.5 T MR-Linac in central nervous system tumour patients. *Radiother Oncol,* 164**,** 155-162.

Le Bihan, D. 2006. Looking into the functional architecture of the brain with diffusion MRI. *International Congress Series,* 1290**,** 1-24.

Le Bihan, D. 2013. Apparent diffusion coefficient and beyond: what diffusion MR imaging can tell us about tissue structure. *Radiology,* 268**,** 318-22.

Le Bihan, D., Mangin, J. F., Poupon, C., Clark, C. A., Pappata, S., Molko, N. & Chabriat, H. 2001. Diffusion tensor imaging: concepts and applications. *J Magn Reson Imaging,* 13**,** 534-46.

Lee, C. C., Wintermark, M., Xu, Z., Yen, C. P., Schlesinger, D. & Sheehan, J. P. 2014. Application of diffusion-weighted magnetic resonance imaging to predict the intracranial metastatic tumor response to gamma knife radiosurgery. *J Neurooncol,* 118**,** 351-361.

Lerner, M., Medin, J., Alkner, S., Olsson, L. E. & Persson, E. 2024. 2432: Intracranial MRI-CT registration uncertainties: a motivation for MRI-only radiotherapy or not? *Radiotherapy and Oncology,* 194**,** S3920-S3923.

Levardon, M., Autret, D., Le Dorze, T., Guillerminet, C. & Dufreneix, S. 2024. Brain MR-only workflow in clinical practice: A comparison among generators for quality assurance and patient positioning. *J Appl Clin Med Phys,* n/a**,** e14583.

Lin, N. U., Lee, E. Q., Aoyama, H., Barani, I. J., Barboriak, D. P., Baumert, B. G., Bendszus, M., Brown, P. D., Camidge, D. R., Chang, S. M., Dancey, J., de Vries, E. G., Gaspar, L. E., Harris, G. J., Hodi, F. S., Kalkanis, S. N., Linskey, M. E., Macdonald, D. R., Margolin, K., Mehta, M. P., Schiff, D., Soffietti, R., Suh, J. H., van den Bent, M. J., Vogelbaum, M. A., Wen, P. Y. & Response Assessment in Neuro-Oncology, g. 2015. Response assessment criteria for brain metastases: proposal from the RANO group. *Lancet Oncol,* 16**,** e270-8.

Liu, F., Yadav, P., Baschnagel, A. M. & McMillan, A. B. 2019. MR-based treatment planning in radiation therapy using a deep learning approach. *Journal of Applied Clinical Medical Physics,* 20**,** 105-114.

Liu, X., Emami, H., Nejad-Davarani, S. P., Morris, E., Schultz, L., Dong, M. & K. Glide-Hurst, C. 2021. Performance of deep learning synthetic CTs for MR-only brain radiation therapy. *Journal of Applied Clinical Medical Physics,* 22**,** 308-317.

Low, R. N., Austin, M. J. & Ma, J. 2011. Fast spin-echo triple echo dixon: Initial clinical experience with a novel pulse sequence for simultaneous fat-suppressed and nonfat-suppressed T2-weighted spine magnetic resonance imaging. *J Magn Reson Imaging,* 33**,** 390-400.

Mahmood, F., Hjorth Johannesen, H., Geertsen, P. & Hansen, R. H. 2020. Diffusion MRI outlined viable tumour volume beats GTV in intra-treatment stratification of outcome. *Radiother Oncol,* 144**,** 121-126.

Manzano Patron, J. P., Moeller, S., Andersson, J. L. R., Ugurbil, K., Yacoub, E. & Sotiropoulos, S. N. 2024. Denoising diffusion MRI: Considerations and implications for analysis. *Imaging Neuroscience,* 2**,** 1-29.

Mardor, Y., Roth, Y., Ochershvilli, A., Spiegelmann, R., Tichler, T., Daniels, D., Maier, S. E., Nissim, O., Ram, Z., Baram, J., Orenstein, A. & Pfeffer, R. 2004. Pretreatment prediction of brain tumors' response to radiation therapy using high b-value diffusion-weighted MRI. *Neoplasia,* 6**,** 136-42.

Martz, N., Salleron, J., Dhermain, F., Vogin, G., Daisne, J. F., Mouttet-Audouard, R., Tanguy, R., Noel, G., Peyre, M., Lecouillard, I., Jacob, J., Attal, J., Charissoux, M., Veresezan, O., Hanzen, C., Huchet, A., Latorzeff, I., Coutte, A., Doyen, J., Stefan, D., Feuvret, L., Garcia, G. & Royer, P. 2023. Target volume delineation for radiotherapy of meningiomas: an ANOCEF consensus guideline. *Radiat Oncol,* 18**,** 113.

Masitho, S., Szkitsak, J., Grigo, J., Fietkau, R., Putz, F. & Bert, C. 2022. Feasibility of artificial-intelligence-based synthetic computed tomography in a magnetic resonance-only radiotherapy workflow for brain radiotherapy: Two-way dose validation and 2D/2D kV-image-based positioning. *Phys Imaging Radiat Oncol,* 24**,** 111-117.

Maspero, M., Bentvelzen, L. G., Savenije, M. H. F., Guerreiro, F., Seravalli, E., Janssens, G. O., van den Berg, C. A. T. & Philippens, M. E. P. 2020. Deep learning-based synthetic CT generation for paediatric brain MR-only photon and proton radiotherapy. *Radiother Oncol,* 153**,** 197-204.

Maspero, M., Seevinck, P. R., Schubert, G., Hoesl, M. A., van Asselen, B., Viergever, M. A., Lagendijk, J. J., Meijer, G. J. & van den Berg, C. A. 2017. Quantification of confounding factors in MRI-based dose calculations as applied to prostate IMRT. *Phys Med Biol,* 62**,** 948-965.

McKinnon, C., Nandhabalan, M., Murray, S. A. & Plaha, P. 2021. Glioblastoma: clinical presentation, diagnosis, and management. *BMJ,* 374**,** n1560.

McRobbie, D. W., Moore, E. A., Graves, M. J. & Prince, M. R. 2009. *MRI from Picture to Proton*.

Miller, K. D., Weathers, T., Haney, L. G., Timmerman, R., Dickler, M., Shen, J. & Sledge Jr, G. W. 2003. Occult central nervous system involvement in patients with metastatic breast cancer: prevalence, predictive factors and impact on overall survival. *Annals of Oncology,* 14**,** 1072-1077.

Miloushev, V. Z., Chow, D. S. & Filippi, C. G. 2015. Meta-Analysis of Diffusion Metrics for the Prediction of Tumor Grade in Gliomas. *American Journal of Neuroradiology,* 36**,** 302-308.

Mohammed, S., Dinesan, M. & Ajayakumar, T. 2022. Survival and quality of life analysis in glioblastoma multiforme with adjuvant chemoradiotherapy: a retrospective study. *Rep Pract Oncol Radiother,* 27**,** 1026-1036.

Nilsson, M., Englund, E., Szczepankiewicz, F., van Westen, D. & Sundgren, P. C. 2018. Imaging brain tumour microstructure. *Neuroimage,* 182**,** 232-250.

Nilsson, M., Szczepankiewicz, F., Brabec, J., Taylor, M., Westin, C. F., Golby, A., van Westen, D. & Sundgren, P. C. 2020. Tensor-valued diffusion MRI in under 3 minutes: an initial survey of microscopic anisotropy and tissue heterogeneity in intracranial tumors. *Magn Reson Med,* 83**,** 608-620.

Niyazi, M., Andratschke, N., Bendszus, M., Chalmers, A. J., Erridge, S. C., Galldiks, N., Lagerwaard, F. J., Navarria, P., Munck Af Rosenschold, P., Ricardi, U., van den Bent, M. J., Weller, M., Belka, C. & Minniti, G. 2023. ESTRO-EANO guideline on target delineation and radiotherapy details for glioblastoma. *Radiother Oncol,* 184**,** 109663.

O'Connor, J. P., Aboagye, E. O., Adams, J. E., Aerts, H. J., Barrington, S. F., Beer, A. J., Boellaard, R., Bohndiek, S. E., Brady, M., Brown, G., Buckley, D. L., Chenevert, T. L., Clarke, L. P., Collette, S., Cook, G. J., deSouza, N. M., Dickson, J. C., Dive, C., Evelhoch, J. L., Faivre-Finn, C., Gallagher, F. A., Gilbert, F. J., Gillies, R. J., Goh, V., Griffiths, J. R., Groves, A. M., Halligan, S., Harris, A. L., Hawkes, D. J., Hoekstra, O. S., Huang, E. P., Hutton, B. F., Jackson, E. F., Jayson, G. C., Jones, A., Koh, D. M., Lacombe, D., Lambin, P., Lassau, N., Leach, M. O., Lee, T. Y., Leen, E. L., Lewis, J. S., Liu, Y., Lythgoe, M. F., Manoharan, P., Maxwell, R. J., Miles, K. A., Morgan, B., Morris, S., Ng, T., Padhani, A. R., Parker, G. J., Partridge, M., Pathak, A. P., Peet, A. C., Punwani, S., Reynolds, A. R., Robinson, S. P., Shankar, L. K., Sharma, R. A., Soloviev, D., Stroobants, S., Sullivan, D. C., Taylor, S. A., Tofts, P. S., Tozer, G. M., van Herk, M., Walker-Samuel, S., Wason, J., Williams, K. J., Workman, P., Yankeelov, T. E., Brindle, K. M., McShane, L. M., Jackson, A. & Waterton, J. C. 2017. Imaging biomarker roadmap for cancer studies. *Nat Rev Clin Oncol,* 14**,** 169-186.

Oldenhuis, C. N., Oosting, S. F., Gietema, J. A. & de Vries, E. G. 2008. Prognostic versus predictive value of biomarkers in oncology. *Eur J Cancer,* 44**,** 946-53.

Owrangi, A. M., Greer, P. B. & Glide-Hurst, C. K. 2018. MRI-only treatment planning: benefits and challenges. *Phys Med Biol,* 63**,** 05TR01.

Palmer, E., Karlsson, A., Nordstrom, F., Petruson, K., Siversson, C., Ljungberg, M. & Sohlin, M. 2021. Synthetic computed tomography data allows for accurate absorbed dose calculations in a magnetic resonance imaging only workflow for head and neck radiotherapy. *Phys Imaging Radiat Oncol,* 17**,** 36-42.

Palmer, E., Persson, E., Ambolt, P., Gustafsson, C., Gunnlaugsson, A. & Olsson, L. E. 2018. Cone beam CT for QA of synthetic CT in MRI only for prostate patients. *J Appl Clin Med Phys,* 19**,** 44-52.

Paradis, E., Cao, Y., Lawrence, T. S., Tsien, C., Feng, M., Vineberg, K. & Balter, J. M. 2015. Assessing the Dosimetric Accuracy of Magnetic Resonance-Generated Synthetic CT Images for Focal Brain VMAT Radiation Therapy. *Int J Radiat Oncol Biol Phys,* 93**,** 1154-61.

Paulson, E. S., Crijns, S. P., Keller, B. M., Wang, J., Schmidt, M. A., Coutts, G. & van der Heide, U. A. 2016. Consensus opinion on MRI simulation for external beam radiation treatment planning. *Radiother Oncol,* 121**,** 187-192.

Persson, E., Jamtheim Gustafsson, C., Ambolt, P., Engelholm, S., Ceberg, S., Bäck, S., Olsson, L. E. & Gunnlaugsson, A. 2020. MR-PROTECT: Clinical feasibility of a prostate MRI-only radiotherapy treatment workflow and investigation of acceptance criteria. *Radiation Oncology,* 15**,** 77.

Persson, E., Svanberg, N., Scherman, J., Jamtheim Gustafsson, C., Fridhammar, A., Hjalte, F., Back, S., Nilsson, P., Gunnlaugsson, A. & Olsson, L. E. 2023. MRI-only radiotherapy from an economic perspective: Can new techniques in prostate cancer treatment be cost saving? *Clin Transl Radiat Oncol,* 38**,** 183-187.

Peters, R. D. & Lawson, S. 2021. AIR Recon DL for diffusion-weighted imaging.

Price, R. G., Kim, J. P., Zheng, W., Chetty, I. J. & Glide-Hurst, C. 2016. Image Guided Radiation Therapy Using Synthetic Computed Tomography Images in Brain Cancer. *Int J Radiat Oncol Biol Phys,* 95**,** 1281-9.

Ranta, I., Wright, P., Suilamo, S., Kemppainen, R., Schubert, G., Kapanen, M. & Keyriläinen, J. 2023. Clinical feasibility of a commercially available MRI-only method for radiotherapy treatment planning of the brain. *J Appl Clin Med Phys,* 24**,** e14044.

Redmond, K. J., Gui, C., Benedict, S., Milano, M. T., Grimm, J., Vargo, J. A., Soltys, S. G., Yorke, E., Jackson, A., El Naqa, I., Marks, L. B., Xue, J., Heron, D. E. & Kleinberg, L. R. 2021. Tumor Control Probability of Radiosurgery and Fractionated Stereotactic Radiosurgery for Brain Metastases. *Int J Radiat Oncol Biol Phys,* 110**,** 53-67.

Regionala Cancercentrum i Samverkan. 2024. *Nationellt vårdprogram: Tumörer i hjärna och ryggmärg* [Online]. Regionala Cancercentrum i Samverkan. Available: https://cancercentrum.se/samverkan/cancerdiagnoser/hjarna-ryggmarg-och-hypofys/hjarna-och-ryggmarg/vardprogram/ [Accessed 2024-11-01 2024].

Rossi, E., Emin, S., Gubanski, M., Gagliardi, G., Hedman, M. & Villegas, F. 2024. Contouring practices and artefact management within a synthetic CT-based radiotherapy workflow for the central nervous system. *Radiation Oncology,* 19**,** 27.

Roth, P., Pace, A., Le Rhun, E., Weller, M., Ay, C., Cohen-Jonathan Moyal, E., Coomans, M., Giusti, R., Jordan, K., Nishikawa, R., Winkler, F., Hong, J. T., Ruda, R., Villà, S., Taphoorn, M. J. B., Wick, W. & Preusser, M. 2021. Neurological and vascular complications of primary and secondary brain tumours: EANO-ESMO Clinical Practice Guidelines for prophylaxis, diagnosis, treatment and follow-up†. *Annals of Oncology,* 32**,** 171-182.

Scaringi, C., Agolli, L. & Minniti, G. 2018. Technical Advances in Radiation Therapy for Brain Tumors. *Anticancer Res,* 38**,** 6041-6045.

Schad, L., S, B., H, H., F, W. & W, L. 1994. Radiosurgical treatment planning of brain metastases based on a fast, three-dimensional MR imaging technique. *Magnetic Resonance Imaging,* 12**,** 811-819.

Shah, A. D., Shridhar Konar, A., Paudyal, R., Oh, J. H., LoCastro, E., Nunez, D. A., Swinburne, N., Vachha, B., Ulaner, G. A., Young, R. J., Holodny, A. I., Beal, K., Shukla-Dave, A. & Hatzoglou, V. 2021. Diffusion and Perfusion MRI Predicts Response Preceding and Shortly After Radiosurgery to Brain Metastases: A Pilot Study. *J Neuroimaging,* 31**,** 317-323.

Sjölund, J., Szczepankiewicz, F., Nilsson, M., Topgaard, D., Westin, C. F. & Knutsson, H. 2015. Constrained optimization of gradient waveforms for generalized diffusion encoding. *J Magn Reson,* 261**,** 157-68.

Socialstyrelsen. 2023. *Statistikområden, Antal nya cancerfall* [Online]. Stockholm: Socialstyrelsen. Available: https://www.socialstyrelsen.se/statistik-och-data/statistik/statistikdatabasen/ [Accessed Aug 1st 2024].

Soliman, H., Ruschin, M., Angelov, L., Brown, P. D., Chiang, V. L. S., Kirkpatrick, J. P., Lo, S. S., Mahajan, A., Oh, K. S., Sheehan, J. P., Soltys, S. G. & Sahgal, A. 2018. Consensus Contouring Guidelines for Postoperative Completely Resected Cavity Stereotactic Radiosurgery for Brain Metastases. *Int J Radiat Oncol Biol Phys,* 100**,** 436-442.

Spadea, M. F., Maspero, M., Zaffino, P. & Seco, J. 2021. Deep learning based synthetic-CT generation in radiotherapy and PET: A review. *Medical Physics,* 48**,** 6537-6566.

Speight, R. 2019. MRI to CT Image Registration. *In:* LINEY, G. & VAN DER HEIDE, U. (eds.) *MRI for Radiotherapy: Planning, Delivery, and Response Assessment.* Cham: Springer International Publishing.

Speight, R., Dubec, M., Eccles, C. L., George, B., Henry, A., Herbert, T., Johnstone, R. I., Liney, G. P., McCallum, H. & Schmidt, M. A. 2021. IPEM topical report: guidance on the use of MRI for external beam radiotherapy treatment planning*. *Physics in Medicine & Biology,* 66**,** 055025.

Sperduto, P. W., Mesko, S., Li, J., Cagney, D., Aizer, A., Lin, N. U., Nesbit, E., Kruser, T. J., Chan, J., Braunstein, S., Lee, J., Kirkpatrick, J. P., Breen, W., Brown, P. D., Shi, D., Shih, H. A., Soliman, H., Sahgal, A., Shanley, R., Sperduto, W. A., Lou, E., Everett, A., Boggs, D. H., Masucci, L., Roberge, D., Remick, J., Plichta, K., Buatti, J. M., Jain, S., Gaspar, L. E., Wu, C.-C., Wang, T. J. C., Bryant, J., Chuong, M., An, Y., Chiang, V., Nakano, T., Aoyama, H. & Mehta, M. P. 2020. Survival in Patients With Brain Metastases: Summary Report on the Updated Diagnosis-Specific Graded Prognostic Assessment and Definition of the Eligibility Quotient. *Journal of Clinical Oncology,* 38**,** 3773-3784.

Srinivasan, S., Dasgupta, A., Chatterjee, A., Baheti, A., Engineer, R., Gupta, T. & Murthy, V. 2022. The Promise of Magnetic Resonance Imaging in Radiation Oncology Practice in the Management of Brain, Prostate, and GI Malignancies. *JCO Glob Oncol,* 8**,** e2100366.

Stupp, R., Mason, W. P., van den Bent, M. J., Weller, M., Fisher, B., Taphoorn, M. J., Belanger, K., Brandes, A. A., Marosi, C., Bogdahn, U., Curschmann, J., Janzer, R. C., Ludwin, S. K., Gorlia, T., Allgeier, A., Lacombe, D., Cairncross, J. G., Eisenhauer, E. & Mirimanoff, R. O. 2005. Radiotherapy plus concomitant and adjuvant temozolomide for glioblastoma. *N Engl J Med,* 352**,** 987-96.

Stupp, R., Taillibert, S., Kanner, A., Read, W., Steinberg, D. M., Lhermitte, B., Toms, S., Idbaih, A., Ahluwalia, M. S., Fink, K., Di Meco, F., Lieberman, F., Zhu, J.-J., Stragliotto, G., Tran, D. D., Brem, S., Hottinger, A. F., Kirson, E. D., Lavy-Shahaf, G., Weinberg, U., Kim, C.-Y., Paek, S.-H., Nicholas, G., Bruna, J., Hirte, H., Weller, M., Palti, Y., Hegi, M. E. & Ram, Z. 2017. Effect of Tumor-Treating Fields Plus Maintenance Temozolomide vs Maintenance Temozolomide Alone on Survival in Patients With Glioblastoma: A Randomized Clinical Trial. *JAMA,* 318**,** 2306-2316.

Szczepankiewicz, F. 2016. Imaging diffusional variance by MRI: The role of tensor-valued diffusion encoding and tissue heterogeneity. *PhD Thesis,* Lund University.

Szczepankiewicz, F., Lasic, S., van Westen, D., Sundgren, P. C., Englund, E., Westin, C. F., Stahlberg, F., Latt, J., Topgaard, D. & Nilsson, M. 2015. Quantification of microscopic diffusion anisotropy disentangles effects of orientation dispersion from microstructure: applications in healthy volunteers and in brain tumors. *Neuroimage,* 104**,** 241-52.

Szczepankiewicz, F., Sjolund, J., Stahlberg, F., Latt, J. & Nilsson, M. 2019a. Tensor-valued diffusion encoding for diffusional variance decomposition (DIVIDE): Technical feasibility in clinical MRI systems. *PLoS One,* 14**,** e0214238.

Szczepankiewicz, F., Sjölund, J., Ståhlberg, F., Lätt, J. & Nilsson, M. 2019b. Tensor-valued diffusion encoding for diffusional variance decomposition (DIVIDE): Technical feasibility in clinical MRI systems. *PLoS One,* 14**,** e0214238.

Szczepankiewicz, F., van Westen, D., Englund, E., Westin, C.-F., Ståhlberg, F., Lätt, J., Sundgren, P. C. & Nilsson, M. 2016. The link between diffusion MRI and tumor heterogeneity: Mapping cell eccentricity and density by diffusional variance decomposition (DIVIDE). *NeuroImage,* 142**,** 522-532.

Szczepankiewicz, F., Westin, C.-F. & Nilsson, M. 2021. Gradient waveform design for tensor-valued encoding in diffusion MRI. *J. Neurosci. Methods,* 348**,** 109007.

Tamimi, A. J., M. 2017. *Epidemiology and Outcome of Glioblastoma,* Brisbane (AU), Codon Publications.

Tax, C. M. W., Bastiani, M., Veraart, J., Garyfallidis, E. & Okan Irfanoglu, M. 2022. What's new and what's next in diffusion MRI preprocessing. *NeuroImage,* 249**,** 118830.

Teh, I., Shelley, D., Boyle, J. H., Zhou, F., Poenar, A. M., Sharrack, N., Foster, R. J., Yuldasheva, N. Y., Parker, G. J. M., Dall'Armellina, E., Plein, S., Schneider, J. E. & Szczepankiewicz, F. 2023. Cardiac q-space trajectory imaging by motion-compensated tensor-valued diffusion encoding in human heart in vivo. *Magn Reson Med,* 90**,** 150-165.

Teoh, M., Clark, C. H., Wood, K., Whitaker, S. & Nisbet, A. 2011. Volumetric modulated arc therapy: a review of current literature and clinical use in practice. *Br J Radiol,* 84**,** 967-96.

Tyagi, N. 2019. Challenges and Requirements. *In:* LINEY, G. & VAN DER HEIDE, U. (eds.) *MRI for Radiotherapy: Planning, Delivery, and Response Assessment.* Cham: Springer International Publishing.

Tyagi, N., Zelefsky, M. J., Wibmer, A., Zakian, K., Burleson, S., Happersett, L., Halkola, A., Kadbi, M. & Hunt, M. 2020. Clinical experience and workflow challenges with magnetic resonance-only radiation therapy simulation and planning for prostate cancer. *Physics and Imaging in Radiation Oncology,* 16**,** 43-49.

Uh, J., Merchant, T. E., Li, Y., Li, X. & Hua, C. 2014. MRI-based treatment planning with pseudo CT generated through atlas registration. *Med Phys,* 41**,** 051711.

Ulin, K., Urie, M. M. & Cherlow, J. M. 2010. Results of a multi-institutional benchmark test for cranial CT/MR image registration. *Int J Radiat Oncol Biol Phys,* 77**,** 1584-9.

van den Bent, M. J., Geurts, M., French, P. J., Smits, M., Capper, D., Bromberg, J. E. C. & Chang, S. M. 2023. Primary brain tumours in adults. *Lancet,* 402**,** 1564-1579.

Vandewinckele, L., Claessens, M., Dinkla, A., Brouwer, C., Crijns, W., Verellen, D. & van Elmpt, W. 2020. Overview of artificial intelligence-based applications in radiotherapy: Recommendations for implementation and quality assurance. *Radiother Oncol.*

Vellayappan, B. A., Lim, M. C., Yong, C., Teo, K., Malone, S. & Lo, S. 2020. Target Delineation for Radiosurgery (Including Postoperative Cavity Radiosurgery) in Brain Metastases. *In:* YAMADA, Y., CHANG, E., FIVEASH, J. B. & KNISELY, J. (eds.) *Radiotherapy in Managing Brain Metastases: A Case-Based Approach.* Cham: Springer International Publishing.

Villegas, F., Dal Bello, R., Alvarez-Andres, E., Dhont, J., Janssen, T., Milan, L., Robert, C., Salagean, G. A., Tejedor, N., Trnkova, P., Fusella, M., Placidi, L. & Cusumano, D. 2024. Challenges and opportunities in the development and clinical implementation of artificial intelligence based synthetic computed tomography for magnetic resonance only radiotherapy. *Radiother Oncol***,** 110387.

Vogelbaum, M. A., Brown, P. D., Messersmith, H., Brastianos, P. K., Burri, S., Cahill, D., Dunn, I. F., Gaspar, L. E., Gatson, N. T. N., Gondi, V., Jordan, J. T., Lassman, A. B., Maues, J., Mohile, N., Redjal, N., Stevens, G., Sulman, E., van den Bent, M., Wallace, H. J., Weinberg, J. S., Zadeh, G. & Schiff, D. 2021. Treatment for Brain Metastases: ASCO-SNO-ASTRO Guideline. *Neuro-Oncology,* 24**,** 331-357.

Vogin, G., Hettal, L., Bartau, C., Thariat, J., Claeys, M.-V., Peyraga, G., Retif, P., Schick, U., Antoni, D., Bodgal, Z., Dhermain, F. & Feuvret, L. 2021. Cranial organs at risk delineation: heterogenous practices in radiotherapy planning. *Radiation Oncology,* 16**,** 26.

Wang, C., Chao, M., Lee, L. & Xing, L. 2008. MRI-based treatment planning with electron density information mapped from CT images: a preliminary study. *Technol Cancer Res Treat,* 7**,** 341-8.

Weller, M., van den Bent, M., Preusser, M., Le Rhun, E., Tonn, J. C., Minniti, G., Bendszus, M., Balana, C., Chinot, O., Dirven, L., French, P., Hegi, M. E., Jakola, A. S., Platten, M., Roth, P., Rudà, R., Short, S., Smits, M., Taphoorn, M. J. B., von Deimling, A., Westphal, M., Soffietti, R., Reifenberger, G. & Wick, W. 2021. EANO guidelines on the diagnosis and treatment of diffuse gliomas of adulthood. *Nature Reviews Clinical Oncology,* 18**,** 170-186.

Westin, C. F., Knutsson, H., Pasternak, O., Szczepankiewicz, F., Ozarslan, E., van Westen, D., Mattisson, C., Bogren, M., O'Donnell, L. J., Kubicki, M., Topgaard, D. & Nilsson, M. 2016. Q-space trajectory imaging for multidimensional diffusion MRI of the human brain. *Neuroimage,* 135**,** 345-62.

Weygand, J., Fuller, C. D., Ibbott, G. S., Mohamed, A. S., Ding, Y., Yang, J., Hwang, K. P. & Wang, J. 2016. Spatial Precision in Magnetic Resonance Imaging-Guided Radiation Therapy: The Role of Geometric Distortion. *Int J Radiat Oncol Biol Phys,* 95**,** 1304-16.

White, N. S., McDonald, C., Farid, N., Kuperman, J., Karow, D., Schenker-Ahmed, N. M., Bartsch, H., Rakow-Penner, R., Holland, D., Shabaik, A., Bjørnerud, A., Hope, T., Hattangadi-Gluth, J., Liss, M., Parsons, J. K., Chen, C. C., Raman, S., Margolis, D., Reiter, R. E., Marks, L., Kesari, S., Mundt, A. J., Kane, C. J., Carter, B. S., Bradley, W. G. & Dale, A. M. 2014. Diffusion-weighted imaging in cancer: physical foundations and applications of restriction spectrum imaging. *Cancer Res,* 74**,** 4638-52.

World Medical Association 2013. World Medical Association Declaration of Helsinki: Ethical Principles for Medical Research Involving Human Subjects. *JAMA,* 310**,** 2191-2194.

Yang, Y., Cao, M., Kaprealian, T., Sheng, K., Gao, Y., Han, F., Gomez, C., Santhanam, A., Tenn, S., Agazaryan, N., Low, D. A. & Hu, P. 2016. Accuracy of UTE-MRI-based patient setup for brain cancer radiation therapy. *Med Phys,* 43**,** 262.

Yip, T. T. Y., Li, Z. & Li, T. 2025. Clinical validation of MR-generated synthetic CT by MRCAT for brain tumor radiotherapy. *J Appl Clin Med Phys,* 26**,** e14494.

Zhao, L., Zhao, M., Liu, J., Yang, H., Zhou, X., Wen, C., Li, G. & Duan, Y. 2021. Mean apparent diffusion coefficient in a single slice may predict tumor response to whole-brain radiation therapy in non-small-cell lung cancer patients with brain metastases. *European Radiology,* 31**,** 5565-5575.

Zheng, W., Kim, J. P., Kadbi, M., Movsas, B., Chetty, I. J. & Glide-Hurst, C. K. 2015. Magnetic Resonance-Based Automatic Air Segmentation for Generation of Synthetic Computed Tomography Scans in the Head Region. *Int J Radiat Oncol Biol Phys,* 93**,** 497-506.

Part II

Research papers

Author contributions

Below is a summary of the author's contribution to each original paper included in this thesis.

Paper I I participated in the study design and development of the methodology. I informed patients. I was responsible for the data analysis, interpretation, and writing the manuscript. I was the main and corresponding author.

Paper II I participated in the study design and development of the methodology. I informed patients, analysed, and interpreted the data and drafted the manuscript. I was the main and corresponding author.

Paper III I participated in the data collection and performed parts of the analysis. I contributed to the interpretation of the results and drafted the manuscript together with P.B. I was the corresponding author.

Paper IV I contributed to the design of the study and development of the methodology. I was responsible for coordinating the logistics of the study and informed most of the patients. I prepared and analysed most of the data. I wrote the manuscript.

Paper V I contributed to the conceptualisation, data collection and interpretation of results. I contributed to writing the manuscript. I was the second author.

Printed by Media-Tryck, Lund 2025 NORDIC SWAN ECOLABEL 3041 0903

LUND UNIVERSITY

FACULTY OF MEDICINE

Department of Translational Medicine
Medical Radiation Physics

Lund University, Faculty of Medicine
Doctoral Dissertation Series 2025:46
ISBN 978-91-8021-699-9
ISSN 1652-8220